nature portfolio

Peer Review File

Engineered bacterial outer membrane vesicles encapsulating oncolytic adenoviruses enhance the efficacy of cancer virotherapy by augmenting tumor cell autophagy

REVIEWER COMMENTS

Reviewer #1 (Remarks to the Author): with expertise in oncolytic viruses, cancer immunology

This manuscript reports on the use of Outer Membrane Vesicles derived from E-Coli and containing P2O as a delivery vehicle for an Adenovirus. The concept of using these OMV to shield the virus from immune neutralization is very interesting.

However, as written at the moment, the manuscript lacks sufficient experimental detail, is poorly written in terms of what experiments were done and how and the data do not address the mechanisms by which OMV protect Ad from, for example, neutralizing antibodies.

I have made some representative comments about how the first two Figures (Figures 2&3)- because there is no Figure 1- could be improved in terms of explanation, clarification, experimental detail and statistical analysis. Similar points can be raised for the remaining 4 Figures and for the additional 27 Supplemental Figures.

There is no Figure 1.

Figure 2A: Unclear as to what we are seeing and what we are supposed to be seeing in this Figure. How many Ad are encapsulated in the OMVs@P2O-Ads?

Figure 2C: SDS Page does not show specificity of the 70KDa P2O and the loading of the lanes is different.

Figure 2D: Experimental details need to be provided.

Figure 2E: Needs to be bigger and explanation of what the arrows are showing.

Figure 2i: needs experimental detail.

Figure 2J should be quantified with statistical analysis.

Figure 3A: Need to show multiple mice. Need experimental detail.

Figure 3C needs error bars for statistical relevance and the legend needs experimental detail.

Figure 3D: n=6 in the Legend is not reflected in the Figure where n=4.

And so on.

Reviewer #2 (Remarks to the Author): with expertise in oncolytic viruses, autophagy

Ban and colleagues provide a report detailing the construction of biomineral engineered OMVs-encapsulating oncolytic adenovirus that exhibit enhanced antitumor efficacy. It was mainly dependent on overactivated autophagy. Some areas where improvements can be made include:

Major concerns:
1. Fig 2f/4f: Grey-scale analysis should be performed, so that the LC3-II/LC3-I ratio can be calculated and statistically analyzed.
2. Fig 3f-k: Since immune response is a dynamic process, from innate immunity to T cell mediated

immunity and B cell mediated immunity, so it is critical to specify at what time point did they collect the tumor samples and explain why they choose this time point.
3. Fig 3j: Grouping information and FDR should also be presented in the GSEA figure. Unexpectedly, the pathway “Activation of immune response” is not included in Fig S11. The authors should explain the representativeness of choosing this pathway.
4. Fig 3k: The individual variations among the three tested samples in OMVs@P2O-Ads group are much too large. This kind of variation severely compromise the accuracy of the data.
5. Fig S11: Most of the GSEA enriched pathways are related to B cells, suggesting that the immune response induced by OMVs@P2O-Ads seems to be mediated by B cells, but not T cells. As far as we know, antitumor immunity is mostly mediated by T cells. Thus, it would be better for the authors to explain why they did not study B cell mediated immunity. Perhaps 18 days post Ads inoculation is too late to monitor the T cell immunity.
6. Fig S13/S14 are extremely important and should be presented in Fig 4. What kind of fluorescent dye did the authors used in Fig S13? This information should be provided in figure legends.
7. Fig 5c: Large amount of tiny green spots, which are unlikely to be normal CD8 staining, are shown in G5 and G6. The authors would be better to provide explanation.
8. Fig 5: The authors try to demonstrate that the antitumor efficacy of CaP-OMVs@P2O-Ads depend on the activation of CD8 T cells. In this case, more solid evidences, including the activation status of CD8 T cells (CD44 and CD69 expression), the tumor killing activity of CD8 T cells (co-culture assay), and dependency of CD8 T cells (depleting CD8 with antibodies), should be provided.
9. Fig 5d-f: The flow cytometry was not well performed. Large amount of death cells leads to serious unspecific staining, which adversely affect the interpretation and quantification of the data. The authors should use live/dead dyes to exclude death cells and debris.
10. Fig 5f: Since most, if not all, antigen presenting cells (APCs) express CD80 and CD86, these two markers are not specific enough to identify DCs. The authors should use CD11c and MHCII, instead.
11. Discussion section is missing in the current manuscript.

Minor concerns:
1. The language of the paper could be improved with some editing.
2. It would be better to have an introduction of the advantages and disadvantages of bacterial outer membrane vesicles. Are OMVs better than other nanomaterials? Are there any potential safety concerns?
3. Figure 1 is missing.
4. Fig 2g is missing.
5. Fig 2j: What do G1~G6 represent? The authors should mention this information in the figure legends.
6. Fig 2k should be mentioned at least once in the manuscript.
7. Fig S7: Only 6 columns are presented, but x-axis has 8 groups.
8. Fig S8/5b/6c: What does “Rr=6/6” or “Rr=5/5” mean?
9. Fig S10: What do G1~G6 represent here. Are they the same with Fig S9? The authors should mention this information in the figure legends.
10. The authors should explain why they use TC-1-hCD46. Indeed, hCD46 is the receptor for adenovirus.
11. Misspell: “wight” in section 2.2
12. Fig 3a: The authors ought to give a brief introduction of DiR dye.
13. Figure 4: It would be better for the authors to explain why CaP-OMVs exhibit better tumor selectivity than OMVs.
14. Fig 4b: What do C, O, P, S, Ca, and Ca+P stand for?
15. Fig S22-23: Gating strategies should also be presented.
16. Fig S9/S16/S17/S24/3c/: What do the dotted lines represent?
17. Section 2.5: Some OVs in clinical trials, including vaccinia virus and reovirus, are systemically delivered. The authors should mention this and compare the CaP-OMVs technology with these intravenous OVs.
18. Section 3: What dose “the oncolytic Ads extracted from E. coli” mean? Ads is grown in HEK293 cells?

Reviewer #3 (Remarks to the Author): with expertise in outer membrane vesicles, immunotherapy

In the current study, the authors design and develop a modified oncolytic adenovirus to address the intrinsic drawbacks of the virus. They used biomineral bacterial outer membrane vesicles encapsulated adenovirus to stimulate autophagy and antitumor immunity. The integrated immunotherapy is timely and critical for improving the clinical applications of the oncologic adenovirus and will attract significant attentions from broad readership. There are some important issues the authors should consider to clarify or improve in the revised version.

1. The logic to integrate various components is rather weak and it is recommended for the authors to clarify in the manuscript. Are these components are replaceable or necessary? It is a complicated system and it is hardly be treated as composite microbe. It is recommended to change the word with nanocomposite or nanosystem.
2. How the adenovirus loaded into OMV? What is the efficacy and any improvement have been tried?
3. Autophagy-overactivated is not proper expression, since overactivated action infers to uncontrolled process and may lead to severe side effects.
4. Quantitative measurement of pyranose oxidase in critical in vivo. What is the contribution for this enzyme for immune activation?
5. The scholarly presentation needs to further improve, such as no OV definition provided in the manuscript.
6. For the immune activation experiments, various critical steps are missing to generate a concrete conclusion of cascade antitumor activation.

Reviewer #4 (Remarks to the Author): with expertise in oncolytic viruses, autophagy, nanotherapy.

This is a meaningful work for the present autophagy-cascade-boosted immunotherapeutic method. The authors stated that OMVs@P2O
promoted Ads replication and resulted in Ads-overactivated autophagy, further remolded immunosuppressive TME. However, several problems that must be clarified need to be solved.

1. As we all known, oncolytic adenovirus enters tumor cells through CAR receptor to play an anti-tumor role. What mechanism does OMVs@P2O or OMVs@P2O-Ads enter tumor cells through? Does it have practical significance in tumor cells with high or low CAR expression?
2.The reason of the low intratumoral content of intravenous-delivered Ads is that the higher level of anti-adenovirus antibody in human body eliminates the exogenous injected Ads. Can OMVs@P2O or OMVs@P2O-Ads effectively avoid the elimination of neutralizing antibodies? Whether the expression level of anti-adenovirus antibody has been improved in the mouse model in advance? This is a very necessary experiment.
3. Infection with oncolytic viruses leads to activation of type I IFN signaling pathways, which are crucial in oncolytic virus-mediated antitumor immunity. The authors stated that OMVs@P2O promoted Ads replication. Is this pathway activated to a greater extent by OMVs@P2O?
4. In vivo experiment on OMVs@P2O-Ads or CaP-OMVs@P2O-Ads regulating tumor immune microenvironment is not enough. The innate and adaptive immune cells, as well as the activation and exhausted markers of T cells, need to be detected.

To sum up, my review opinion is that unless the authors can completely and effectively supplement the above experiments, it is unacceptable.

Responses to the reviewers' comments

Reviewer #1: This manuscript reports on the use of Outer Membrane Vesicles derived from *E-Coli* and containing P_2O as a delivery vehicle for an Adenovirus. The concept of using these OMV to shield the virus from immune neutralization is very interesting. However, as written at the moment, the manuscript lacks sufficient experimental detail, is poorly written in terms of what experiments were done and how and the data do not address the mechanisms by which OMV protect Ad from, for example, neutralizing antibodies. I have made some representative comments about how the first two Figures (Figures 2&3)- because there is no Figure 1- could be improved in terms of explanation, clarification, experimental detail and statistical analysis. Similar points can be raised for the remaining 4 Figures and for the additional 27 Supplemental Figures.

Question 1: There is no Figure 1.

Response: We are sorry that Figure 1 had been not shown in the manuscript. We have attached Figure 1 here and added it to the revised manuscript (page 6).

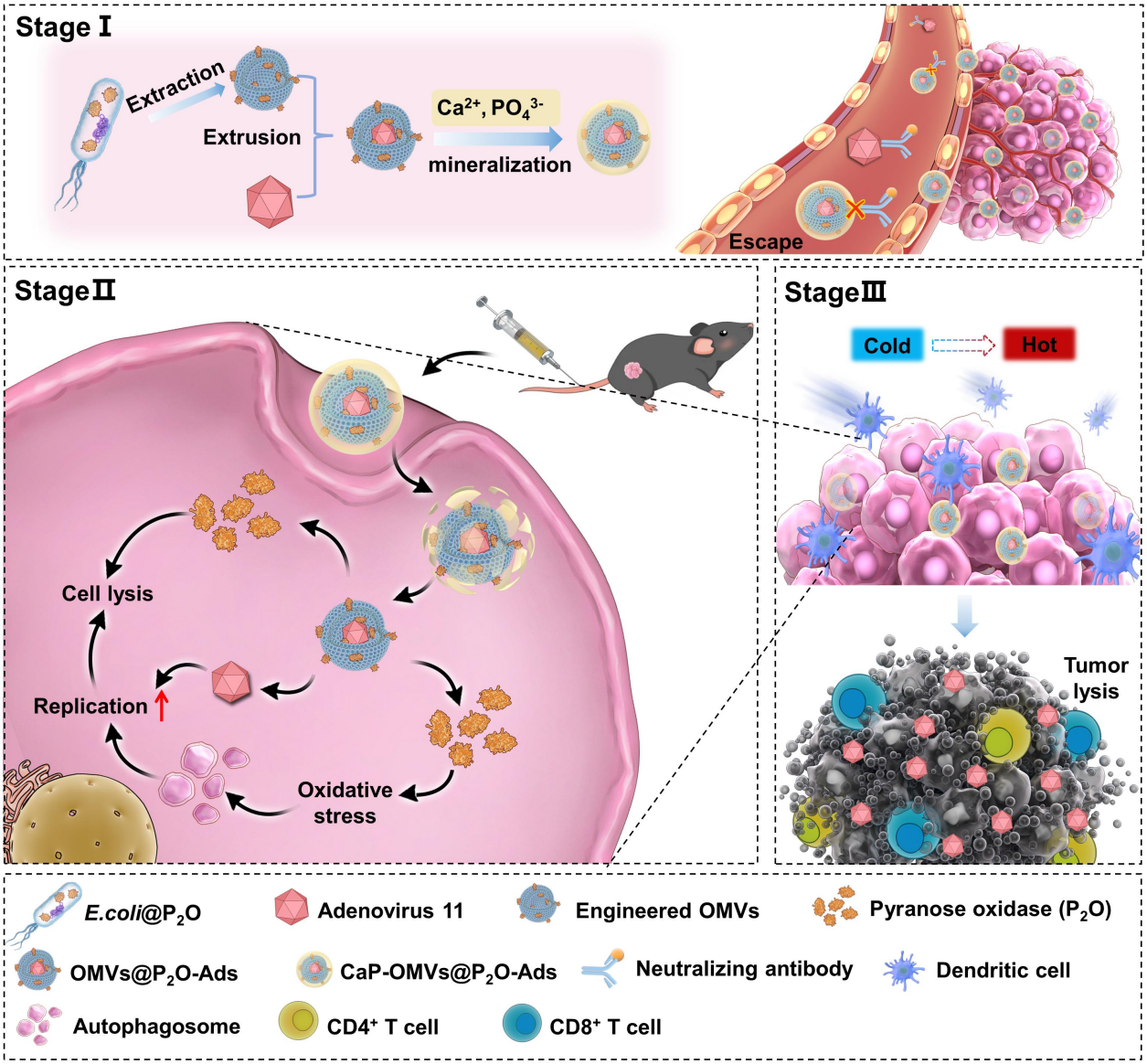

Figure 1. Schematic diagram. The biomineralized microbial nanocomposite engineered from OVs for autophagy-cascade-augmented immunotherapy.

Question 2: Figure 2A: Unclear as to what we are seeing and what we are supposed to be seeing in this Figure. How many Ad are encapsulated in the OMVs@P_2O-Ads?

Response: Thanks for the reviewer's kind questions. Figure 2A showed the particle size and size distribution of Ads, OMVs@P_2O and OMVs@P_2O-Ads (measured by Malvern laser granulometer), as well as the morphology of these under the transmission electron microscope (TEM). In TEM images, Ads possessed a hexagonal core, and OMVs@P_2O presented a spherical shell. The "core-shell" structure of OMVs@P_2O-Ads had been shown in Figure 2A, indicating that the successful construction of this microbial nanocomposite. In this study, Ads themselves have a

steady particle size of 90-100 nm. The *E. coli*-secreted OMVs possessed an even size about 130 nm through the extraction method. Thurs, we ensure that each microbial nanocomposite contained only one Ad particle, which are consistent with image of TEM.

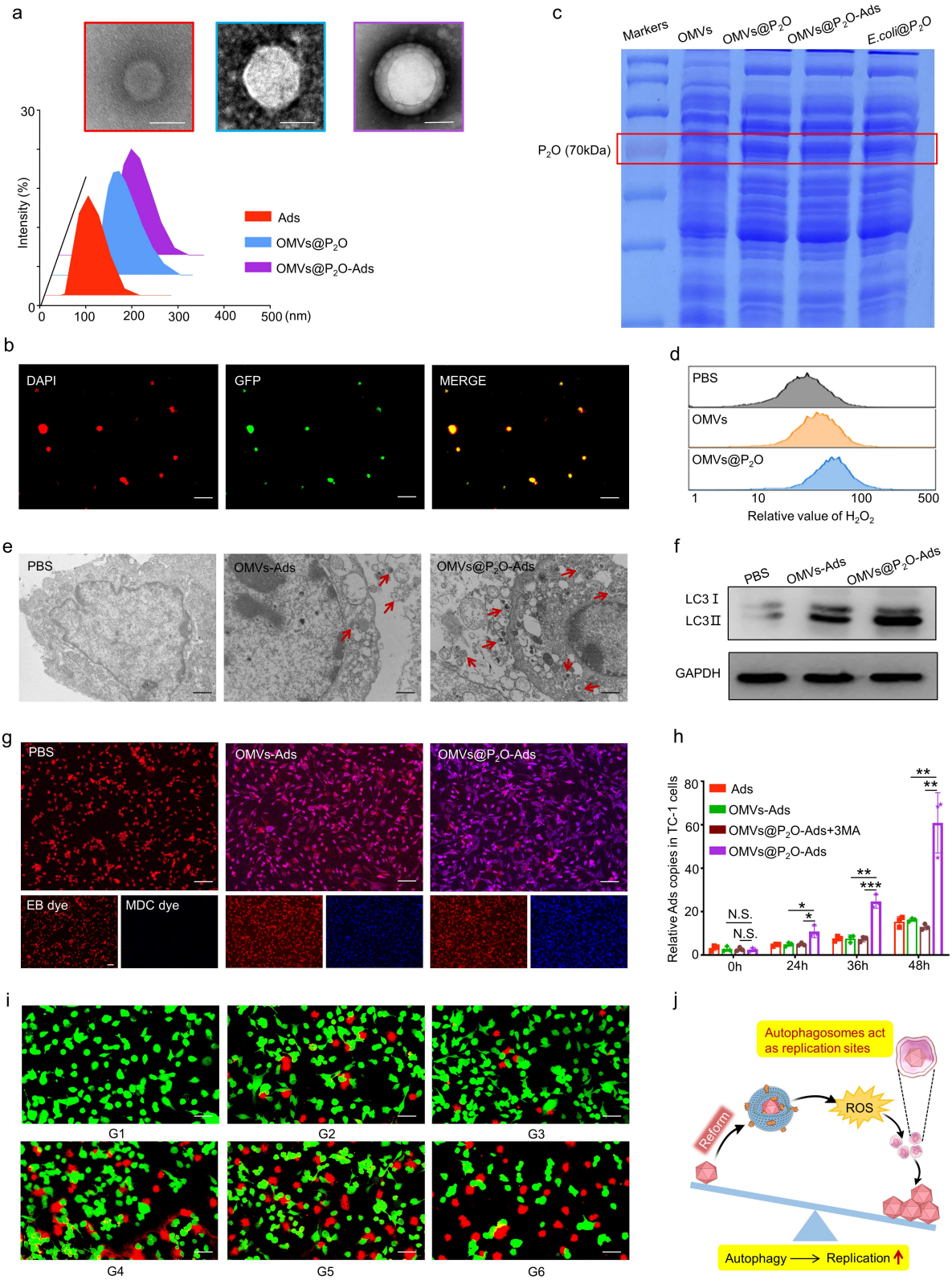

Figure 2. Preparation and *in vitro* evaluation of the microbial nanocomposite. (a) TEM and size distribution images of Ads, OMVs@P_2O, and OMVs@P_2O-Ads. Scale bar=100 nm. (b) CLSM images of the microbial nanocomposite. Ads were stained with DAPI dye (red) and OMVs carried a GFP marker (green). Scale bar=1 μm. (c) The expression of P_2O was investigated by the SDS-PAGE method. (d) The ROS level assessment in TC-1 cells by flow cytometry. (e) TEM images of autophagosomes. Scale bar=200 nm. (f) The expression of autophagy-related protein LC3-I and LC3-II by western bolt analyses. (g) CLSM images of autophagosomes. Cells were stained with EB dye (red) and autophagosomes were stained with MDC dye (blue). Scale bar=50 μm. (h) The Ads replication in TC-1 cells was quantified using real-time PCR at 0, 24, 36, and 48 h sequentially. 3MA is an autophagy inhibitor: 3-Methyladenine. (i) Cytotoxicity of different formulations in TC-1 cells by CLSM. Living cells were stained with Calcein (green) and dead cells were stained with PI (red). Scale bar=20 μm. (j) Schematic diagram of bridging ROS with oncolytic Ads replication. *p<0.05, **p<0.01, ***p<0.001, ****p<0.0001 versus control. G1: PBS, G2: Ads, G3: OMVs, G4: OMVs@P_2O, G5: OMVs-Ads, G6: OMVs@P_2O-Ads.

Question 3: Figure 2C: SDS Page does not show specificity of the 70 KDa P_2O and the loading of the lanes is different.

Response: We appreciate the reviewer's comments. Pyranose oxidase (P_2O) is an enzyme with a molecular mass of 70KDa. As shown in Figure 2C, compared with OMVs group, there are clearer 70KDa lanes observed in OMVs@P_2O, OMVs@P_2O-Ads and *E. coli*@P_2O groups. However, due to the limitations of SDS Page method, the expression of the P_2O can't be specifically confirmed. So, in our study, a chemical chromogenic reaction approach was conducted to further verify the function of the P_2O, thereby indirectly proving the existence of P_2O (Figure S1- S4).

In our study, to ensure the rigor of SDS experiments, the total protein content of the samples from all groups was measured by BCA protein quantification kit and the loading quantity of all groups were kept in a consistent value. Here, we had re-modified experiments and obtained experimental results in the revised manuscript as follow (Figure 2C):

Figure S1. Qualitative analysis of P_2O expression in OMVs, *E. coli*@P_2O and OMVs@P_2O.

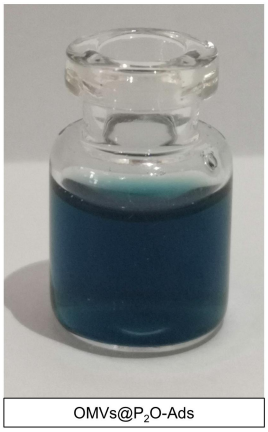

Figure S2. Qualitative analysis of P_2O expression in OMVs@P_2O-Ads.

Figure S3. Qualitative analysis of different concentration P_2O expression in OMVs@P_2O.

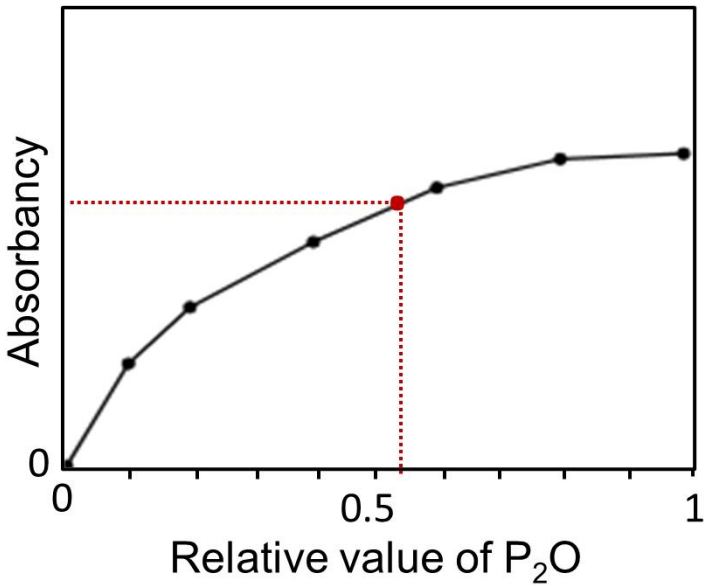

Figure S4. The function curve illustrated the relationship between the absorbance and P_2O with different concentrations. The red point revealed the relative P_2O concentration within the microbial nanocomposite.

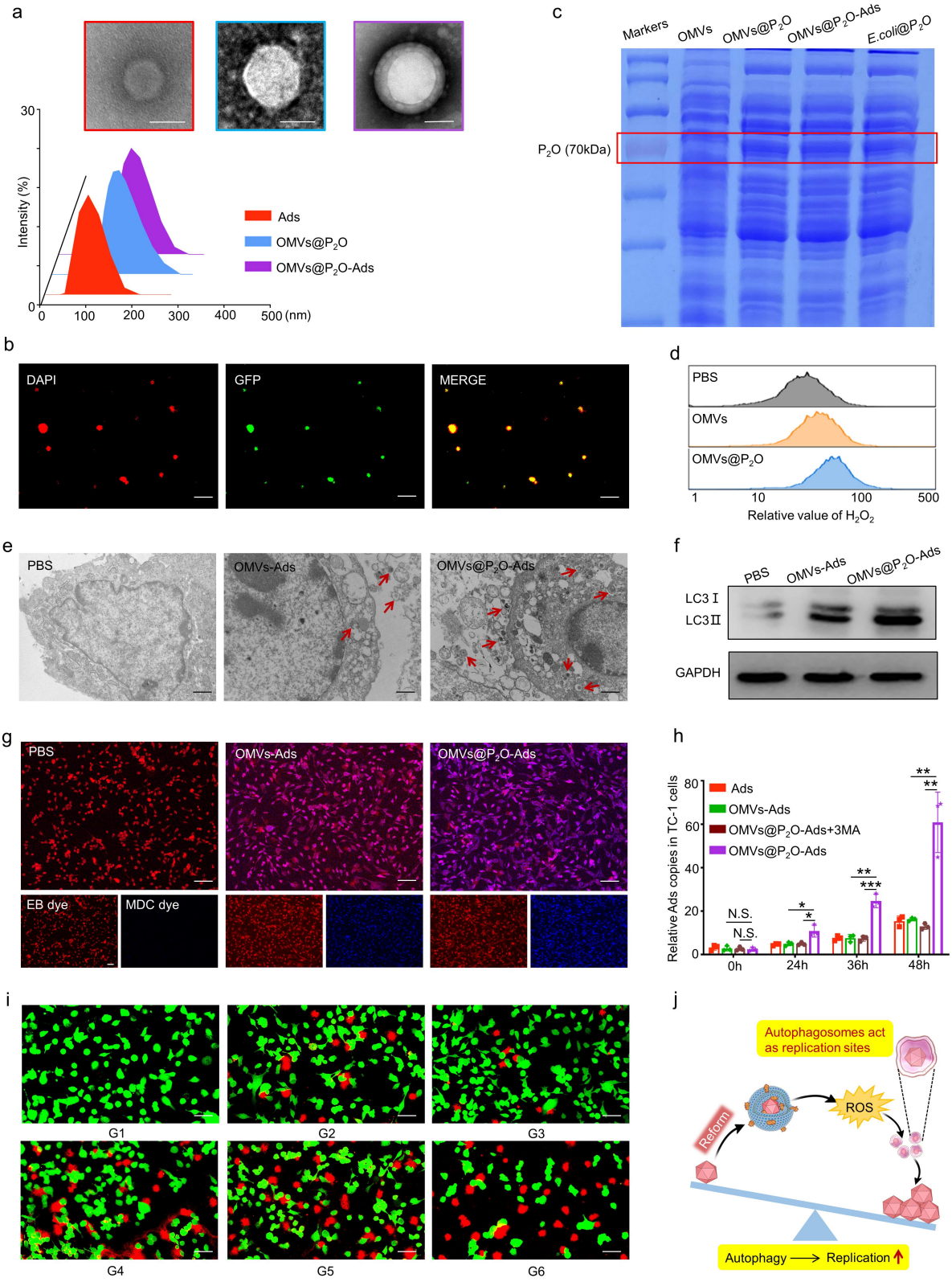

Figure 2. Preparation and *in vitro* evaluation of the microbial nanocomposite. (a) TEM and size distribution images of Ads, OMVs@P_2O, and OMVs@P_2O-Ads. Scale bar=100 nm. (b) CLSM images of the microbial nanocomposite. Ads were stained with DAPI dye (red) and OMVs carried a GFP marker (green). Scale bar=1 μm. (c) The expression of P_2O was investigated by the SDS-PAGE method. (d) The ROS level assessment in TC-1

cells by flow cytometry. (e) TEM images of autophagosomes. Scale bar=200 nm. (f) The expression of autophagy-related protein LC3-I and LC3-II by western bolt analyses. (g) CLSM images of autophagosomes. Cells were stained with EB dye (red) and autophagosomes were stained with MDC dye (blue). Scale bar=50 μm. (h) The Ads replication in TC-1 cells was quantified using real-time PCR at 0, 24, 36, and 48 h sequentially. 3MA is an autophagy inhibitor: 3-Methyladenine. (i) Cytotoxicity of different formulations in TC-1 cells by CLSM. Living cells were stained with Calcein (green) and dead cells were stained with PI (red). Scale bar=20 μm. (j) Schematic diagram of bridging ROS with oncolytic Ads replication. *p<0.05, **p<0.01, ***p<0.001, ****p<0.0001 versus control. G1: PBS, G2: Ads, G3: OMVs, G4: OMVs@P_2O, G5: OMVs-Ads, G6: OMVs@P_2O-Ads.

Question 4: Figure 2D: Experimental details need to be provided.

Response: We appreciate the reviewer's comments. In the revised manuscript, this part was modified in section 4.6 as (page 23): "TC-1 mouse lung cancer cells were cultured in DMEM medium supplemented with 10% FBS, penicillin (100 U mL^{-1}), and streptomycin (100 μg mL^{-1}). The cells were maintained in a humidified atmosphere of 5% CO_2 at 37 °C. TC-1 cells were cultured and divided into three groups (PBS, OMVs, and OMVs@P_2O). After the cells occupied 80% of the bottom, the medium was discarded, and the cells were rinsed twice using PBS. DCFH-DA fluorescent dye (10 μM, 1mL) (Meilun ROS Assay Kit MA0219) was added to the blank medium working solution. The cells were then incubated at 37 ℃ for 1 h in the dark. Next, the medium was discarded, and the cells were rinsed with PBS again. Then, PBS, OMVs, and OMVs@P_2O blank medium dispersion were added sequentially and further incubated at 37℃ for 3 h in the dark. After rinsing with PBS, the cells were collected, and their ROS concentration was determined by flow cytometry. The extracellular DCFH-DA has no fluorescence even after possessing the capability of crossing the cell membrane freely. After entering the cell, it can be hydrolyzed by intracellular esterase to translate into DCFH, which cannot pass through the cell membrane. In the presence of ROS, DCFH is oxidized to produce the fluorescent substance DCF (the excitation wavelength: 502nm; the emission wavelength: 530nm)."

Question 5: Figure 2E: Needs to be bigger and explanation of what the arrows are showing.

Response: We appreciate the reviewer's comments. In order to make this article more intuitive for reviewers and readers, we tried to put the equal-scaling amplifying pictures in the supplement (Figure S7).

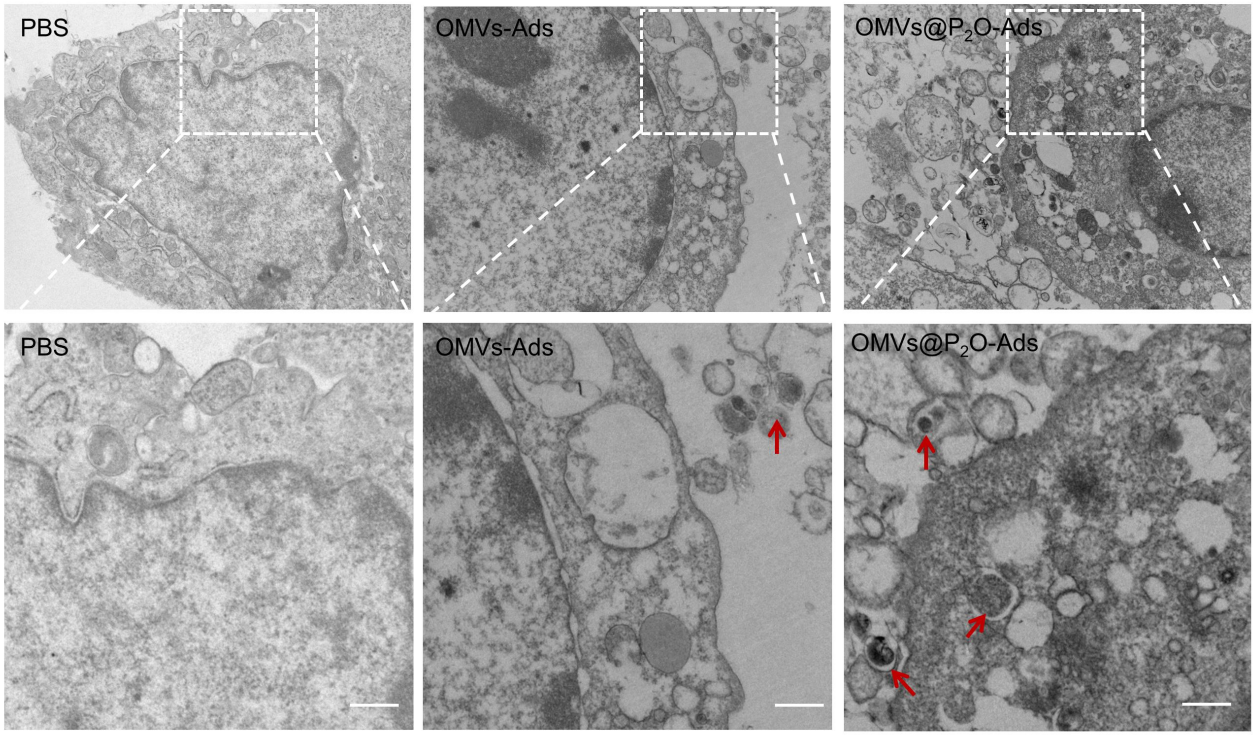

Figure S7. The equal-scaling amplifying TEM images of autophagosomes, scale bar=500 nm.

Question 6: Figure 2i: needs experimental detail.

Response: We appreciate the reviewer's comments. In the revised manuscript, this part (replaced by Figure 2h) was modified in section 4.9 as (page 25): "TC-1 cells were cultured in cell culture plates. After the cells occupied 80% of the bottom, the medium was sucked out with a 2 mL syringe and washed with PBS twice. Ads, OMVs-Ads, OMVs@P_2O-Ads + 3MA, and OMVs@P_2O-Ads were added to each group and incubated for 3h at 37℃. 3MA is an autophagy inhibitor: 3-Methyladenine. The drug solution was dumped out, the cells were rinsed twice with PBS, and the same volume of blank medium was added. Plates were put in 37 ℃ and moved after 0, 24 h, 36 h, and 48 h, and were placed at -80℃ for three times to ensure complete cell breakdown. The freeze-thaw solution was collected and centrifuged at 2800 rpm/min at 4℃ for 0.5 h. Precipitation was discarded, and 1% triton was added to the supernatant. Then, the liquid was pre-denatured at 98℃, and the precipitate of deformed protein was removed by centrifugation at 12000 rpm/min for 10 min. Finally, the RT-qPCR technique collected and processed the supernatant for quantitative Ads detection. All the reagents of the RT-qPCR technique were purchased from Vazyme."

Question 7: Figure 2J should be quantified with statistical analysis.

Response: We appreciate the reviewer's comments. The statistical analysis result had been shown in Figure S10 in the revised manuscript:

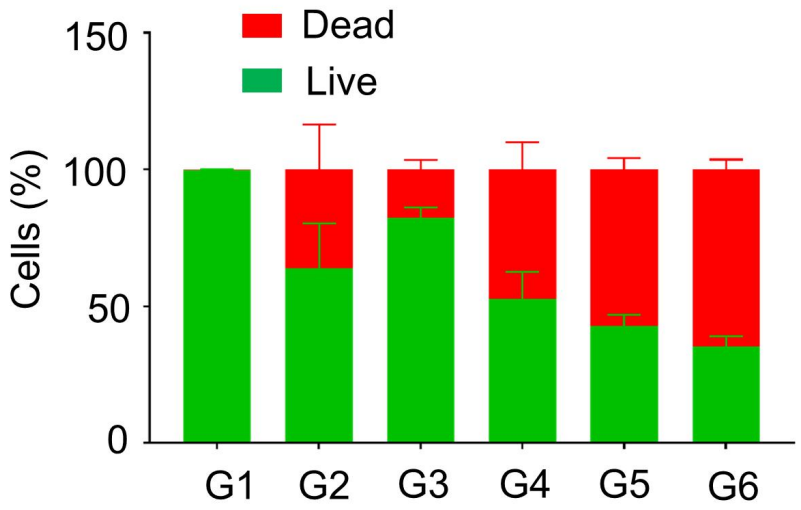

Figure S10. The statistical analysis result of live/dead cellular staining (n=3). (G1: PBS, G2: Ads, G3: OMVs, G4: OMVs@P_2O, G5: OMVs-Ads, G6: OMVs@P_2O-Ads).

Question 8: Figure 3A: Need to show multiple mice. Need experimental detail.

Response: We agree with the reviewer's comments. The more mice are shown below. In the revised manuscript, this part was modified in section 4.11 as (page 25):

"Female C57 mice were obtained from the Laboratory Animal Center of Shenyang Pharmaceutical University. The animal experiments were performed by following the Guidelines for the Care and Use of Laboratory Animals approved by the Institutional Animal Ethical Care Committee (IAEC) of Shenyang Pharmaceutical University.

OMVs@P_2O-Ads was prepared as described in section 4.4, and an excess of DIR staining solution was subsequently added to label OMVs. The free DIR dye was removed by centrifugation at 3,000 × g for 3 min using an ultrafiltration tube with a 100 kDA pore size. DIR-labeled OMVs@P_2O-Ads were injected intratumorally using Ads content of 7×10^5 PFU as a standard. DIR fluorescent imaging of the microbial nanocomposite *in vivo* in TC-1-hCD46 xenograft tumor-bearing mice by IVIS."

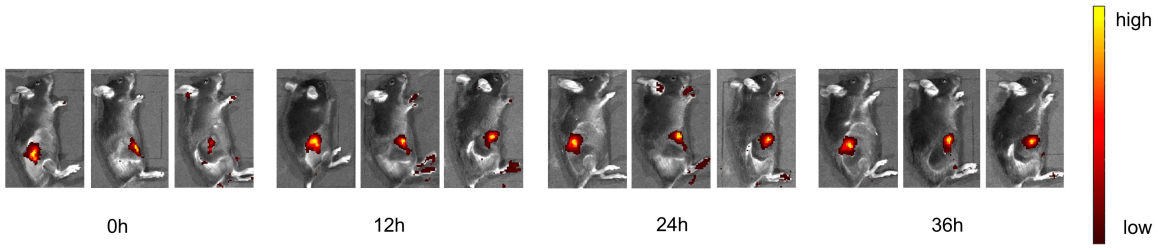

Figure S11. *In vivo* DIR fluorescent imaging of the nanocomposite in TC-1-hCD46 xenograft tumor-bearing mice by IVIS (n=3).

Question 9: Figure 3C needs error bars for statistical relevance and the legend needs experimental detail.

Response: We appreciate the reviewer's comments. Error bars are represented by dotted lines in Figure 3C. To make the figure information more intuitive for reviewers and readers, we replace the dotted lines with the traditional error bars. Furthermore, the experimental detail was attached as follow (page 12):

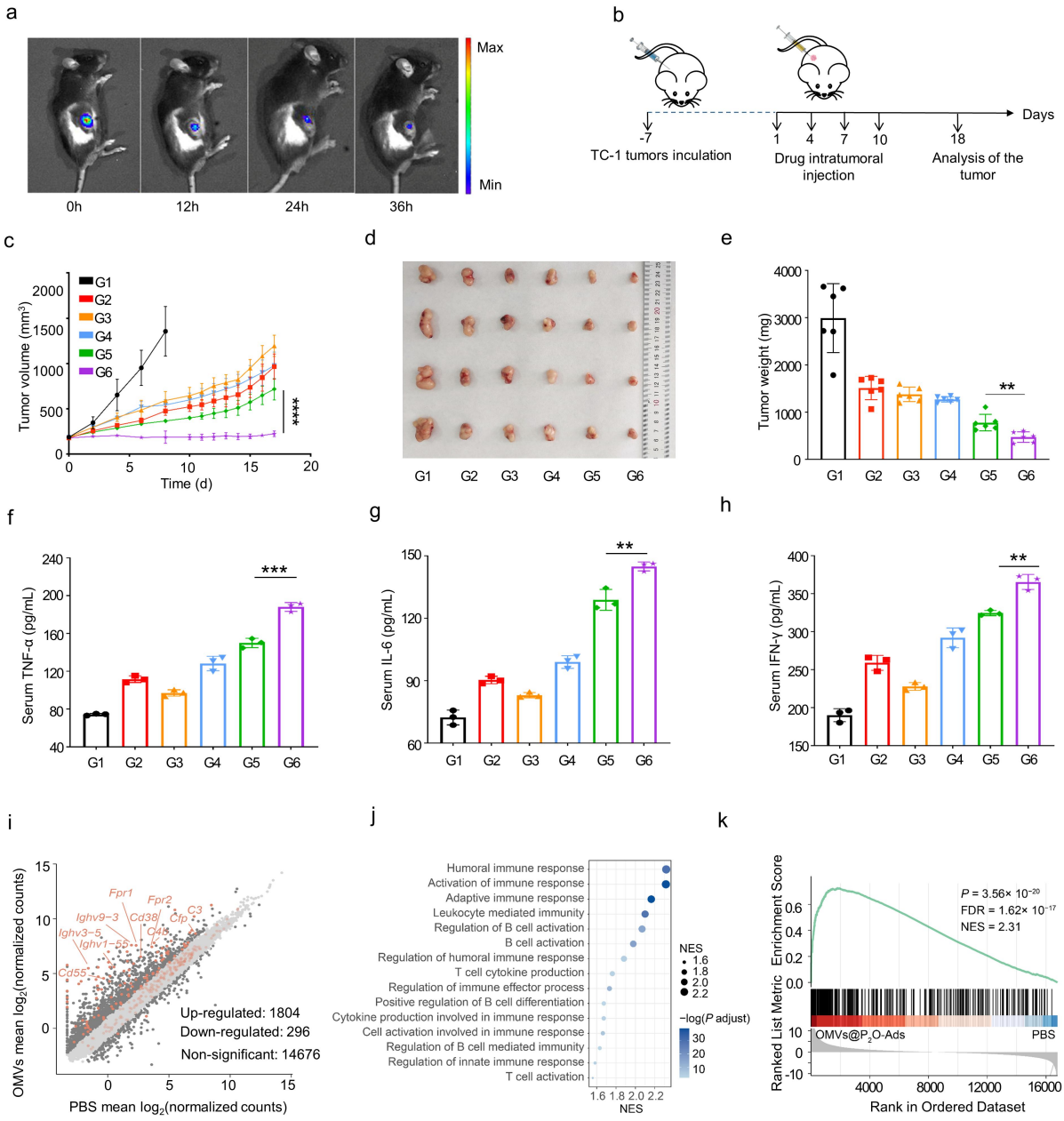

Figure 3. *In vivo* oncolytic efficacy of the microbial nanocomposite. (a) *In vivo* DIR fluorescent imaging of the microbial nanocomposite in TC-1-hCD46 xenograft tumor-bearing mice by IVIS. (b) Schematic illustration of the antitumor activity and immunology assessment experiments of the microbial nanocomposite using TC-1-hCD46 xenograft tumor-bearing C57 female mice model. TC-1 cells (10^6) were subcutaneously injected into the waist of female C57 mice, and the tumor-bearing mice were divided into six groups (n=6). When the tumor reached 100-150 mm^3, the mice were injected intratumorally with PBS, Ads (7×10^5 PFU), OMVs, OMVs@P_2O, OMVs-Ads (7×10^5 PFU), and OMVs@P_2O-Ads (7×10^5 PFU). The drug was given every three days for four consecutive times, the tumor volume was measured with a vernier caliper, and mice were weighed daily. (c) Tumor volume growth profiles of C57 mice bearing TC-1 xenografts. (d) Images of representative tumors of different treated groups on the 18th day (n=6). (e) Statistical graph of tumor weight of different treated groups on the 18th day (n=6). (f-h) Images of concentration of main cytokines in serum. (i) The differential gene expression between the samples treated with OMVs@P_2O-Ads and PBS, using the absolute value of logFC greater than 1 as

the threshold. (j) GSEA enriched pathways of the up-regulated genes in the samples treated with OMVs@P_2O-Ads, showing immune-related terms. (k) Gene set enrichment analysis (GSEA) of the term "Activation of immune response", and the genes included in this pathway are highlighted in (i) with light yellow brown. *p<0.05, **p<0.01, ***p<0.001, ****p<0.0001 versus control. (G1: PBS, G2: Ads, G3: OMVs, G4: OMVs@P_2O, G5: OMVs-Ads, G6: OMVs@P_2O-Ads).

Question 10: Figure 3D: n=6 in the Legend is not reflected in the Figure where n=4.

Response: We are sorry that we made an error in the process of typesetting, which resulted in Figure 3D not being fully presented. We have attached the original documents here and modified in the revised manuscript.

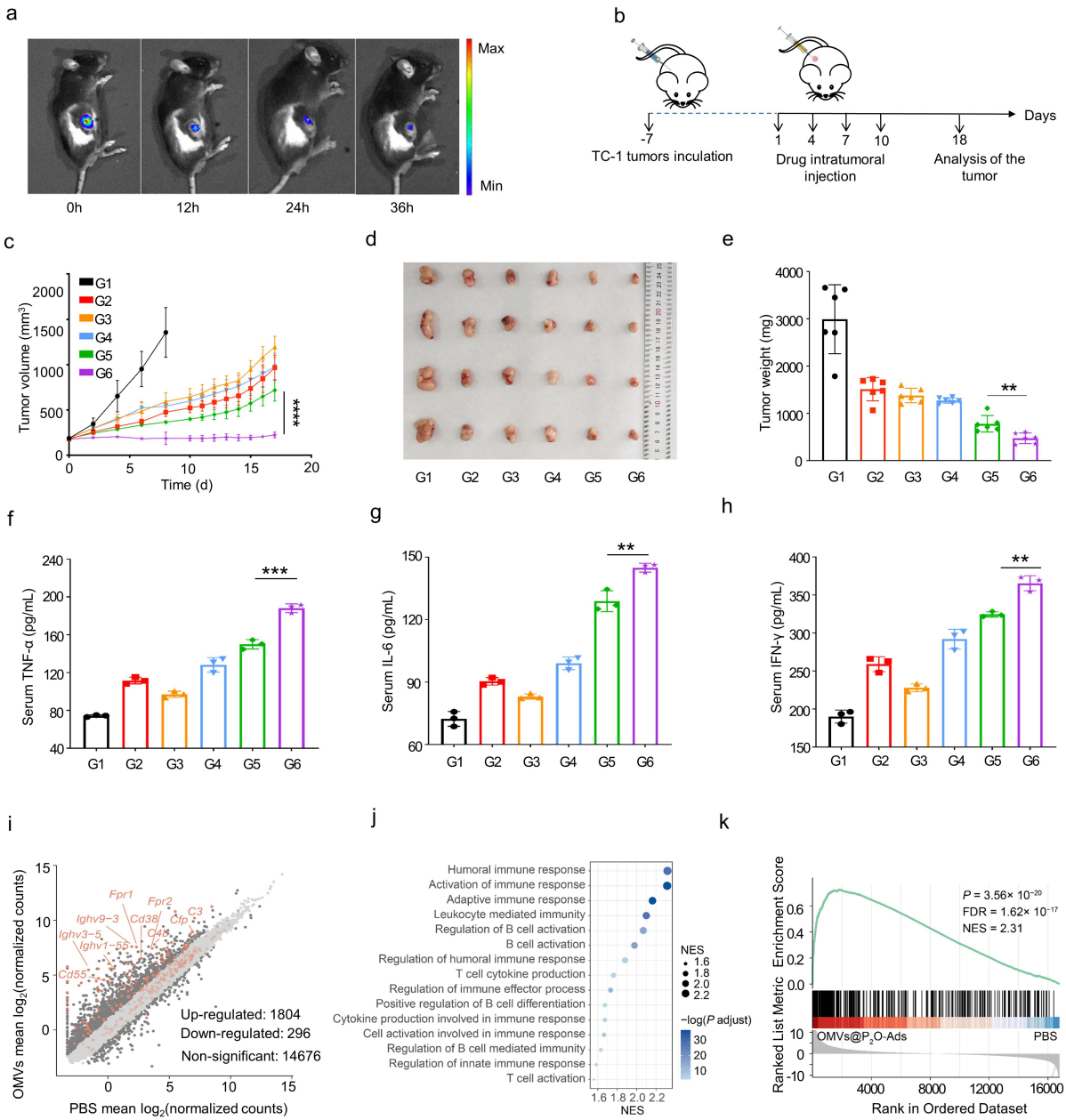

153

Figure 3. *In vivo* oncolytic efficacy of the microbial nanocomposite. (a) *In vivo* DIR fluorescent imaging of the microbial nanocomposite in TC-1-hCD46 xenograft tumor-bearing mice by IVIS. (b) Schematic illustration of the antitumor activity and immunology assessment experiments of the microbial nanocomposite using TC-1-hCD46 xenograft tumor-bearing C57 female mice model. TC-1 cells (10^6) were subcutaneously injected into the waist of female C57 mice, and the tumor-bearing mice were divided into six groups (n=6). When the tumor reached 100-150 mm^3, the mice were injected intratumorally with PBS, Ads (7×10^5 PFU), OMVs, OMVs@P_2O, OMVs-Ads (7×10^5 PFU), and OMVs@P_2O-Ads (7×10^5 PFU). The drug was given every three days for four consecutive times, the tumor volume was measured with a vernier caliper, and mice were weighed daily. (c) Tumor volume growth profiles of C57 mice bearing TC-1 xenografts. (d) Images of representative tumors of different treated groups on the 18^{th} day (n=6). (e) Statistical graph of tumor weight of different treated groups on the 18^{th} day (n=6). (f-h) Images of concentration of main cytokines in serum. (i) The differential gene expression between the samples treated with OMVs@P_2O-Ads and PBS, using the absolute value of logFC greater than 1 as the threshold. (j) GSEA enriched pathways of the up-regulated genes in the samples treated with OMVs@P_2O-Ads, showing immune-related terms. (k) Gene set enrichment analysis (GSEA) of the term "Activation of immune response", and the genes included in this pathway are highlighted in (i) with light yellow brown. *p<0.05, **p<0.01, ***p<0.001, ****p<0.0001 versus control. (G1: PBS, G2: Ads, G3: OMVs, G4: OMVs@P_2O, G5: OMVs-Ads, G6: OMVs@P_2O-Ads).

Reviewer #2: Ban and colleagues provide a report detailing the construction of biomineral engineered OMVs-encapsulating oncolytic adenovirus that exhibit enhanced antitumor efficacy. It was mainly dependent on overactivated autophagy. Some areas where improvements can be made include:

Major concerns:

Question 1: Fig 2f/4f: Grey-scale analysis should be performed, so that the LC3-II/LC3-I ratio can be calculated and statistically analyzed.

Response: We appreciate the reviewer's comments. The grey-scale analysis in Figure2f/4f had been conducted, and LC3-II/LC3-I ratio had been calculated and statistically analyzed in the revised manuscript.

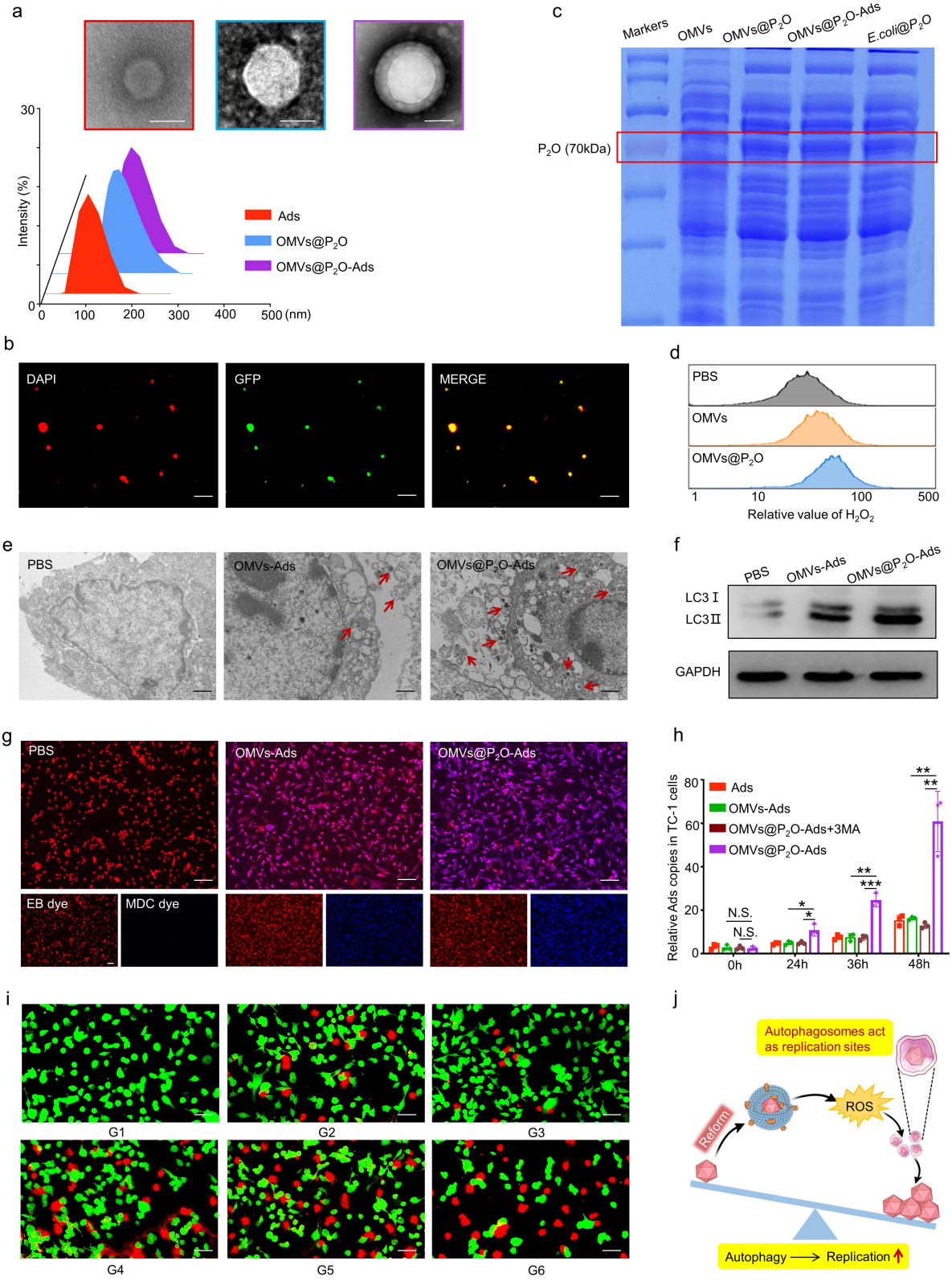

181 **Figure 2. Preparation and *in vitro* evaluation of the microbial nanocomposite.** (a) TEM and size distribution
182 images of Ads, OMVs@P_2O, and OMVs@P_2O-Ads. Scale bar=100 nm. (b) CLSM images of the microbial
183 nanocomposite. Ads were stained with DAPI dye (red) and OMVs carried a GFP marker (green). Scale bar=1 μm.
184 (c) The expression of P_2O was investigated by the SDS-PAGE method. (d) The ROS level assessment in TC-1

cells by flow cytometry. (e) TEM images of autophagosomes. Scale bar=200 nm. (f) The expression of autophagy-related protein LC3-I and LC3-II by western bolt analyses. (g) CLSM images of autophagosomes. Cells were stained with EB dye (red) and autophagosomes were stained with MDC dye (blue). Scale bar=50 μm. (h) The Ads replication in TC-1 cells was quantified using real-time PCR at 0, 24, 36, and 48 h sequentially. 3MA is an autophagy inhibitor: 3-Methyladenine. (i) Cytotoxicity of different formulations in TC-1 cells by CLSM. Living cells were stained with Calcein (green) and dead cells were stained with PI (red). Scale bar=20 μm. (j) Schematic diagram of bridging ROS with oncolytic Ads replication. *p<0.05, **p<0.01, ***p<0.001, ****p<0.0001 versus control. G1: PBS, G2: Ads, G3: OMVs, G4: OMVs@P_2O, G5: OMVs-Ads, G6: OMVs@P_2O-Ads.

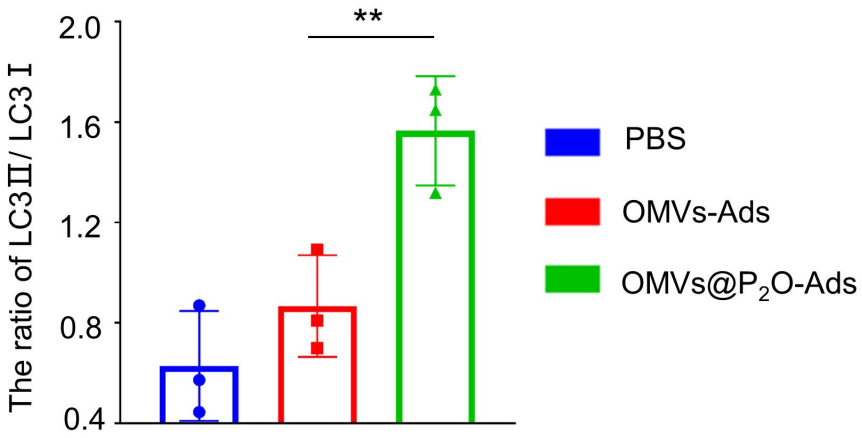

Figure S8. The LC3-II/LC3-I ratio *in vitro* (n=3).

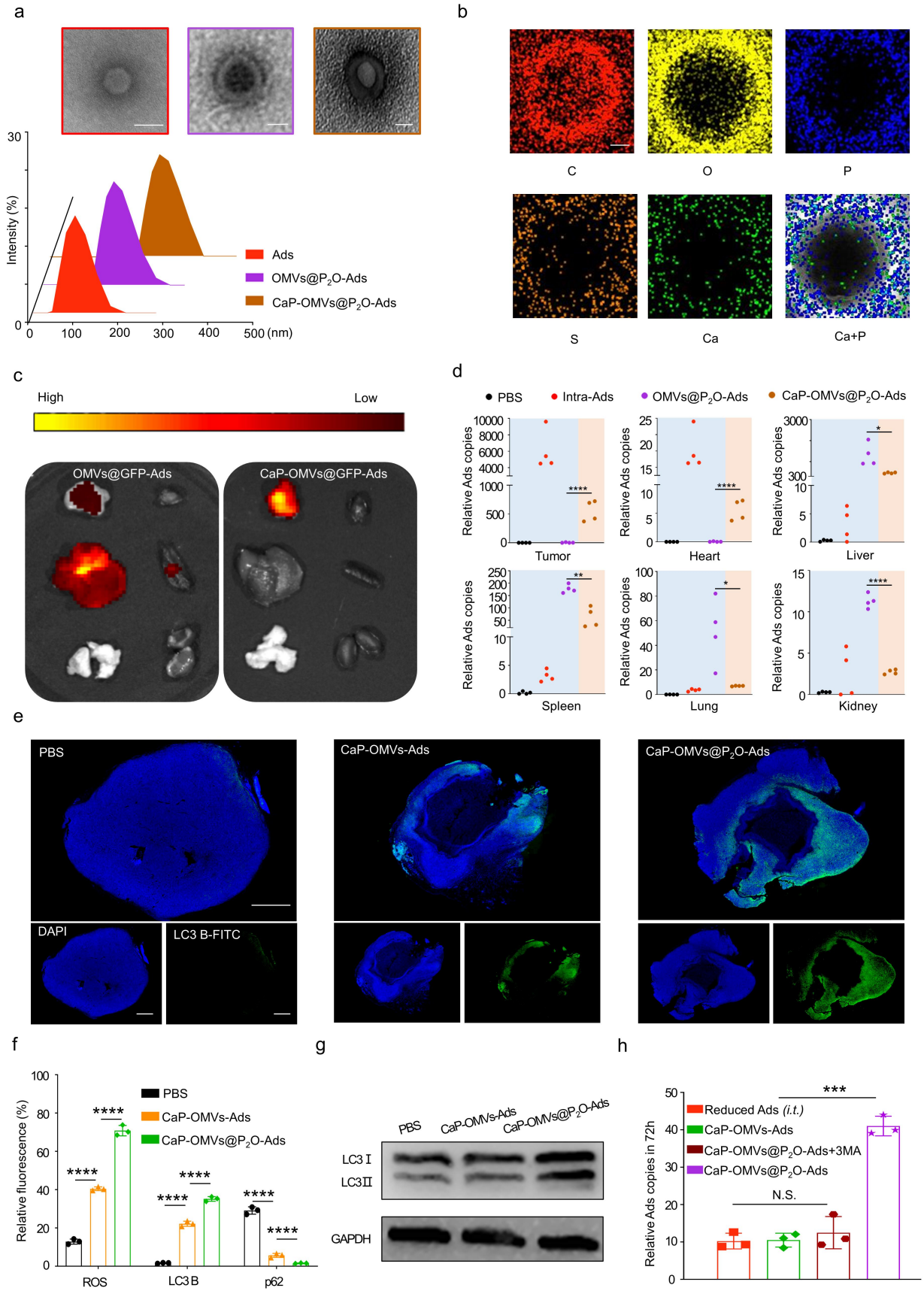

Figure 4. Preparation and *in vivo* evaluation of the biomineralized microbial nanocomposite. (a) TEM and size distribution images of Ads, OMVs@P_2O-Ads, and CaP-OMVs@P_2O-Ads. Scale bar=100 nm. (b) Energy

spectrum analysis image of the biomineralized composite microbe. Scale bar=50 nm. (c) *In vivo* fluorescence imaging of the multiple organs and tumors collected from the mice at 24 h post *i.v.* injection. From left to right: tumor, heart, liver, spleen, lung, and kidney. (d) Quantitation of the biodistribution of relative Ads contents in multiple organs and tumors after 24 h of different treatments by RT-qPCR (n=4). (e) Immunofluorescence images of LC3 autophagic proteins in tumor tissues. Blue represents DAPI-stained tumor cells and the green represents FITC-stained LC3 autophagic protein. Scale bar=2 mm. (f) Quantitative analysis of fluorescence intensity. (g) The expression of autophagy-related protein LC3-I and LC3-II examined by western blot. (h) Quantitation of relative Ads content in the tumor after 72 h of different treatments by RT-qPCR technique (n=3). *p<0.05, **p<0.01, ***p<0.001, ****p<0.0001 versus control. *p<0.05, **p<0.01, ***p<0.001, ****p<0.0001 versus control.

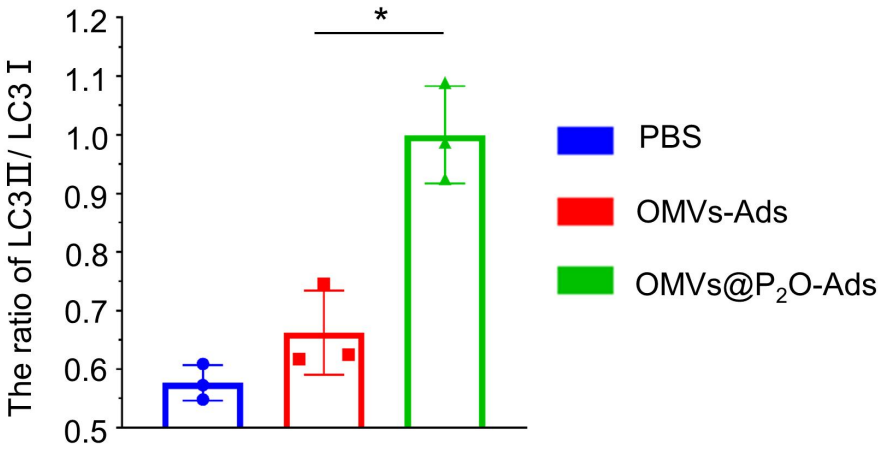

Figure18. The LC3-II/LC3-I ratio *in vivo* (n=3).

Question 2: Fig 3f-k: Since immune response is a dynamic process, from innate immunity to T cell mediated immunity and B cell mediated immunity, so it is critical to specify at what time point did they collect the tumor samples and explain why they choose this time point.

Response: We appreciate the reviewer's comments. As for Figure 3f-h, the collection of samples for immunological studies was performed on the basis of pharmacodynamic studies. Concretely, as shown in Figure 3b, the mice were injected different drugs at 1, 4, 7 and 10 days and dissected at the 18th day. And as for Figure 3i-k, the collection of samples for transcriptomic analysis of the tumor xenografts 7 days after the first administration. Compared with the expression of cytokines and the visualization of tumor volume, relevant transcriptomic change of the tumor xenografts is earlier, this is why we accomplished the transcriptomic analysis of the tumor xenografts after two consecutive administration (on the seventh day). However, as described by the reviewer's **Question2 - Question5**, we have been aware that the collection of samples for transcriptomic analysis of the tumor xenografts at 7 day is too early. In the revised manuscript, we redesigned the

experiment and collected samples for transcriptomic analysis on the twelfth day after the fourth administration. And the relevant results are shown in Figure 3i-k.

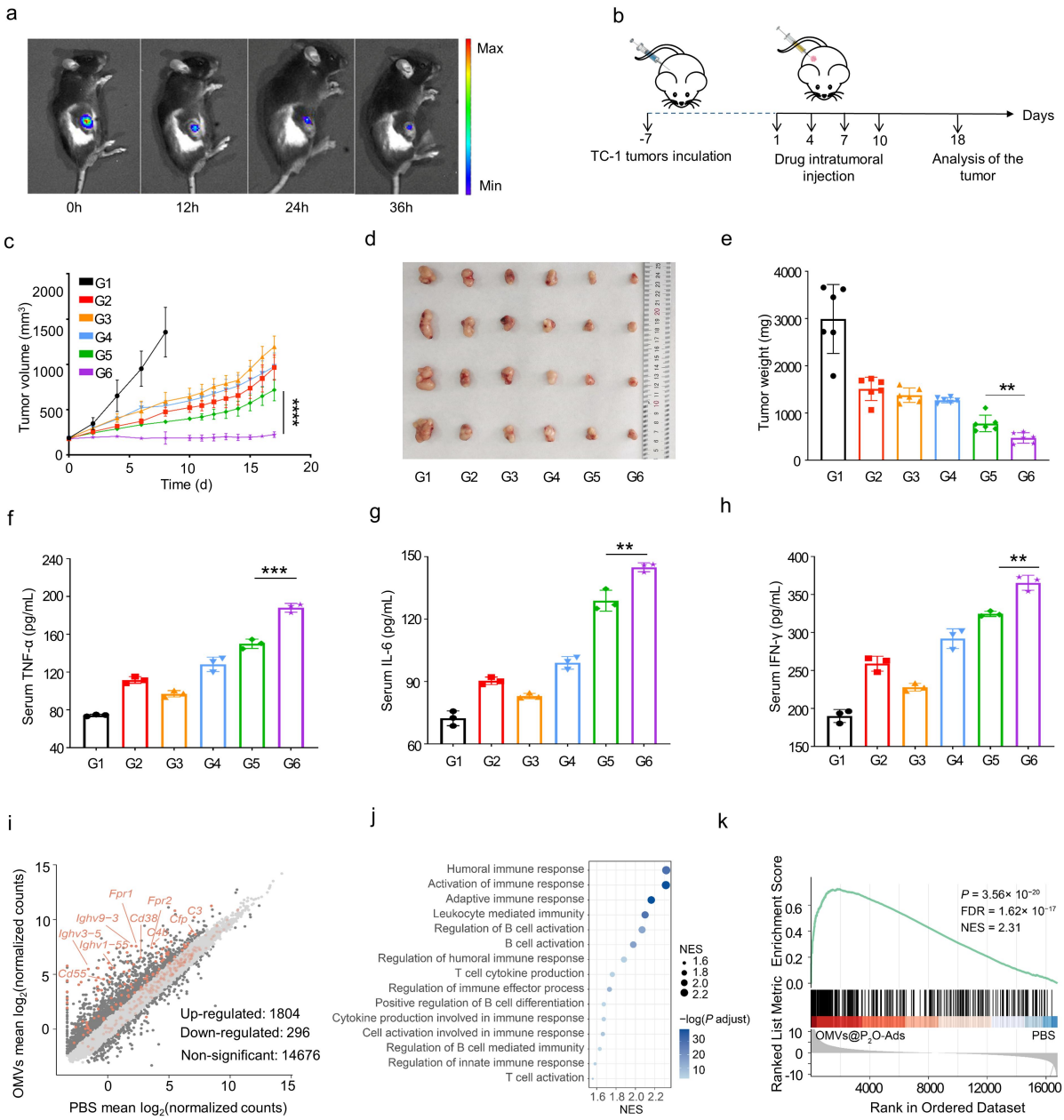

Figure 3. *In vivo* oncolytic efficacy of the microbial nanocomposite. (a) *In vivo* DIR fluorescent imaging of the microbial nanocomposite in TC-1-hCD46 xenograft tumor-bearing mice by IVIS. (b) Schematic illustration of the antitumor activity and immunology assessment experiments of the microbial nanocomposite using TC-1-hCD46 xenograft tumor-bearing C57 female mice model. TC-1 cells (10^6) were subcutaneously injected into the waist of female C57 mice, and the tumor-bearing mice were divided into six groups (n=6). When the tumor reached 100-150 mm^3, the mice were injected intratumorally with PBS, Ads (7×10^5 PFU), OMVs, OMVs@P_2O, OMVs-Ads (7×10^5 PFU), and OMVs@P_2O-Ads (7×10^5 PFU). The drug was given every three days for four consecutive times, the tumor volume was measured with a vernier caliper, and mice were weighed daily. (c) Tumor volume growth profiles of C57 mice bearing TC-1 xenografts. (d) Images of representative tumors of

different treated groups on the 18th day (n=6). (e) Statistical graph of tumor weight of different treated groups on the 18th day (n=6). (f-h) Images of concentration of main cytokines in serum. (i) The differential gene expression between the samples treated with OMVs@P_2O-Ads and PBS, using the absolute value of logFC greater than 1 as the threshold. (j) GSEA enriched pathways of the up-regulated genes in the samples treated with OMVs@P_2O-Ads, showing immune-related terms. (k) Gene set enrichment analysis (GSEA) of the term "Activation of immune response", and the genes included in this pathway are highlighted in (i) with light yellow brown. *p<0.05, **p<0.01, ***p<0.001, ****p<0.0001 versus control. (G1: PBS, G2: Ads, G3: OMVs, G4: OMVs@P_2O, G5: OMVs-Ads, G6: OMVs@P_2O-Ads).

Question 3: Fig 3j: Grouping information and FDR should also be presented in the GSEA figure. Unexpectedly, the pathway "Activation of immune response" is not included in Fig S11. The authors should explain the representativeness of choosing this pathway.

Response: Thanks for this kind suggestion, and grouping information and FDR had been added in the GSEA figure (Fig. 3k) in the revised manuscript. The original Fig S11 was ranked by the P value and also limited terms were shown, thus the pathway "Activation of immune response" was not included. In the revised manuscript, we improved the time-point to acquire the samples and re-performed the transcriptomic analysis and showed that the pathway "Activation of immune response" is significantly up-regulated 12 days after OMVs@P_2O-Ads injection (Fig 3j).

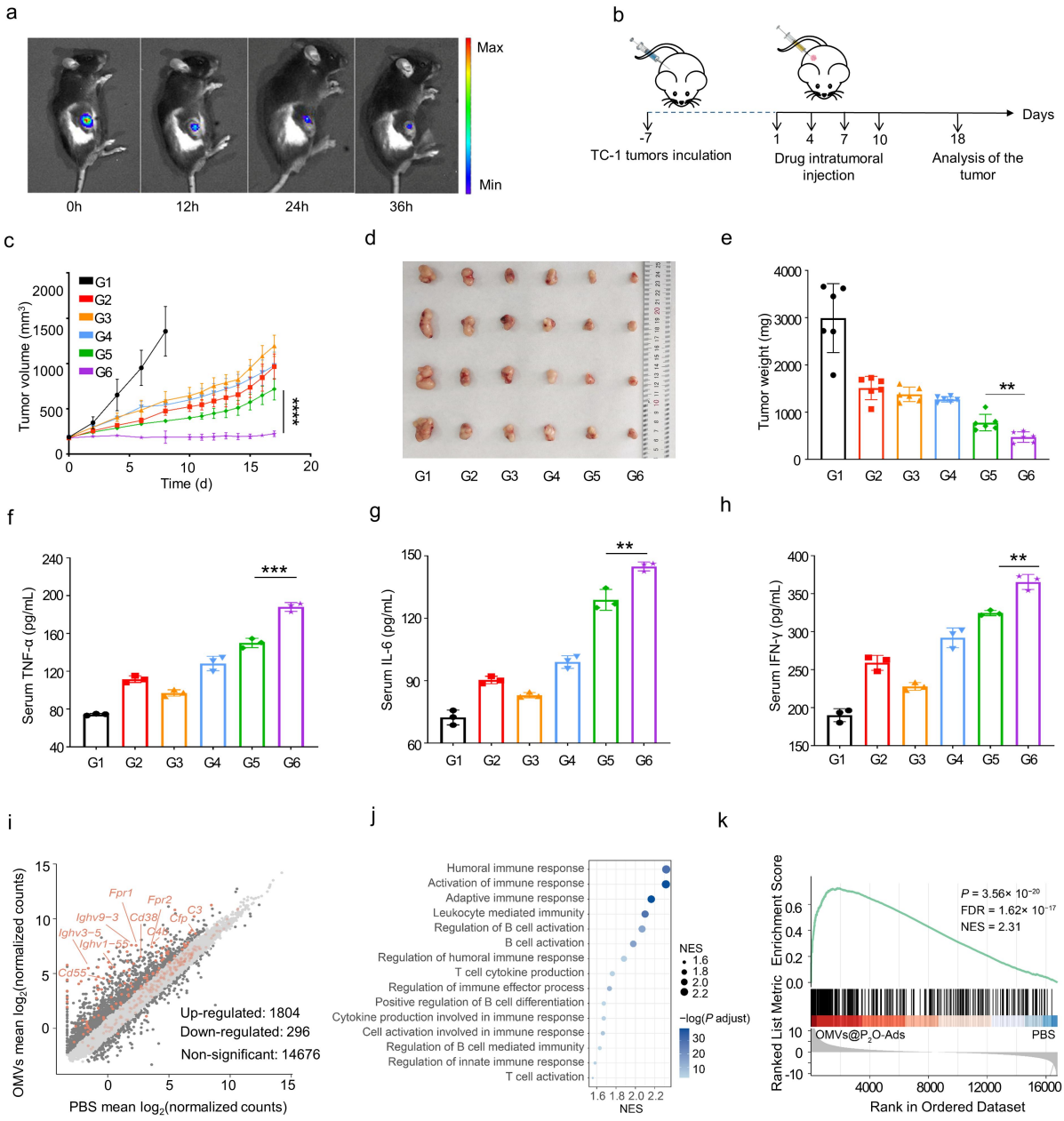

Figure 3. *In vivo* oncolytic efficacy of the microbial nanocomposite. (a) *In vivo* DIR fluorescent imaging of the microbial nanocomposite in TC-1-hCD46 xenograft tumor-bearing mice by IVIS. (b) Schematic illustration of the antitumor activity and immunology assessment experiments of the microbial nanocomposite using TC-1-hCD46 xenograft tumor-bearing C57 female mice model. TC-1 cells (10^6) were subcutaneously injected into the waist of female C57 mice, and the tumor-bearing mice were divided into six groups (n=6). When the tumor reached 100-150 mm^3, the mice were injected intratumorally with PBS, Ads (7×10^5 PFU), OMVs, OMVs@P_2O, OMVs-Ads (7×10^5 PFU), and OMVs@P_2O-Ads (7×10^5 PFU). The drug was given every three days for four consecutive times, the tumor volume was measured with a vernier caliper, and mice were weighed daily. (c) Tumor volume growth profiles of C57 mice bearing TC-1 xenografts. (d) Images of representative tumors of different treated groups on the 18th day (n=6). (e) Statistical graph of tumor weight of different treated groups on the 18th day (n=6). (f-h) Images of concentration of main cytokines in serum. (i) The differential gene expression between the samples treated with OMVs@P_2O-Ads and PBS, using the absolute value of logFC greater than 1 as

the threshold. (j) GSEA enriched pathways of the up-regulated genes in the samples treated with OMVs@P_2O-Ads, showing immune-related terms. (k) Gene set enrichment analysis (GSEA) of the term "Activation of immune response", and the genes included in this pathway are highlighted in (i) with light yellow brown. *p<0.05, **p<0.01, ***p<0.001, ****p<0.0001 versus control. (G1: PBS, G2: Ads, G3: OMVs, G4: OMVs@P_2O, G5: OMVs-Ads, G6: OMVs@P_2O-Ads).

Question 4: Fig 3k: The individual variations among the three tested samples in OMVs@P_2O-Ads group are much too large. This kind of variation severely compromise the accuracy of the data.

Response: Thanks for this kind suggestion. In our original experiment, the samples were acquired earlier (on the seventh day), so that the immune response in some mice had not been invoked. According to the reviewer's suggestion and the result of our phenotypic experiment, samples were acquired uniformly 11 days after OMVs@P_2O-Ads injection. And the experimental results obtained according to the modified experimental plan are shown in the Figure 3i-k in the revised manuscript.

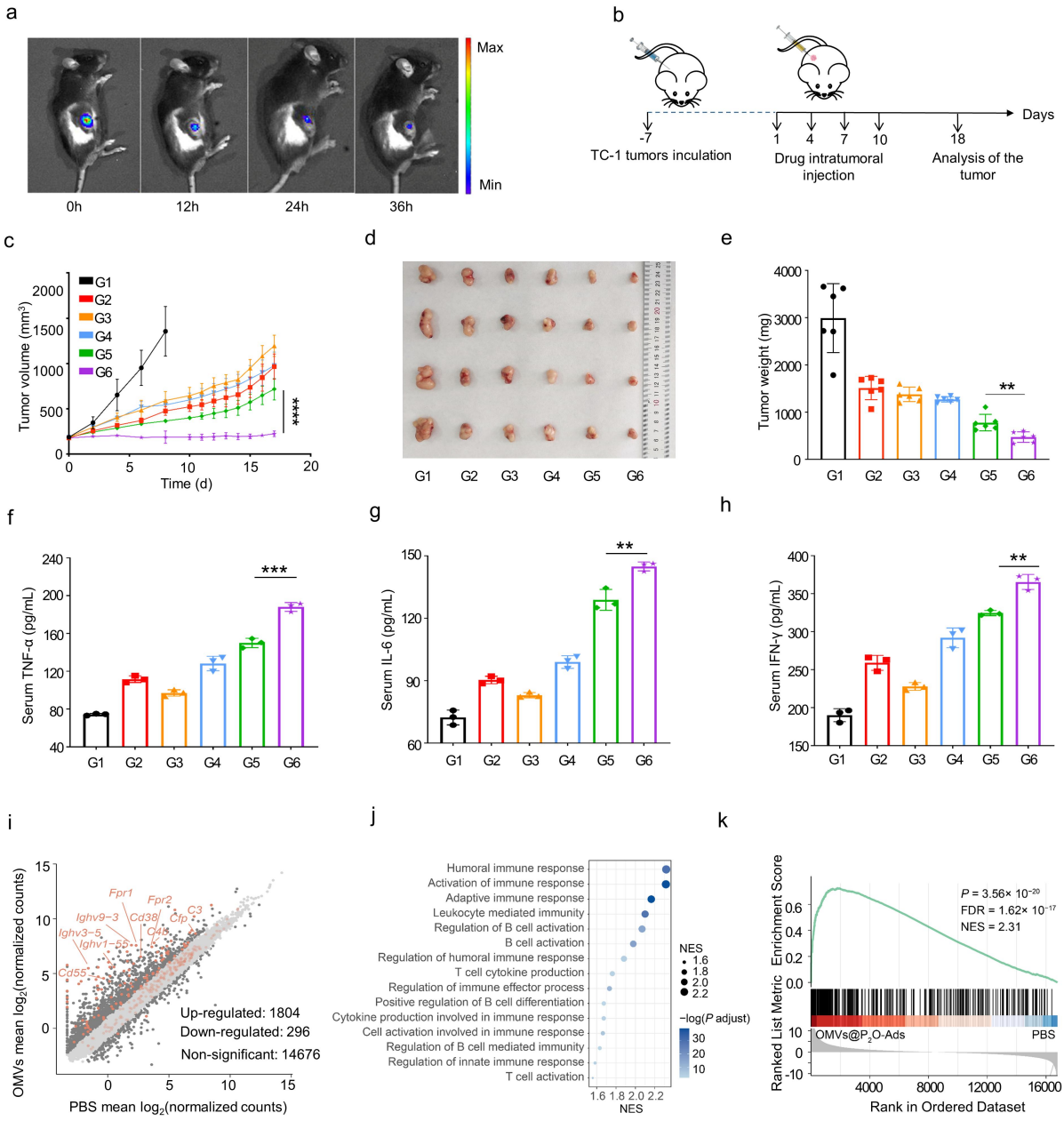

Figure 3. *In vivo* oncolytic efficacy of the microbial nanocomposite. (a) *In vivo* DIR fluorescent imaging of the microbial nanocomposite in TC-1-hCD46 xenograft tumor-bearing mice by IVIS. (b) Schematic illustration of the antitumor activity and immunology assessment experiments of the microbial nanocomposite using TC-1-hCD46 xenograft tumor-bearing C57 female mice model. TC-1 cells (10^6) were subcutaneously injected into the waist of female C57 mice, and the tumor-bearing mice were divided into six groups (n=6). When the tumor reached 100-150 mm^3, the mice were injected intratumorally with PBS, Ads (7×10^5 PFU), OMVs, OMVs@P_2O, OMVs-Ads (7×10^5 PFU), and OMVs@P_2O-Ads (7×10^5 PFU). The drug was given every three days for four consecutive times, the tumor volume was measured with a vernier caliper, and mice were weighed daily. (c) Tumor volume growth profiles of C57 mice bearing TC-1 xenografts. (d) Images of representative tumors of different treated groups on the 18th day (n=6). (e) Statistical graph of tumor weight of different treated groups on the 18th day (n=6). (f-h) Images of concentration of main cytokines in serum. (i) The differential gene expression between the samples treated with OMVs@P_2O-Ads and PBS, using the absolute value of logFC greater than 1 as

the threshold. (j) GSEA enriched pathways of the up-regulated genes in the samples treated with OMVs@P_2O-Ads, showing immune-related terms. (k) Gene set enrichment analysis (GSEA) of the term "Activation of immune response", and the genes included in this pathway are highlighted in (i) with light yellow brown. *p<0.05, **p<0.01, ***p<0.001, ****p<0.0001 versus control. (G1: PBS, G2: Ads, G3: OMVs, G4: OMVs@P_2O, G5: OMVs-Ads, G6: OMVs@P_2O-Ads).

Question 5: Fig S11: Most of the GSEA enriched pathways are related to B cells, suggesting that the immune response induced by OMVs@P_2O-Ads seems to be mediated by B cells, but not T cells. As far as we know, antitumor immunity is mostly mediated by T cells. Thus, it would be better for the authors to explain why they did not study B cell mediated immunity. Perhaps 18 days post Ads inoculation is too late to monitor the T cell immunity.

Response: Thanks for this kind suggestion. Looking at the latest research progress of microbe-mediated tumor immunotherapy, although the role of B cells in anti-tumor immunity is gradually being discovered, as mentioned by the reviewer, anti-tumor immunity is mainly mediated by T cells[1, 2, 3]. In the experimental results of mice tumor transcriptome analysis shown in the revised Figure 3j, most of the GSEA enriched pathways are related to B cells, which is consistent with the results of other experiments (such as the increase of serum IL-6 in Fig 3g, which is capable of promoting the differentiation of B cell) and is foreseen. Based on the experimental data of this project and related literature reports, we believe that the activation of the B cell-associated transcriptome is mainly caused by antiviral immunity instead of anti-tumor immunity. Although the amplified anti-tumor immunity after injection of OMVs@P_2O-Ads is what we expect, as was reviewed in our previous work, the occurrence of antiviral immunity was earlier and stronger than anti-tumor immunity and the number of virus particles free in the tumor microenvironment is much more than the number of viruses infected into the tumor cells during the whole immunity process[4]. In the initial stage, free virions are mainly engulfed and eliminated by macrophages. After the activation of specific antiviral immunity, B cell-mediated humoral immunity is mainly responsible for the elimination of free Ads in tumor fluids. Overall, compared with innate immune cells and specific antiviral T cells, B cells play a more significant role during the process of virus clearance, which is the main reason why B cell-associated transcriptomes was distinctly activated as is shown in the revised Figure 3j (the Fig S11 was removed to Figure 3j). However, in this study, we attempted to focus on the anti-tumor immune response triggered by OMVs@P_2O-Ads instead of

antiviral immunity. Therefore, there is no doubt that it’s more significant for us to meticulously investigate the role of T cells in anti-tumor immunity process in our manuscripts even though most GSEA-enriched pathways are associated with B cells. In addition, we agree with the reviewer's opinion that perhaps 18 days post Ads inoculation is too late. In the revised manuscript, we have re-modified the experiment and the transcriptome analysis of tumor tissues was performed on day 11, and the new results had been presented in Figure 3i-k in the revised manuscript. As shown in Figure 3i-k, although some GSEA-enriched pathways were associated with B cells, T-cell-associated GSEA-enriched pathways were also detected, indicating that the earlier detection time points (on day 11 after the first administration) was more proper to investigate the change situation of transcriptome in tumor tissue of mice, and the microbial nanocomposite OMVs@P_2O-Ads possessed the ability to invoke T cell-mediated antitumor immunity.

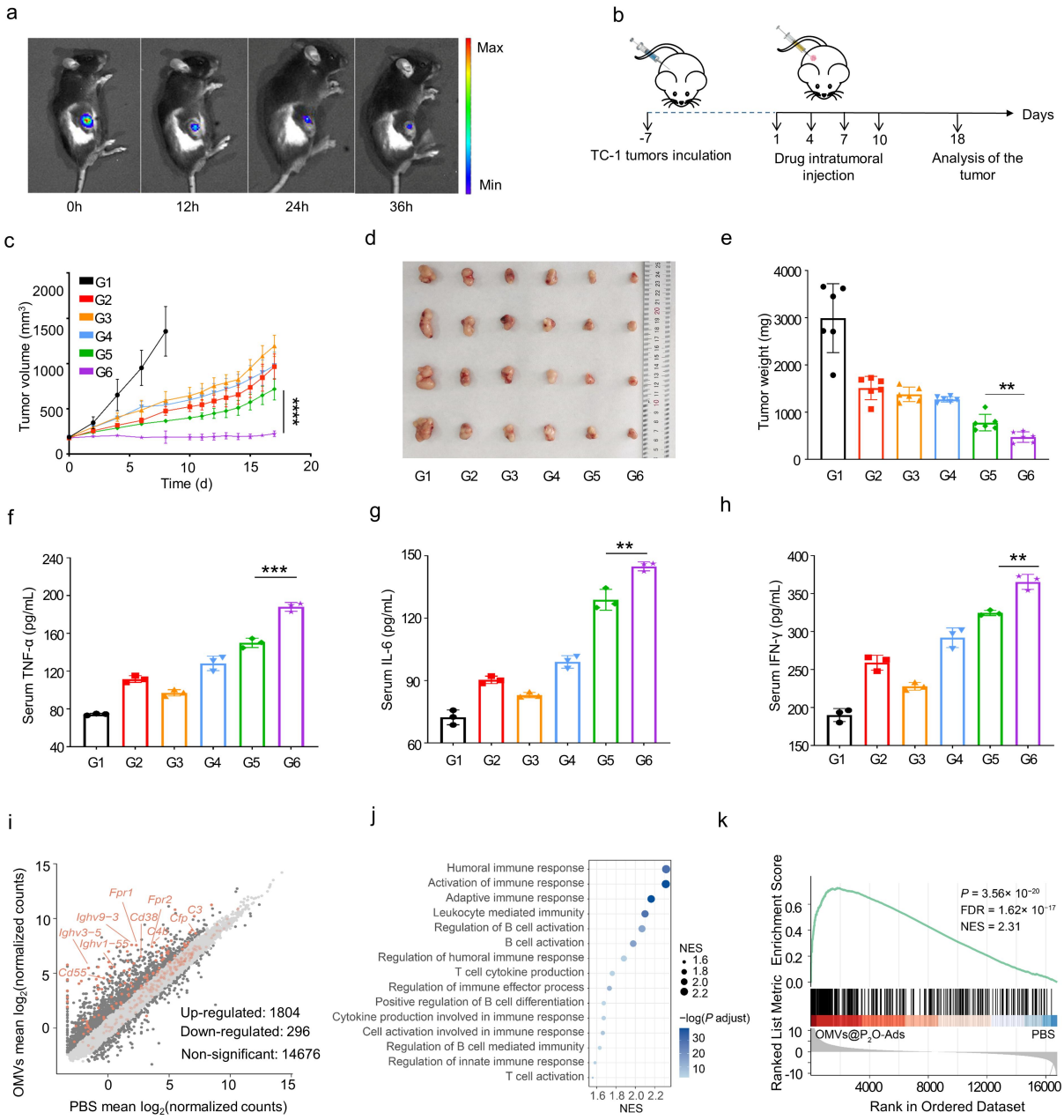

Figure 3. *In vivo* oncolytic efficacy of the microbial nanocomposite. (a) *In vivo* DIR fluorescent imaging of the microbial nanocomposite in TC-1-hCD46 xenograft tumor-bearing mice by IVIS. (b) Schematic illustration of the antitumor activity and immunology assessment experiments of the microbial nanocomposite using TC-1-hCD46 xenograft tumor-bearing C57 female mice model. TC-1 cells (10^6) were subcutaneously injected into the waist of female C57 mice, and the tumor-bearing mice were divided into six groups (n=6). When the tumor reached 100-150 mm^3, the mice were injected intratumorally with PBS, Ads (7×10^5 PFU), OMVs, OMVs@P_2O, OMVs-Ads (7×10^5 PFU), and OMVs@P_2O-Ads (7×10^5 PFU). The drug was given every three days for four consecutive times, the tumor volume was measured with a vernier caliper, and mice were weighed daily. (c) Tumor volume growth profiles of C57 mice bearing TC-1 xenografts. (d) Images of representative tumors of different treated groups on the 18th day (n=6). (e) Statistical graph of tumor weight of different treated groups on the 18th day (n=6). (f-h) Images of concentration of main cytokines in serum. (i) The differential gene expression between the samples treated with OMVs@P_2O-Ads and PBS, using the absolute value of logFC greater than 1 as

the threshold. (j) GSEA enriched pathways of the up-regulated genes in the samples treated with OMVs@P_2O-Ads, showing immune-related terms. (k) Gene set enrichment analysis (GSEA) of the term "Activation of immune response", and the genes included in this pathway are highlighted in (i) with light yellow brown. *p<0.05, **p<0.01, ***p<0.001, ****p<0.0001 versus control. (G1: PBS, G2: Ads, G3: OMVs, G4: OMVs@P_2O, G5: OMVs-Ads, G6: OMVs@P_2O-Ads).

References

1. Cabrita R, et al. Tertiary lymphoid structures improve immunotherapy and survival in melanoma. Nature 577, 561-565 (2020).
2. Petitprez F, et al. B cells are associated with survival and immunotherapy response in sarcoma. Nature 577, 556-560 (2020).
3. Helmink BA, et al. B cells and tertiary lymphoid structures promote immunotherapy response. Nature 577, 549-555 (2020).
4. Ban W, et al. Emerging systemic delivery strategies of oncolytic viruses: A key step toward cancer immunotherapy. Nano Res 15, 4137-4153 (2022).

Question 6: Fig S13/S14 are extremely important and should be presented in Fig 4. What kind of fluorescent dye did the authors used in Fig S13? This information should be provided in figure legends.

Response: We appreciate the reviewer's comments. In the revised manuscript, we have presented Fig S13/S14 in Figure 4a and 4b. In Fig S13 (Figure 4a in the revised manuscript), we used engineered eubacterial outer membrane vesicles that can express green fluorescent protein (OMVs@GFP).

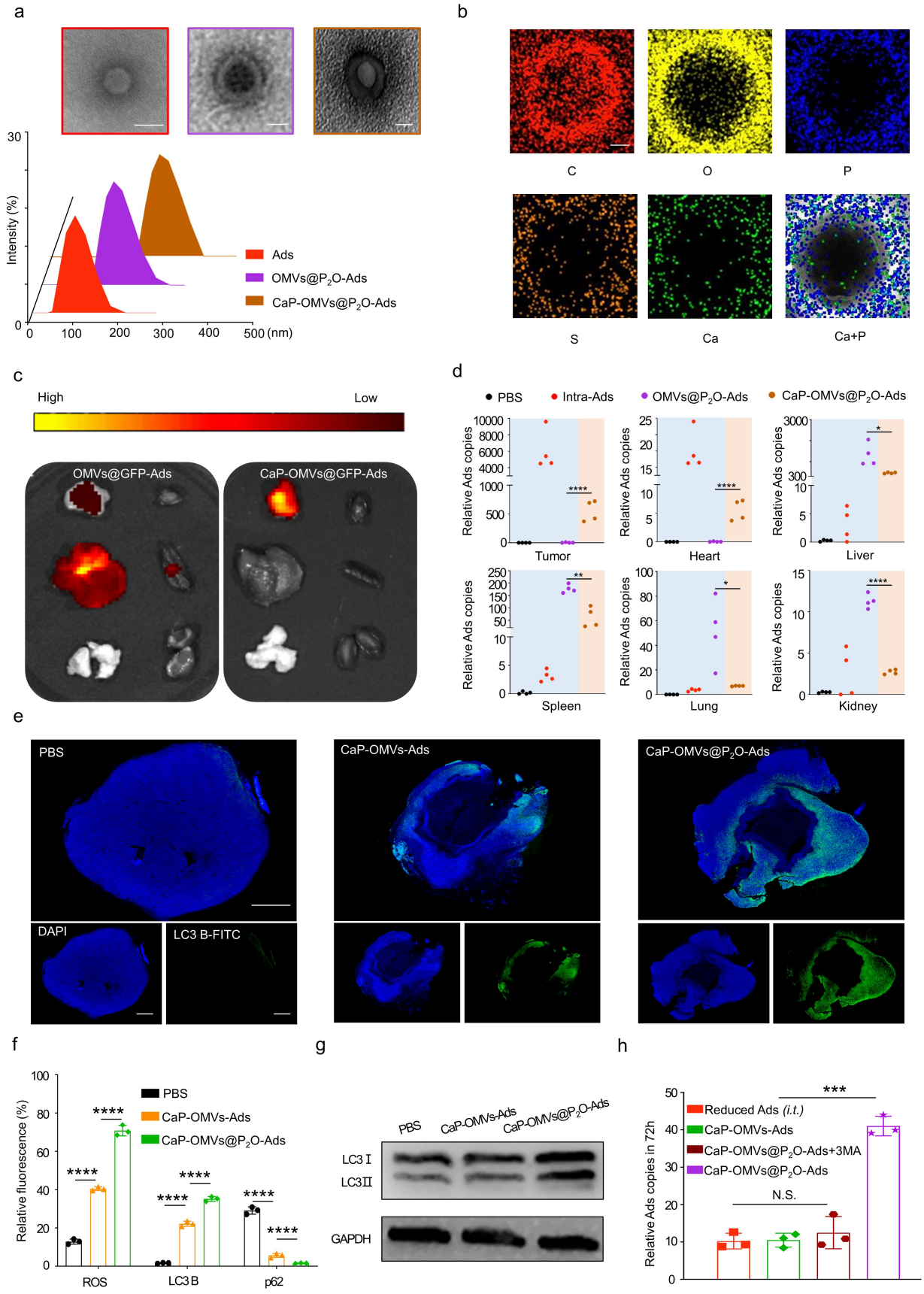

358 **Figure 4. Preparation and *in vivo* evaluation of the biomineralized microbial nanocomposite.** (a) TEM and
359 size distribution images of Ads, OMVs@P2O-Ads, and CaP-OMVs@P2O-Ads. Scale bar=100 nm. (b) Energy

spectrum analysis image of the biomineralized composite microbe. Scale bar=50 nm. (c) *In vivo* fluorescence imaging of the multiple organs and tumors collected from the mice at 24 h post *i.v.* injection. From left to right: tumor, heart, liver, spleen, lung, and kidney. (d) Quantitation of the biodistribution of relative Ads contents in multiple organs and tumors after 24 h of different treatments by RT-qPCR (n=4). (e) Immunofluorescence images of LC3 autophagic proteins in tumor tissues. Blue represents DAPI-stained tumor cells and the green represents FITC-stained LC3 autophagic protein. Scale bar=2 mm. (f) Quantitative analysis of fluorescence intensity. (g) The expression of autophagy-related protein LC3-I and LC3-II examined by western blot. (h) Quantitation of relative Ads content in the tumor after 72 h of different treatments by RT-qPCR technique (n=3). *p<0.05, **p<0.01, ***p<0.001, ****p<0.0001 versus control. *p<0.05, **p<0.01, ***p<0.001, ****p<0.0001 versus control.

Question 7: Fig 5c: Large amount of tiny green spots, which are unlikely to be normal CD8 staining, are shown in G5 and G6. The authors would be better to provide explanation.

Response: We appreciate the reviewer's comments. In original Figure 5c, the tiny green spots indeed were CD8 staining, but the image quality was not satisfactory. In revised manuscript, we modified the CD8 immunofluorescence section experiments using confocal fluorescence microscopy, and the representative images and the fluorescence quantitative statistics are shown as follows:

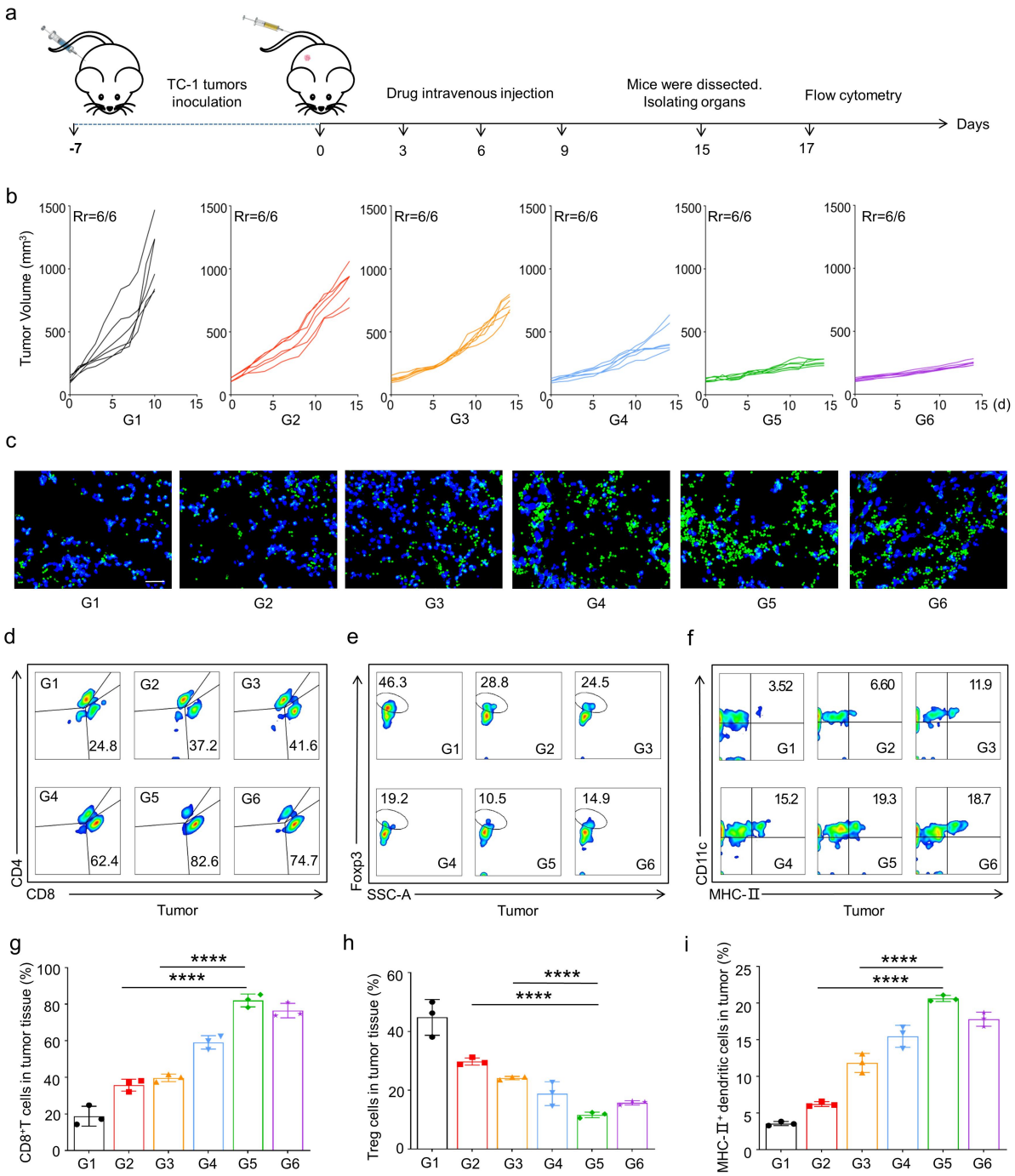

Figure 5. ***In vivo*** **oncolytic efficacy and immuneactivation capacity of the biomineralized microbial nanocomposite.** (a) Schematic illustration of the antitumor activity and immunity investigation of the biomineralized microbial nanocomposite on TC-1-hCD46 xenograft tumor-bearing C57 female mice model. (b) Individual tumor growth kinetics in different groups (n=6). (c) The immunofluorescence images of $CD8^+$ T cells in tumor tissues. Scale bars=50μm. (d) Representative flow cytometric evolution images (g) as well as relative quantification of $CD8^+$ T cells ($CD45^+CD3^+CD8^+$) in the tumor (n=3). (e) Representative flow cytometric evolution images (h) as well as relative quantification of Treg cells ($CD45^+CD3^+CD4^+Foxp3^+$) in the tumor (n=3). (f) Representative flow cytometric evolution images (i) and relative quantification of MHC-II^+ DC cells ($CD45^+CD11C^+$MHC-II^+) in the tumor (n=3). *p<0.05, **p<0.01, ***p<0.001, ****p<0.0001 versus control. (G1:

PBS, G2: OMVs@P_2O-Ads, G3: CaP-OMVs-Ads, G4: Intra-Ads, G5: CaP-OMVs@P_2O-Ads, G6: Intra-Ads high does).

Question 8: Fig 5: The authors try to demonstrate that the antitumor efficacy of CaP-OMVs@P2O-Ads depend on the activation of CD8 T cells. In this case, more solid evidences, including the activation status of CD8 T cells (CD44 and CD69 expression), the tumor killing activity of CD8 T cells (co-culture assay), and dependency of CD8 T cells (depleting CD8 with antibodies), should be provided.

Response: We appreciate the reviewer's comments. To refine the content of our experiments, we supplemented the relevant experiments one by one as suggested by reviewer. First, we measured the proportion of $CD45^+CD3^+CD8^+CD44^+$ and $CD45^+CD3^+CD8^+CD69^+$ T cells in tumor tissue after four consecutive treatment of Cap-OMVs@P_2O-Ads *via* flow cytometry. As is shown in the Figure, $CD44^-$ T cells and $CD44^+$ T cells clusters could be obviously observed. However, the cell cluster of $CD69^+$ T cells cannot be found in the figure, indicating that there is few T cell expressing $CD69^+$ after four consecutive treatments of Cap-OMVs@P_2O-Ads. By reviewing the related papers, the rationality of our experimental results was confirmed. Concretely, CD69 is one of the earliest markers upregulated after T cell activation, whose expression increased in a time-dependent manner between 3 and 12 hours, remained elevated until 24 hours, and then decreased[1]. In our study, the $CD45^+CD3^+CD8^+CD69^+$ T cells were measured after four consecutive treatment of Cap-OMVs@P_2O-Ads. Therefore, we held the opinion that the T cells go through the primary $CD69^+$ activation phase and enter into the next activation stage.

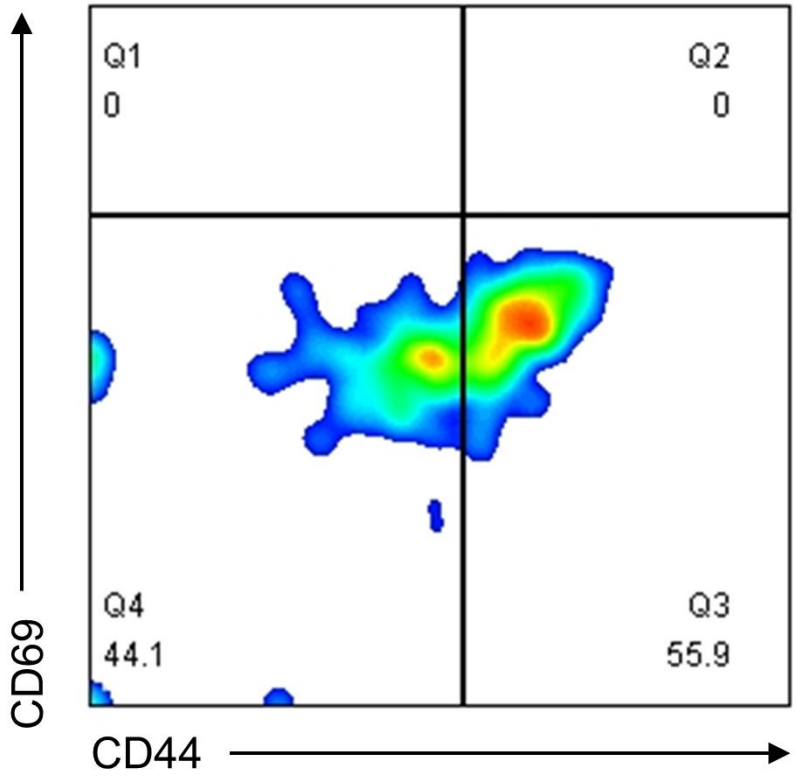

405 **Figure.** Representative flow cytometric evolution image of $CD45^+CD3^+CD8^+CD44^+$ T cells and
406 $CD45^+CD3^+CD8^+CD69^+$ T cells in tumor tissue.

407 Next, we have accomplished the co-culture assay *in vitro* to verify the tumor killing activity of
408 $CD8^+$ T cells in different administration groups. The detailed experimental method (section 4.23)
409 and the experimental result (Figure S32) are as follows:

410 Method: "First, TC-1 cells (10^6) were subcutaneously injected into the waist of female C57 mice,
411 and tumor-bearing mice were divided into six groups (n=6). When the tumor reached 100−150 mm^3,
412 the mice were intravenously injected with PBS, OMVs@P_2O-Ads, CaP-OMVs-Ads, and
413 CaP-OMVs@P_2O-Ads, while the Ads (7×10^5 and 10^7) were injected intratumorally. $CD8^+$ T cells
414 were extracted from each administration group based on the instructions of the BeaverBeads™
415 mouse $CD8^+$ T cell sorting kit (purchased from Beaver, 70903-100). Then, TC-1 cells were cultured
416 in cell culture plates. After the cells occupied 80% of the bottom, the medium was sucked out with a
417 2 mL syringe and washed twice with PBS. Then, $CD8^+$ T cells extracted from each administration
418 group were added into the holes based on the proportion of TC-1 cells: $CD8^+$ T cells =1:100 and
419 subsequently incubated at 37℃ for 24 h. Next, the MTT assay helped investigate the tumor-killing

rate in each group."

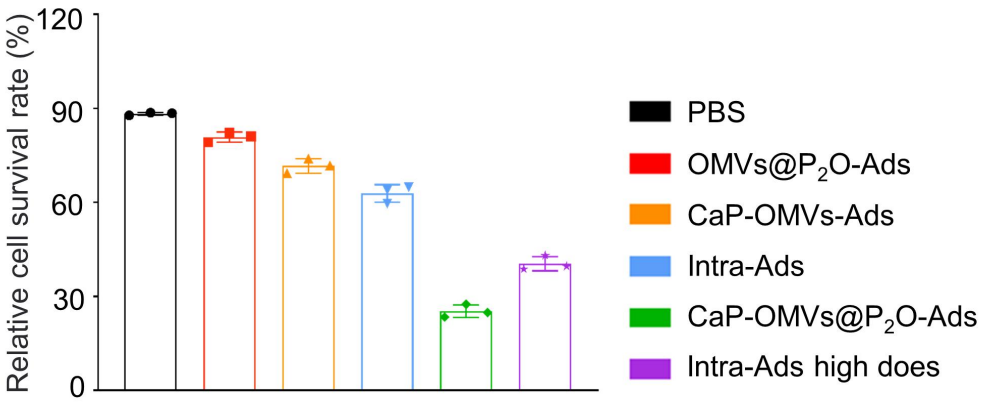

Figure S32. The experimental result of the co-culture assay. (It's worth noting here that PBS represents T cells extracted from mice in the PBS group, and other groups as above.)

In addition, the dependency of CD8 T cells was investigated *via* injecting $CD8^+$ T cells antibody. The detailed experimental method (section 4.24) and the experimental result (Figure S33) are as follows:

Method: "TC-1 cells (10^6) were subcutaneously injected into the waist of female C57 mice, and tumor-bearing mice were divided into three groups (n=5). When the tumor reached the size of 100−150 mm^3, the mice were intravenously injected with PBS, CaP-OMVs@P_2O-Ads, and CaP-OMVs@P_2O-Ads plus $CD8^+$ T cells antibody (anti-CD8 antibodies, clone: 2.43, Bio X cell, cat. no.: BP0061, injected *i.v.* every two days starting one day before the CaP-OMVs@P_2O-Ads injection) at 0, 3, 6, 9 day. On the 12^{th} day of the efficacy experiment, the mice were sacrificed by cervical spine removal, and the tumor tissue was isolated, weighed, and photographed. The effects of the different preparations on tumor growth were analyzed and compared."

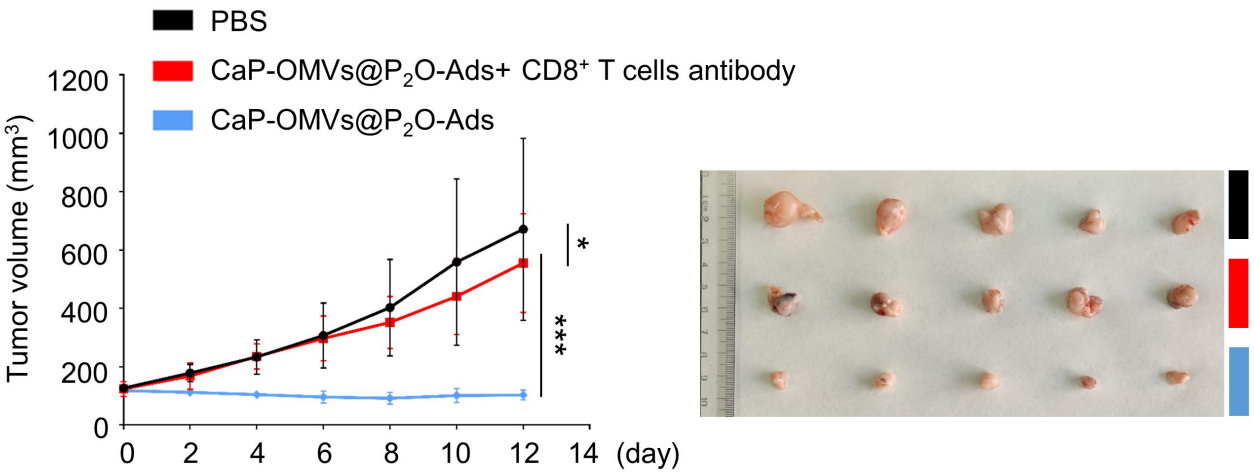

Figure S33. Tumor volume during the treatments and images of representative tumors of different treated groups on the 12th day (n=5).

References

1. Hamann J, Fiebig H, Strauss M. Expression cloning of the early activation antigen CD69, a type II integral membrane protein with a C-type lectin domain. J Immunol 150, 4920-4927 (1993).

Question 9: Fig 5d-f: The flow cytometry was not well performed. Large amount of death cells leads to serious unspecific staining, which adversely affect the interpretation and quantification of the data. The authors should use live/dead dyes to exclude death cells and debris.

Response: We appreciate the reviewer's comments. Due to the interference of a large number of dead cells, the Fig 5d-f data were not satisfactory. Therefore, we re-modified the experiment as suggested by the reviewer including using live/dead dyes, and the results were shown below:

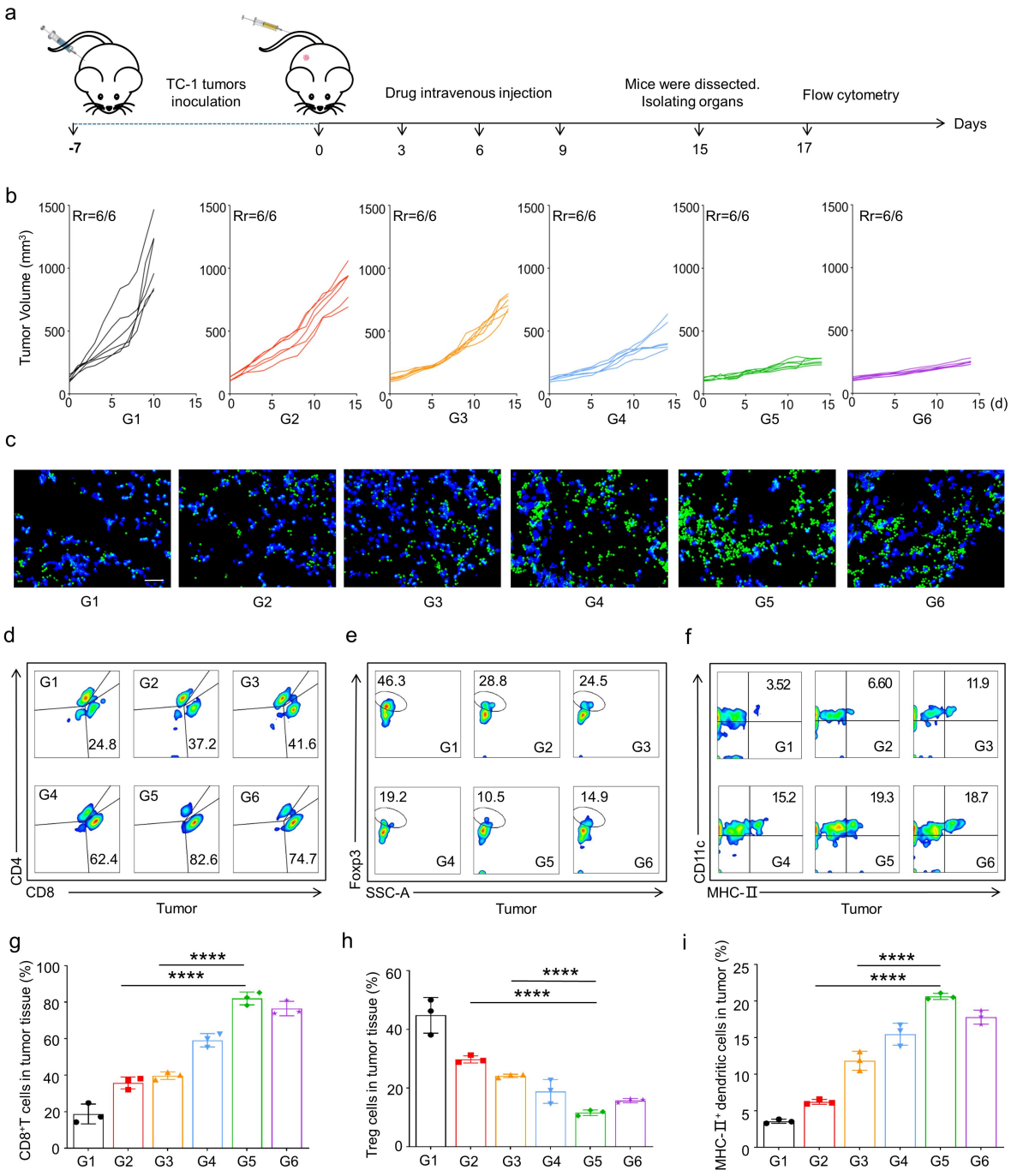

Figure 5. ***In vivo*** **oncolytic efficacy and immuneactivation capacity of the biomineralized microbial nanocomposite.** (a) Schematic illustration of the antitumor activity and immunity investigation of the biomineralized microbial nanocomposite on TC-1-hCD46 xenograft tumor-bearing C57 female mice model. (b) Individual tumor growth kinetics in different groups (n=6). (c) The immunofluorescence images of $CD8^+$ T cells in tumor tissues. Scale bars=50μm. (d) Representative flow cytometric evolution images (g) as well as relative quantification of $CD8^+$ T cells ($CD45^+CD3^+CD8^+$) in the tumor (n=3). (e) Representative flow cytometric evolution images (h) as well as relative quantification of Treg cells ($CD45^+CD3^+CD4^+Foxp3^+$) in the tumor (n=3). (f) Representative flow cytometric evolution images (i) and relative quantification of MHC-II^+ DC cells ($CD45^+CD11C^+$MHC-II^+) in the tumor (n=3). *p<0.05, **p<0.01, ***p<0.001, ****p<0.0001 versus control. (G1:

PBS, G2: OMVs@P_2O-Ads, G3: CaP-OMVs-Ads, G4: Intra-Ads, G5: CaP-OMVs@P_2O-Ads, G6: Intra-Ads high does).

Question 10: Fig 5f: Since most, if not all, antigen presenting cells (APCs) express CD80 and CD86, these two markers are not specific enough to identify DCs. The authors should use CD11c and MHCII, instead.

Response: We appreciate the reviewer's comments. In Figure 5f and 5i, we have replaced $CD80^+CD86^+$ DC cells with $CD11c^+$MHC-II^+ DC cells in the revised manuscript. The statistical result (n=3) and the gating strategies of DCs ($CD45^+CD11c^+$MHC-II^+) were shown as follows:

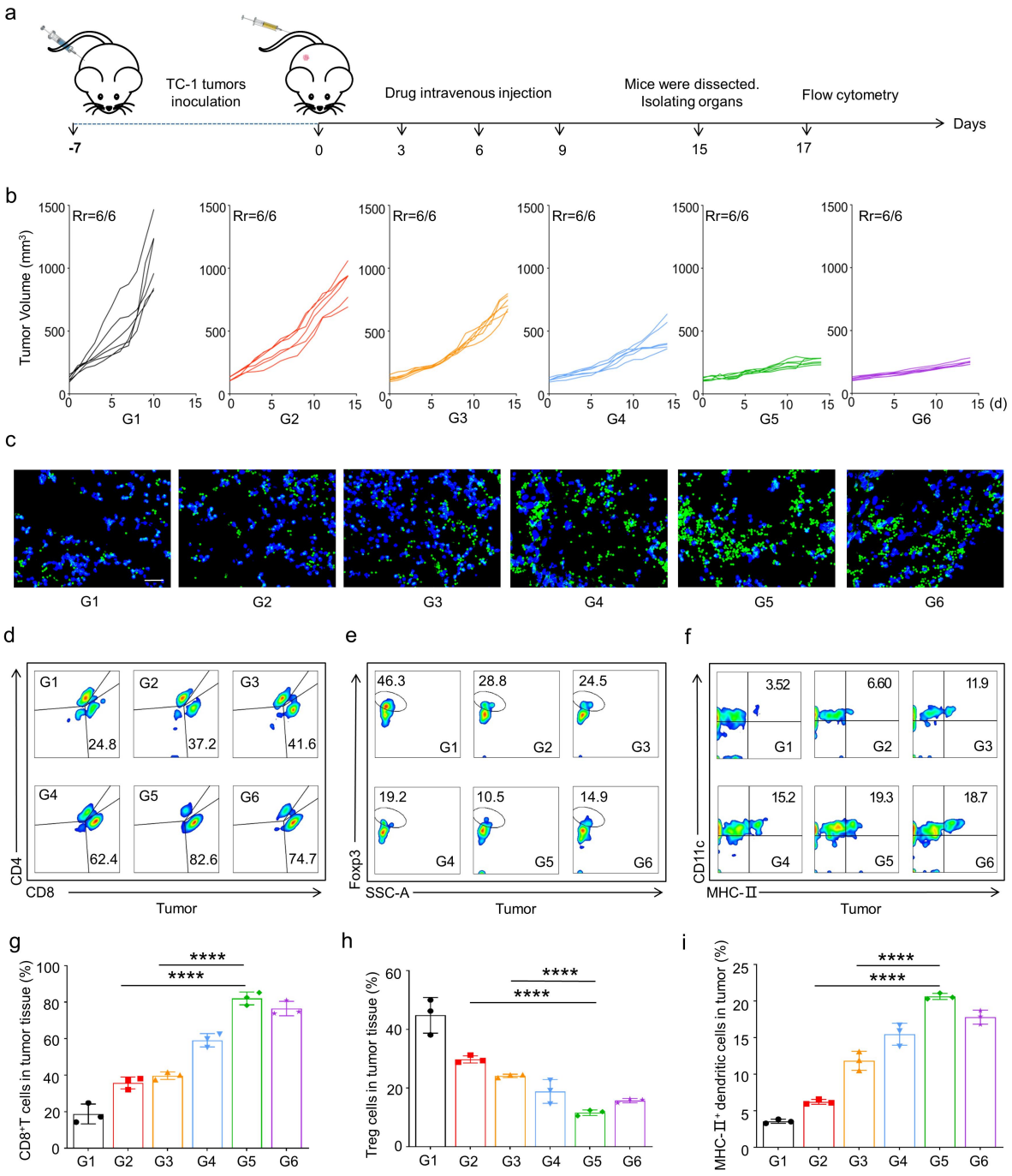

Figure 5. ***In vivo*** **oncolytic efficacy and immuneactivation capacity of the biomineralized microbial nanocomposite.** (a) Schematic illustration of the antitumor activity and immunity investigation of the biomineralized microbial nanocomposite on TC-1-hCD46 xenograft tumor-bearing C57 female mice model. (b) Individual tumor growth kinetics in different groups (n=6). (c) The immunofluorescence images of $CD8^+$ T cells in tumor tissues. Scale bars=50μm. (d) Representative flow cytometric evolution images (g) as well as relative quantification of $CD8^+$ T cells ($CD45^+CD3^+CD8^+$) in the tumor (n=3). (e) Representative flow cytometric evolution images (h) as well as relative quantification of Treg cells ($CD45^+CD3^+CD4^+Foxp3^+$) in the tumor (n=3). (f) Representative flow cytometric evolution images (i) and relative quantification of MHC-II^+ DC cells ($CD45^+CD11C^+$MHC-II^+) in the tumor (n=3). *p<0.05, **p<0.01, ***p<0.001, ****p<0.0001 versus control. (G1:

PBS, G2: OMVs@P_2O-Ads, G3: CaP-OMVs-Ads, G4: Intra-Ads, G5: CaP-OMVs@P_2O-Ads, G6: Intra-Ads high does).

Question 11: Discussion section is missing in the current manuscript.

Response: We appreciate the reviewer's comments. To help reviewers and readers better understand the research content of this project, we have included the discussion section in the revised manuscript (page 22):

"Oncolytic virotherapy is a novel type of immunotherapy inducing antitumor responses through selective self-replication inside cancer cells and oncolytic virus (OV)-mediated immunostimulation. It has attracted more attention recently. However, although OVT has incredible advantages in cancer treatment, the clinical practice of commercial OVs is not perfect. The three oncolytic viral drugs marketed globally are administered by intratumoral injection. This significantly increases the difficulty of clinical treatment and decreases medication compliance in patients. In addition, some clinical trials have attempted to deliver OVs systematically, with unsatisfactory clinical results.

We constructed the microbial nanocomposite for the first time for autophagy-cascade-augmented immunotherapy. The oncolytic Ads were encapsulated using the engineered OMVs extracted from *E. coli* and transfected with plasmid to express P_2O. CaP biomineral shells were added to protect Ads from the clearance of the innate immune system. Therefore, it extends the *in vivo* circulation time and promotes Ads enrichment after systemic administration. More importantly, P_2O-catalyzed H_2O_2 elevated the level of oxidative stress in the tumor site, leading to autophagy formation. The increase in the number of autophagy-induced autophagosomes would significantly augment the replication efficiency of Ads in OVs-infected cancer cells. Meanwhile, enhanced OVs intratumoral enrichment augmented OVs replication in tumors and immunosuppressive TEM remolding based on the advantage of the immunostimulatory capability of OMVs. This would enhance OVs-mediated immune responses. Overall, the current autophagy-cascade-boosted immunotherapy strategy would be promising in OVs-based biomedical therapy applications."

Minor concerns:

Question 1: The language of the paper could be improved with some editing.

Response: We appreciate the reviewer's comments. The revised manuscript was checked out

carefully by ourselves and to better improve the readability of the manuscript, we had sent it for language revision by language revision by Mogoedit language editing service on 23-Feb-2023.

MogoEdit

CERTIFICATE OF ENGLISH EDITING

This is to certify that the manuscript entitled

Autophagy-overactivated microbial nanocomposite engineered from oncolytic adenoviruses for the cascade enhancement of cancer immunotherapy

commissioned to us has been carefully edited by a native English-speaking editor of MogoEdit, and the grammar, spelling, and punctuation have been verified and corrected where needed. Based on this review, we believe that the language in this paper meets academic journal requirements. Please contact us with any questions.

MOGOEDIT MOGO INTERNET TECHNOLOGY CO., LTD.

Gang Zhang

Dr. Gang Zhang
Founder & CEO of MogoEdit

Date of Issue
February 22, 2023

Disclaimer: The changes in the document may be accepted or rejected by the authors in their sole discretion after our editing. However, MogoEdit is not responsible for revisions made to the document after our edit on **February 22, 2023**.

MogoEdit is a professional English editing company who provides English language editing, translation, and publication support services to individuals and corporate customers worldwide. As a company invested by the affiliate fund of Chinese Academy of Science, MogoEdit is one of the leading language editing service providers in China, whose clients come from more than 1000 universities and research institutes.
MogoEdit Website: http://en.mogoedit.com/
500+ native English editors: http://en.mogoedit.com/editors

Mogo make the world flatter

Mogo Internet Technology Co., LTD.
No. 57, 3rd Keji Road, Xi'an 710075, PR China +86 02988317483 support@mogoedit.com

Figure. The certificate of MogoEdit language editing services on 23-Feb-2023.

Question 2: It would be better to have an introduction of the advantages and disadvantages of bacterial outer membrane vesicles. Are OMVs better than other nanomaterials? Are there any potential safety concerns?

Response: We appreciate the reviewer's comments. The application of OMVs in the field of drug delivery has been extensively reported recently ascribed to its intuitive advantages. First, it has nanoscale particle size, sufficient internal space and wide membrane area to act as a delivery carrier for a variety of drugs such as Ads. In addition, inheriting various immunostimulatory components such as lipopolysaccharide (LPS) from their parent bacteria, OMVs also represent a natural immune activator possessing abilitiy to turn the "cold tumor" into "hot tumor"[1]. Furthermore, abandoning the proliferation ability of the parent bacteria, OMVs has higher controllability and safety than bacteria[2]. In our subject, engineered bacterial outer membrane vesicles (OMVs@P_2O) are an irreplaceable component. On the one hand, as mentioned above, serving as the vector for systemic delivery of the Ads, OMVs@P_2O could protect Ads from recognition and clearance by neutralizing antibodies. And as the natural immune activator, OMVs@P_2O could remould the suppressive tumor immune microenvironment for the further oncolytic viral immunotherapy. On the other hand, OMVs@P_2O naturally carries pyranose oxidase, which could catalyze the production of ROS at the tumor site and trigger excessive autophagy, thereby improving the replication of Ads in tumor cells. Overall, OMVs represents an irreplaceable carrier material for the construction of autophagy-overactivated microbial nanocomposite.

References

1. Cheng K, et al. Bioengineered bacteria-derived outer membrane vesicles as a versatile antigen display platform for tumor vaccination via Plug-and-Display technology. Nat Commun 12, 2041 (2021).

2. Jahromi LP, Fuhrmann G. Bacterial extracellular vesicles: Understanding biology promotes applications as nanopharmaceuticals. Adv Drug Deliv Rev 173, 125-140 (2021).

Question 3: Figure 1 is missing.

Response: We are sorry that Figure 1 had been not shown in the manuscript. We have attached Figure 1 here and added it to the revised manuscript (page 6).

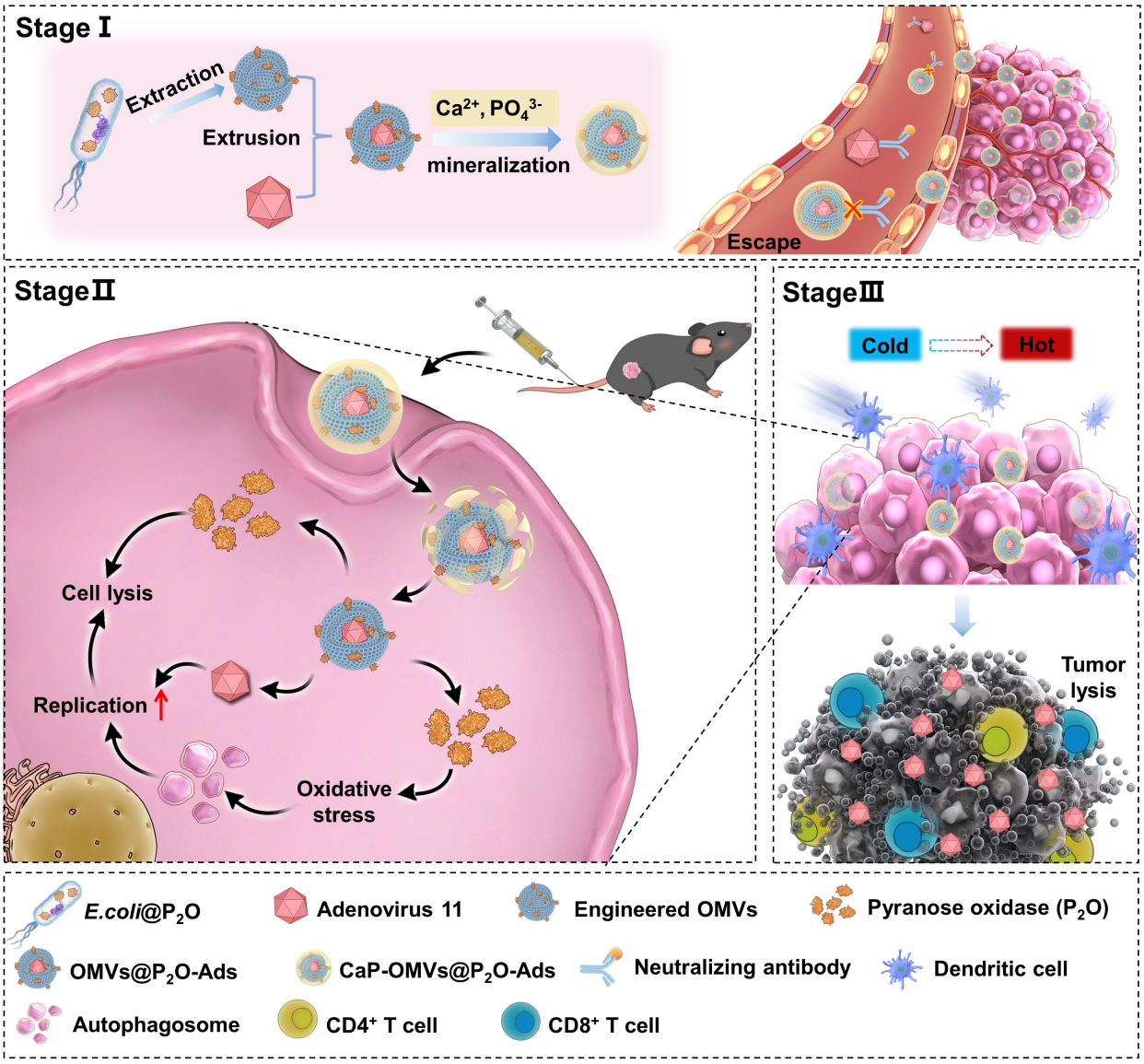

Figure 1. Schematic diagram. The biomineralized microbial nanocomposite engineered from OVs for autophagy-cascade-augmented immunotherapy.

Question 4: Fig 2g is missing.

Response: We appreciate the reviewer's comments. The Figure 2 had been added as follow:

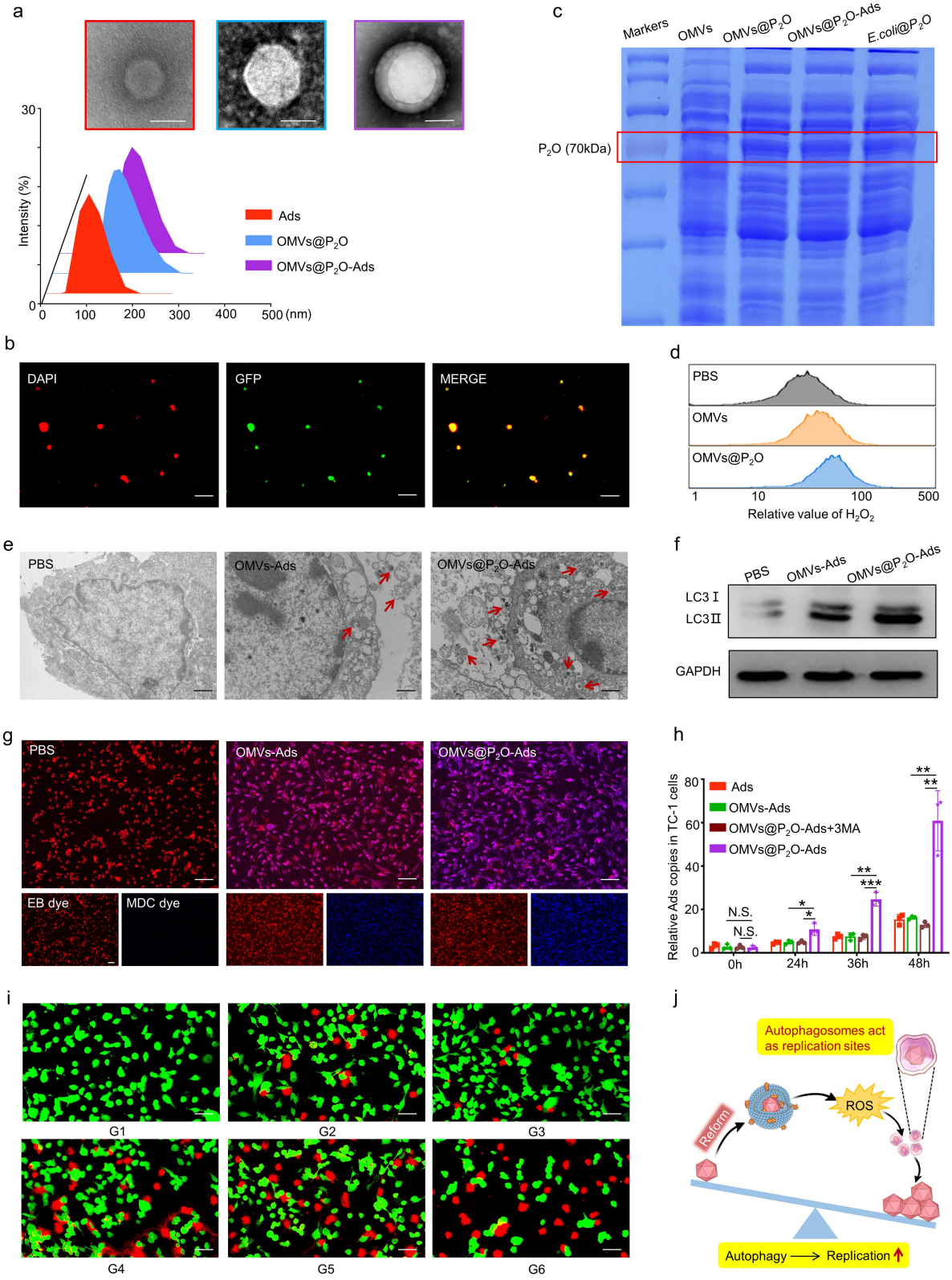

535 **Figure 2. Preparation and *in vitro* evaluation of the microbial nanocomposite.** (a) TEM and size distribution
536 images of Ads, OMVs@P_2O, and OMVs@P_2O-Ads. Scale bar=100 nm. (b) CLSM images of the microbial
537 nanocomposite. Ads were stained with DAPI dye (red) and OMVs carried a GFP marker (green). Scale bar=1 μm.
538 (c) The expression of P_2O was investigated by the SDS-PAGE method. (d) The ROS level assessment in TC-1

cells by flow cytometry. (e) TEM images of autophagosomes. Scale bar=200 nm. (f) The expression of autophagy-related protein LC3-I and LC3-II by western bolt analyses. (g) CLSM images of autophagosomes. Cells were stained with EB dye (red) and autophagosomes were stained with MDC dye (blue). Scale bar=50 μm. (h) The Ads replication in TC-1 cells was quantified using real-time PCR at 0, 24, 36, and 48 h sequentially. 3MA is an autophagy inhibitor: 3-Methyladenine. (i) Cytotoxicity of different formulations in TC-1 cells by CLSM. Living cells were stained with Calcein (green) and dead cells were stained with PI (red). Scale bar=20 μm. (j) Schematic diagram of bridging ROS with oncolytic Ads replication. *p<0.05, **p<0.01, ***p<0.001, ****p<0.0001 versus control.

Question 5: Fig 2j: What do G1~G6 represent? The authors should mention this information in the figure legends.

Response: We are sorry to make the reviewer confused. The meaning of G1~G6 are as follows: G1: PBS, G2: Ads, G3: OMVs, G4: OMVs@P2O, G5: OMVs-Ads, G6: OMVs@P2O-Ads. And we also present this information in the legend in the manuscripts (page 10).

Question 6: Fig 2k should be mentioned at least once in the manuscript.

Response: We agree with the reviewer's comments. In the revised manuscript, this part was modified as (page 8): "Autophagy-generated internal double-membrane-bound vesicles (autophagosomes) could be Ads replication sites within Ads-infected tumor cells. This effectively enhanced Ads replication through the autophagy pathway (Figure 2j)."

Question 7: Fig S7: Only 6 columns are presented, but x-axis has 8 groups.

Response: We are sorry for the mistake of marking the number in the post-processing of the Figure S9. The amendatory Figure S9 was updated as follow:

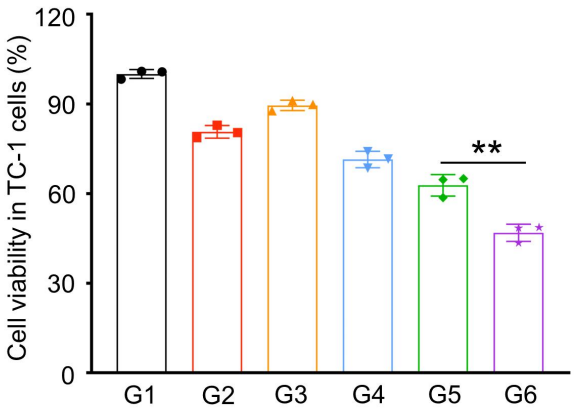

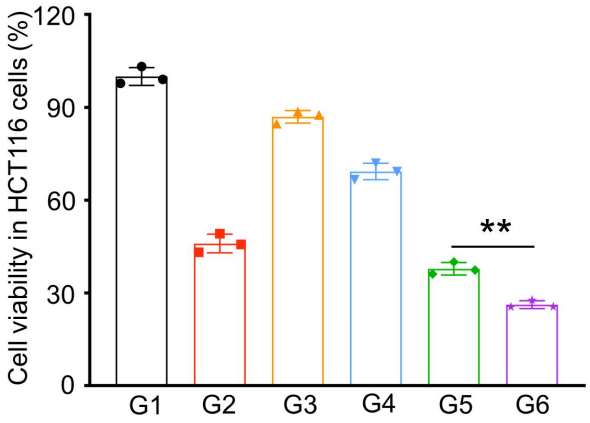

Figure S9. Cytotoxicity of different formulations in TC-1 cells and HCT116 cells by MTT assay. (G1: PBS, G2: Ads, G3: OMVs, G4: OMVs@P_2O, G5: OMVs-Ads, G6: OMVs@P_2O-Ads).

Question 8: Fig S8/5b/6c: What does "Rr=6/6" or "Rr=5/5" mean?

Response: We appreciate the reviewer's comments. "Rr" represents the real survival rate of mice in each group during pharmacodynamic investigation. "Rr=6/6" or "Rr=5/5" represents that there was no death of 6 (5) mice in each group (n=6 or n=5) during pharmacodynamic investigation.

Question 9: Fig S10: What do G1~G6 represent here. Are they the same with Fig S9? The authors should mention this information in the figure legends.

Response: We are sorry to make the reviewer confused. The meanings of G1~G6 were the same with Figure S9, namely G1: PBS, G2: Ads, G3: OMVs, G4: OMVs@P_2O, G5: OMVs-Ads, G6: OMVs@P_2O-Ads. In the revised manuscript, the revisionary legends of Figure S10 was mentioned.

Question 10: The authors should explain why they use TC-1-hCD46. Indeed, hCD46 is the receptor for adenovirus.

Response: We appreciate the reviewer's question. The oncolytic ad11-tel (ad11) was supplied by Beijing Bio-Targeting Therapeutics Technology Co., Ltd (China). Oncolytic viruses cannot infect most murine tumor cells because there are no marker molecules on the murine cancer cell surface that are recognizable to the oncolytic virus. To investigate the use of oncolytic virus in mouse animal models, we used engineered TC-1-hCD46 murine tumor cell lines by introducing human CD46 receptor expression plasmid into the murine cancer cells. The oncolytic virus could infect and

replicate in TC-1 cells *via* human CD46 receptors expressed on the cell surface.

Question 11: Misspell: "wight" in section 2.2.

Response: We appreciate the reviewer's comments. In the revised manuscript, this misspell was modified as (page 10): "weight".

Question 12: Fig 3a: The authors ought to give a brief introduction of DiR dye.

Response: We agree with the reviewer's comments. In the revised manuscript, this part was modified in section 4.11 as (page 27): "DIR is a type of long-chain lipophilic dialkylcarbocyanine dye. Owing to its lipophilicity, DIR is often used to label cell membranes as well as other liposoluble biological structures including OMVs. The maximum excitation and emission wavelengths of DIR are 750nm and 780nm, respectively. Because the infrared light emitted by DiR can efficiently pass through cells and tissues, it is of great significance in *in vivo* imaging or tracking."

Question 13: Figure 4: It would be better for the authors to explain why CaP-OMVs exhibit better tumor selectivity than OMVs.

Response: We appreciate the reviewer's comments. OMVs might still rapidly cause severe systemic inflammatory response and antibody-mediated clearance. Thurs, a "masking" strategy was adopted in which we used the highly biocompatible calcium phosphate (CaP) to encapsulate OMVs. Upon the microbial nanocomposite arrival at tumors through EPR effect, the slightly acidic pH of TME triggered the dissolution of CaP shells, thereby OMVs@P_2O and Ads would be exposed and play their functions severally.

Question 14: Fig 4b: What do C, O, P, S, Ca, and Ca+P stand for?

Response: We appreciate the reviewer's comments. C, O, P, S, Ca, and Ca+P represent element abbreviations, namely carbon, oxygen, phosphorus, sulphur, calcium and co-localization of calcium with phosphorus. The revised figure was removed to Figure S14.

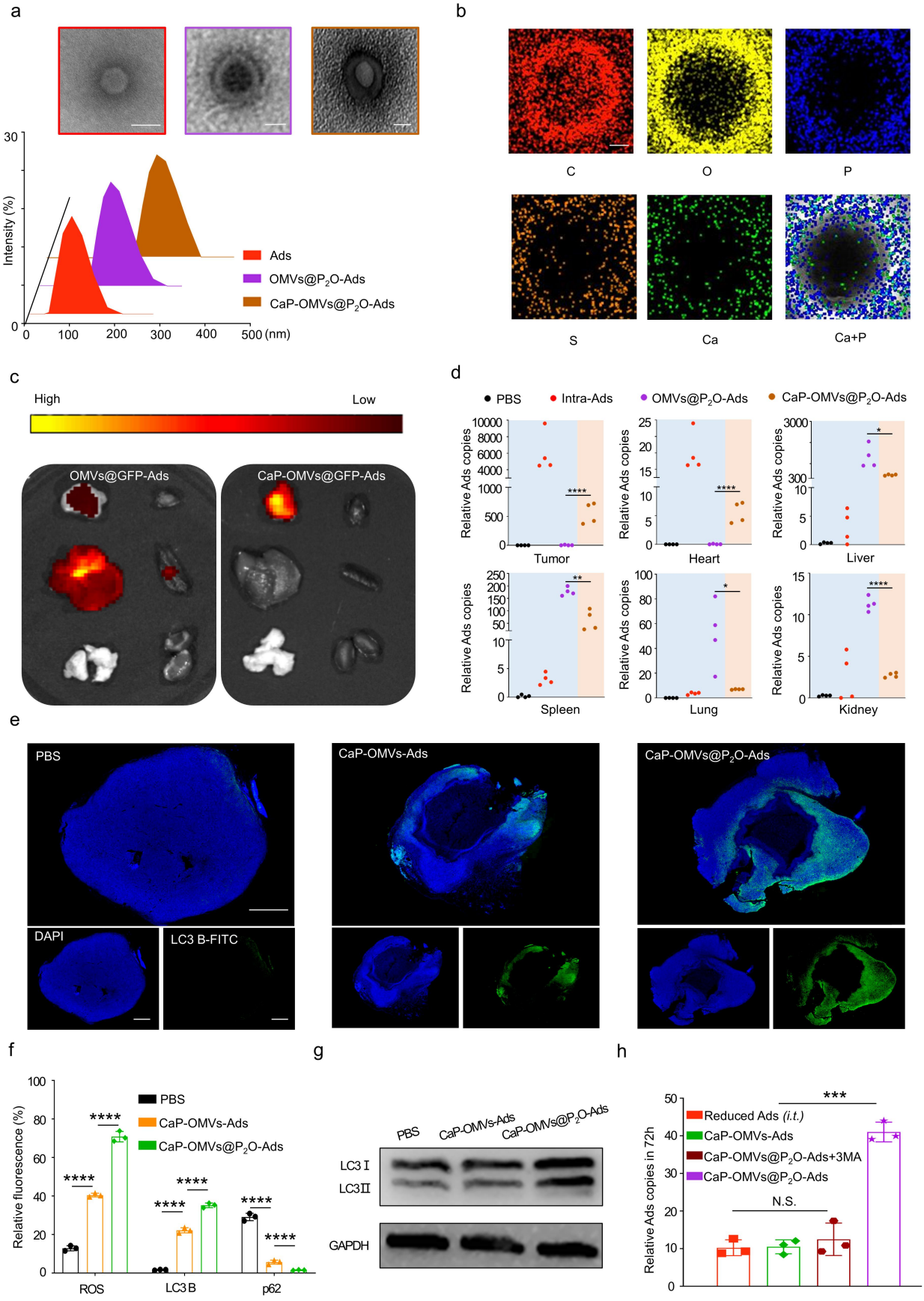

603 **Figure 4. Preparation and *in vivo* evaluation of the biomineralized microbial nanocomposite.** (a) TEM and
604 size distribution images of Ads, OMVs@P_2O-Ads, and CaP-OMVs@P_2O-Ads. Scale bar=100 nm. (b) Energy

spectrum analysis image of the biomineralized composite microbe. Scale bar=50 nm. (c) *In vivo* fluorescence imaging of the multiple organs and tumors collected from the mice at 24 h post *i.v.* injection. From left to right: tumor, heart, liver, spleen, lung, and kidney. (d) Quantitation of the biodistribution of relative Ads contents in multiple organs and tumors after 24 h of different treatments by RT-qPCR (n=4). (e) Immunofluorescence images of LC3 autophagic proteins in tumor tissues. Blue represents DAPI-stained tumor cells and the green represents FITC-stained LC3 autophagic protein. Scale bar=2 mm. (f) Quantitative analysis of fluorescence intensity. (g) The expression of autophagy-related protein LC3-I and LC3-II examined by western blot. (h) Quantitation of relative Ads content in the tumor after 72 h of different treatments by RT-qPCR technique (n=3). *p<0.05, **p<0.01, ***p<0.001, ****p<0.0001 versus control. *p<0.05, **p<0.01, ***p<0.001, ****p<0.0001 versus control.

Question 15: Fig S22-23: Gating strategies should also be presented.

Response: We appreciate the reviewer's comments. Gating strategies had been presented in Figure S30 in the revised manuscript.

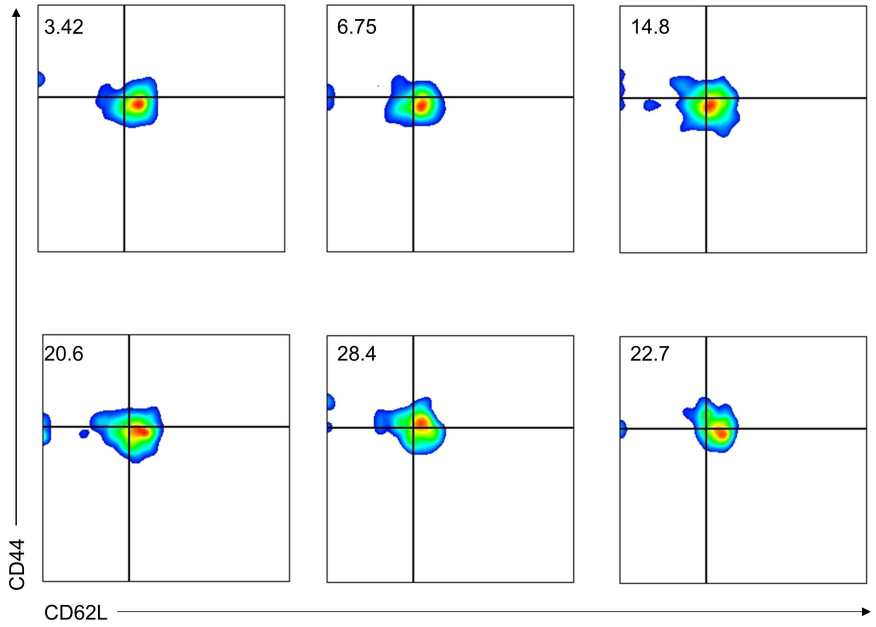

Figure S30. The gating strategy of effector memory T cells ($CD3^+$ $CD8^+$ $CD62L^-$ $CD44^+$) in spleen (n=3). (G1: PBS, G2: OMVs@P_2O-Ads, G3: CaP-OMVs-Ads, G4: Intra-Ads, G5: CaP-OMVs@P_2O-Ads, G6: Intra-Ads high does).

Question 16: Fig S9/S16/S17/S24/3c/: What do the dotted lines represent?

Response: We are sorry to make the reviewer confused. The dotted lines represent error bars here. To make the figure information more intuitive for reviewers and readers, we replace the dotted lines with the traditional error bars.

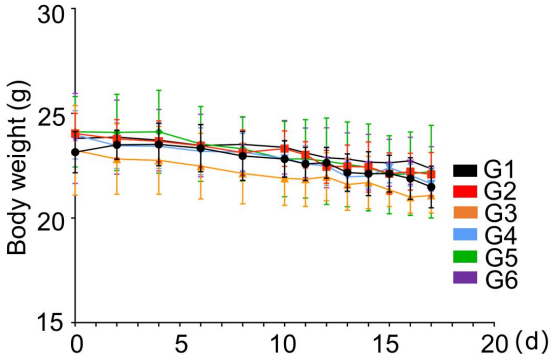

624 **Figure S13.** Body weight changes of TC-1-bearing mice after intratumoral administration of different
625 formulations (n=6). (G1: PBS, G2: Ads, G3: OMVs, G4: OMVs@P_2O, G5: OMVs-Ads, G6: OMVs@P_2O-Ads).

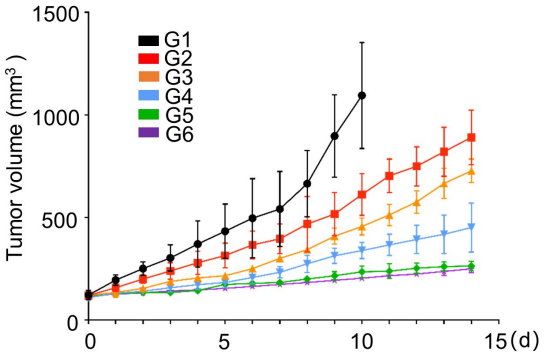

626 **Figure S19.** The tumor of TC-1-bearing mice model volume change for TC-1 xenograft tumor model during
627 different treatments (n=6). ****p<0.0001 versus control. (G1: PBS, G2: OMVs@P_2O-Ads, G3: CaP-OMVs-Ads,
628 G4: Intra-Ads, G5: CaP-OMVs@P_2O-Ads, G6: Intra-Ads high does).

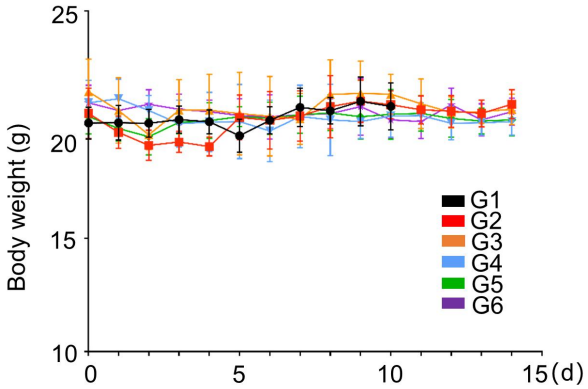

629 **Figure S20.** Body weight changes of TC-1-bearing mice after administration of different formulations (n=6). (G1:
630 PBS, G2: OMVs@P_2O-Ads, G3: CaP-OMVs-Ads, G4: Intra-Ads, G5: CaP-OMVs@P_2O-Ads, G6: Intra-Ads high
631 does).

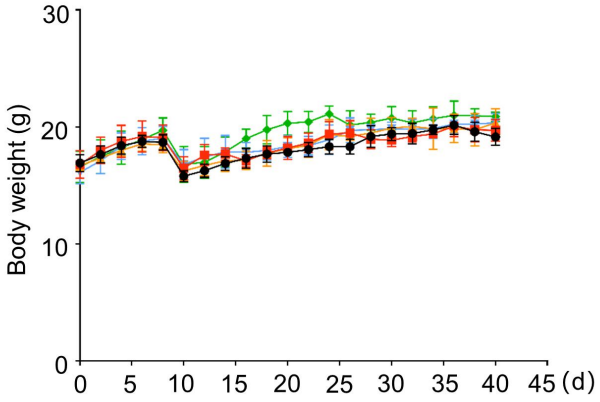

632 **Figure S34.** Body weight changes of TC-1-bearing mice after administration of different formulations (n=5). (G1:
633 PBS, G2: OMVs@P_2O-Ads, G3: CaP-OMVs-Ads, G4: Intra-Ads, G5: CaP-OMVs@P_2O-Ads).

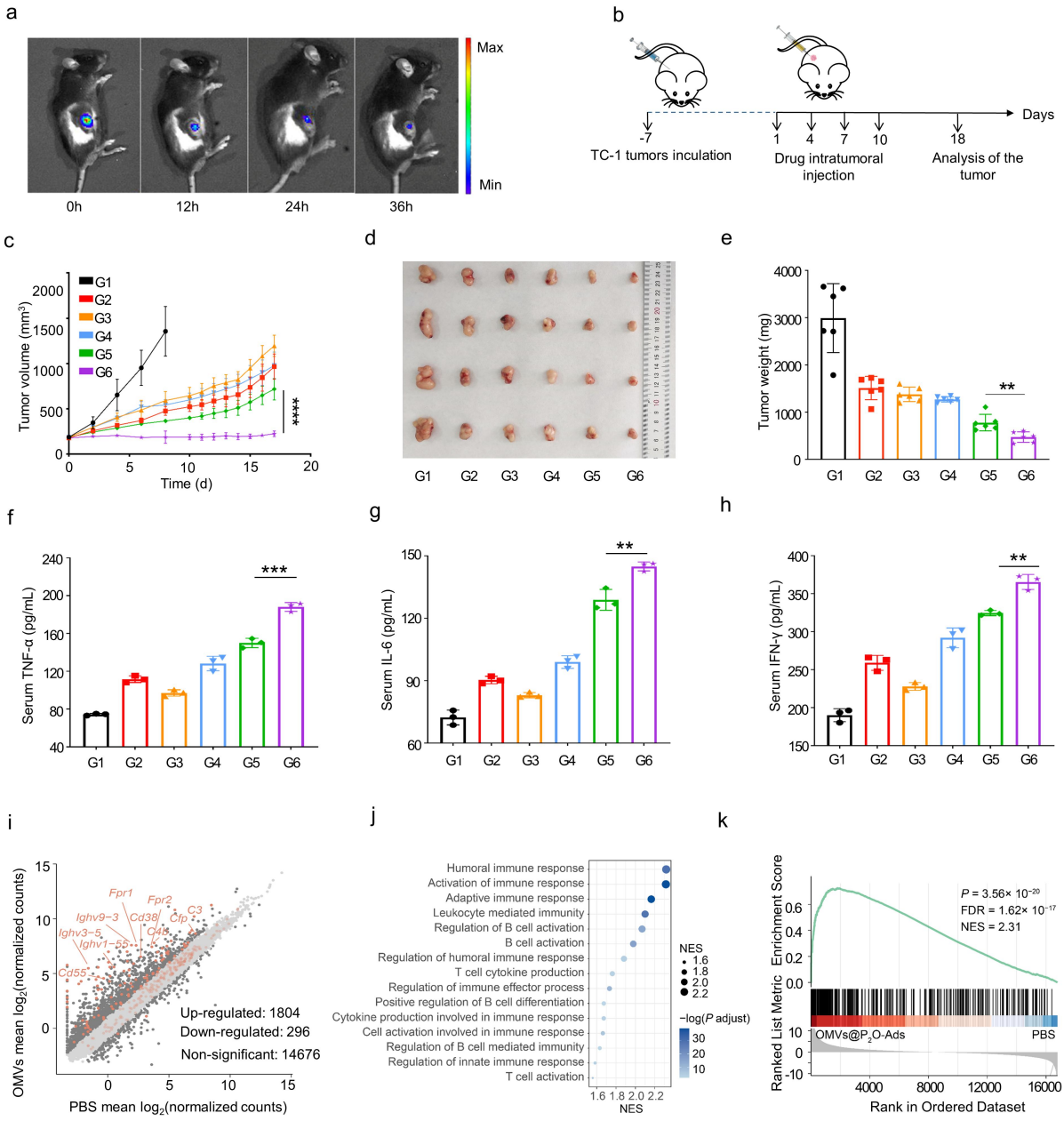

Figure 3. *In vivo* oncolytic efficacy of the microbial nanocomposite. (a) *In vivo* DIR fluorescent imaging of the microbial nanocomposite in TC-1-hCD46 xenograft tumor-bearing mice by IVIS. (b) Schematic illustration of the antitumor activity and immunology assessment experiments of the microbial nanocomposite using TC-1-hCD46 xenograft tumor-bearing C57 female mice model. TC-1 cells (10^6) were subcutaneously injected into the waist of female C57 mice, and the tumor-bearing mice were divided into six groups (n=6). When the tumor reached 100-150 mm^3, the mice were injected intratumorally with PBS, Ads (7×10^5 PFU), OMVs, OMVs@P_2O, OMVs-Ads (7×10^5 PFU), and OMVs@P_2O-Ads (7×10^5 PFU). The drug was given every three days for four consecutive times, the tumor volume was measured with a vernier caliper, and mice were weighed daily. (c) Tumor volume growth profiles of C57 mice bearing TC-1 xenografts. (d) Images of representative tumors of different treated groups on the 18th day (n=6). (e) Statistical graph of tumor weight of different treated groups on the 18th day (n=6). (f-h) Images of concentration of main cytokines in serum. (i) The differential gene expression between the samples treated with OMVs@P_2O-Ads and PBS, using the absolute value of logFC greater than 1 as

the threshold. (j) GSEA enriched pathways of the up-regulated genes in the samples treated with OMVs@P_2O-Ads, showing immune-related terms. (k) Gene set enrichment analysis (GSEA) of the term "Activation of immune response", and the genes included in this pathway are highlighted in (i) with light yellow brown. *p<0.05, **p<0.01, ***p<0.001, ****p<0.0001 versus control. (G1: PBS, G2: Ads, G3: OMVs, G4: OMVs@P_2O, G5: OMVs-Ads, G6: OMVs@P_2O-Ads).

Question 17: Section 2.5: Some OVs in clinical trials, including vaccinia virus and reovirus, are systemically delivered. The authors should mention this and compare the CaP-OMVs technology with these intravenous OVs.

Response: We appreciate the reviewer's comments. In the beginning of section 2.5, we mistakenly said "marketed product" instead of "clinical research stage". In the revised manuscript, this part was modified in section 2.5 as (page 19): "All marketed OVs products are delivered by intratumoral or topical administration rather than intravenous administration."

We published a review article entitled "Emerging systemic delivery strategies of oncolytic viruses: A key step toward cancer immunotherapy" in 2021, which introduces the foundation of clinical trials of OVT to date[1]. Although, in clinical trials, there are cases of systemic delivery of vaccinia virus and reovirus products, it's still necessary to develop the systemic Ads products due to its innate advantages. On the one hand, compared with RNA oncolytic virus such as reovirus, Ads possess higher genetic stability in the process of self-replication in tumor cells, which could ensure the ability of the virus to infect and kill tumor cells after repetitive replication, thereby maintaining a low toxicity and high efficiency cancer treatment. On the other hand, compared with vaccinia virus, Ads have the prospect of product transformation because of lower cost of production.

Herein, constructing the biomineralized microbial nanocomposite *via* OMVs encapsulation and biomimetic mineralization technology, we successfully resolved the problem in Ads' systemic delivery, including recognition and clearance of neutralizing antibodies, low replication efficiency in tumor cells and unsatisfactory capacity for immune activation in tumor site. Overall, we firmly believe that Ads-based systemic delivery possesses the development necessity and we have provided an ideal strategy in this manuscript.

References

1. Ban W, et al. Emerging systemic delivery strategies of oncolytic viruses: A key step toward

cancer immunotherapy. Nano Res 15, 4137-4153 (2022).

Question 18: Section 3: What dose “the oncolytic Ads extracted from E. coli” mean? Ads is grown in HEK293 cells?

Response: We are sorry to make the reviewer confused. In the revised manuscript, this part was modified in section 3 as (page 21): “The oncolytic Ads were encapsulated using the engineered OMVs extracted from *E. coli* and transfected with plasmid to express P_2O.”

Reviewer #3: In the current study, the authors design and develop a modified oncolytic adenovirus to address the intrinsic drawbacks of the virus. They used biomineral bacterial outer membrane vesicles encapsulated adenovirus to stimulate autophagy and antitumor immunity. The integrated immunotherapy is timely and critical for improving the clinical applications of the oncologic adenovirus and will attract significant attentions from broad readership. There are some important issues the authors should consider to clarify or improve in the revised version.

Question 1: The logic to integrate various components is rather weak and it is recommended for the authors to clarify in the manuscript. Are these components being replaceable or necessary? It is a complicated system and it is hardly be treated as composite microbe. It is recommended to change the word with nanocomposite or nanosystem.

Response: We accept the reviewer's proposal to replace “composite microbe” with "microbial nanocomposite". Oncolytic virotherapy (OVT) is a novel type of immunotherapy that induces anti-tumor response through selective self-replication within cancer cells and oncolytic virus (OV)-mediated immunostimulation. However, there are some disadvantages impeding the clinical practice of commercial OVs, including the poor immune activation capacity and the neutralizing antibodies elimination. In our study, the engineered OMVs@P_2O was applied to activate anti-tumor immunity and increasing the replication of Ads in tumor tissue through inducing overactivated autophagy of tumor cells. Besides, the biomineral calcium phosphate (CaP) shell was used to protect OMVs@P_2O-Ads from neutralizing antibodies and immune cells. Overall, this Ads delivery platform described in our manuscript provides the unique insight for clinical applications of enhanced OVs-mediated cancer immunotherapy, and all of the various components are obbligato and irreplaceable.

Question 2: How the adenovirus loaded into OMV? What is the efficacy and any improvement have been tried?

Response: We appreciate the reviewer’s questions. In our manuscript, the adenovirus was entered into the OMV by continuous extrusion through the 200 nm filtration membrane. We demonstrated that the encapsulation efficiency of OMVs-Ads was more than 90% by fluorescence quenching experiments with heavy metal ions.

In addition to the extrusion method, we also tried the ultrasound method and the combination of

the two methods to encapsulate adenovirus in OMV. As shown in following Figure, the encapsulation efficiency of OMVs-Ads obtained *via* the ultrasound method was lower than the extrusion method, and there was no significant improvement observed in the combination group. The experimental procedures for fluorescence quenching experiments were as follows. Overall, the extrusion method was selected as the most appropriate preparation method of OMVs-Ads in the manuscript.

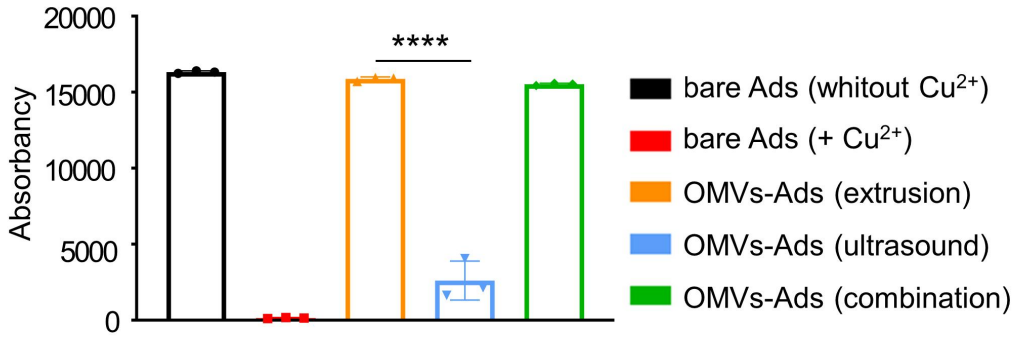

Figure. results of fluorescence quenching experiments for OMVs-Ads obtained by different preparation methods.

Method: "Excess Cy7 fluorescent dye was mixed with 10^8 Ads and incubated at 37 ° C for 3h. And free Cy7 was filtered off by ultrafiltration method using a 30kDA ultrafiltration tube. 1mM Cu^{2+} solution was configured as fluorescence quenching agent. Ads-Cy7 was divided into 5 parts. The extrusion method, the ultrasound method and the combination of the two methods were used respectively to encapsulate adenovirus in OMV. 150 μL of bare Ads, bare Ads, and OMVs-Ads (extrusion, ultrasound, and combinnation) were successively added to a black 96-well plate (n=3) and designated G1 to G5. In G2, G3, G4 and G5, 50 μL of 1mM Cu^{2+} solution was added and shaken. The fluorescence intensity of each group was measured by microplate reader (wavelength of excitation: 730; wavelength of emission: 770)."

Question 3: Autophagy-overactivated is not proper expression, since overactivated action infers to uncontrolled process and may lead to severe side effects.

Response: We appreciate the reviewer's comments. The original intention of using "Autophagy-overactivated" is to express the following two meanings: One the one hand, there have been many studies reported that host tumor cells would autophagy after being infected by Ads.

However, the clinical effect of Ads against tumor cells was not ideal. Herein, we proposed that more powerful autophagy induced by ROS could enhance intratumoral Ads replication to enhance tumor killing efficacy. Therefore, to distinguish between the two, we use "autophagy-overactivated" to refer to the more intense autophagy induced by ROS. One the other hand, the mildly activated autophagy is a self-protection mechanism for cells to cope with the harsh micro-environment, while the severe autophagy would lose cyto-protective function and lead to cell death by triggering autophagic cell death pathway. In our manuscript, we intended to enhance the anti-tumor ability of Ads *via* autophagy of tumor cells, which required us to induce strong autophagy in tumor cells instead of mildly activated autophagy. Therefore, to make clear to reviewers and readers the extent of autophagy referred to in our project, we used the term of "autophagy-overactivated".

Question 4: Quantitative measurement of pyranose oxidase in critical *in vivo*. What is the contribution for this enzyme for immune activation?

Response: We appreciate the reviewer's kind suggestion. The important role of pyranose oxidase *in vivo* is to promote the generation of ROS in the tumor microenvironment, thereby inducing more stronger autophagy and enhancing the antitumor efficacy of oncolytic viral immunotherapy. Therefore, we had evaluated the level of ROS at the tumor site instead of measuring the concentration of pyranose oxidase *in vivo* (Figure S16).

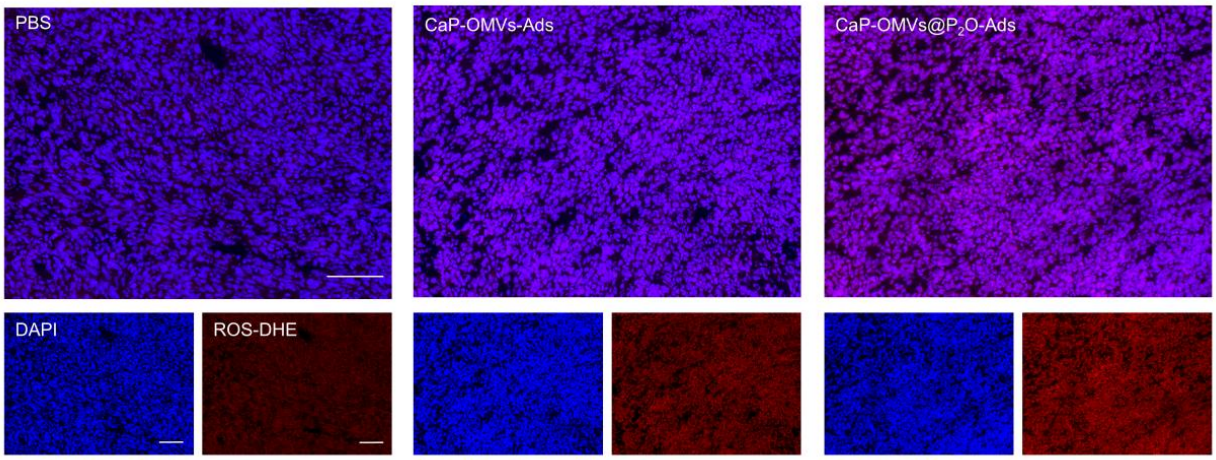

Figure S16. Immunofluorescence images of ROS in tumor tissues. Blue represents DAPI-stained tumor cells and red represents DHE. Scale bar=100 μm.

Question 5: The scholarly presentation needs to further improve, such as no OV definition provided

in the manuscript.

Response: We appreciate the reviewer's comments. We are sorry for the confusion caused to the reviewer's reading due to the loopholes in scholarly expression. The revised manuscript was checked out carefully by ourselves and to better improve the readability of the manuscript, we had sent it for language revision by language revision by MogoEdit language editing service on 23-Feb-2023. Futhermore, we have rechecked the expressive holes in the manuscript, such as no OV definition provided here, and the revised content has been added in the revised manuscript (page 4): "An attractive immunotherapeutic strategy is oncolytic viral biotherapy against cancer. It could selectively kill cancer cells and activate the systemic immune response using oncolytic viruses (OVs). Oncolytic adenoviruses (Ads) are commonly employed OVs due to their safety and efficacy."

MogoEdit

CERTIFICATE OF ENGLISH EDITING

This is to certify that the manuscript entitled

Autophagy-overactivated microbial nanocomposite engineered from oncolytic adenoviruses for the cascade enhancement of cancer immunotherapy

commissioned to us has been carefully edited by a native English-speaking editor of MogoEdit, and the grammar, spelling, and punctuation have been verified and corrected where needed. Based on this review, we believe that the language in this paper meets academic journal requirements. Please contact us with any questions.

MOGOEDIT MOGO INTERNET TECHNOLOGY CO., LTD.

Gang Zhang

Dr. Gang Zhang
Founder & CEO of MogoEdit

Date of Issue
February 22, 2023

Disclaimer: The changes in the document may be accepted or rejected by the authors in their sole discretion after our editing. However, MogoEdit is not responsible for revisions made to the document after our edit on **February 22, 2023**.

MogoEdit is a professional English editing company who provides English language editing, translation, and publication support services to individuals and corporate customers worldwide. As a company invested by the affiliate fund of Chinese Academy of Science, MogoEdit is one of the leading language editing service providers in China, whose clients come from more than 1000 universities and research institutes.
MogoEdit Website: http://en.mogoedit.com/
500+ native English editors: http://en.mogoedit.com/editors

Mogo make the world flatter

Mogo Internet Technology Co., LTD.
No. 57, 3rd Keji Road, Xi'an 710075, PR China +86 02988317483 support@mogoedit.com

Figure. The certificate of MogoEdit language editing services on 23-Feb-2023.

Question 6: For the immune activation experiments, various critical steps are missing to generate a concrete conclusion of cascade antitumor activation.

Response: We appreciate the reviewer's comments. Oncolytic adenovirus (Ad) was an immune activation element attracting widespread attention recent years. However, the immune activation

capacity and anti-tumor ability of commercial Ads in clinical stage were unsatisfactory actually. Herein, to address the the clinical obstacles of Ads, the engineered OMVs@P_2O have been constructed and introduced in our study. Concretely, when the microbial nanocomposite injected into the tumor, there would be a plenty of ROS producing through glucose enzymatic hydrolysis by P_2O, then the excessive accumulation of ROS at the tumor site would sequentially trigger overactivated autophagy of tumor cells, thereby triggering autophagic immunogenic cells death and the production of autophagosomes. As reported in relative paper, due to the "imprisonment" effect of tumor stromal cells on Ads and the rapid death of infected tumor cells, there are no sufficient condition for the replication of Ads in tumor tissue. Here, a large number of autophagosomes provide a site for Ads to replicate, and then enhance the Ads-mediated immune response.

In our manuscript, as shown in Figure 2h, this result suggested that the engineered OMVs-generated ROS could promote autophagy, thereby improving the replication of Ads. After 48 hours, compared with OMVs-Ads group and OMVs@P_2O-Ads plus 3MA group (3MA is an autophagy inhibitor: 3-Methyladenine), the Ads replication ability of OMVs@P_2O-Ads was increased by 3.74± 0.86 times. And in Figure S14, compared with the group without P_2O (G3 and G5), the agents with P_2O (G4 and G6) remarkably promote the immune activation in the tumor tissue. Concretely, compared with OMVs group, the proportion of $CD8^+$ T cells in OMVs@P_2O group increased to 1.2 times; compared with OMVs-Ads group, the proportion of $CD8^+$ T cells in OMVs@P_2O-Ads group increased to 1.24 times and compared with PBS group, the proportion of $CD8^+$ T cells in OMVs@P_2O-Ads group increased to 6.15 times. Overall, the introduction of engineered OMVs@P_2O could draw a concrete conclusion of cascade antitumor activation.

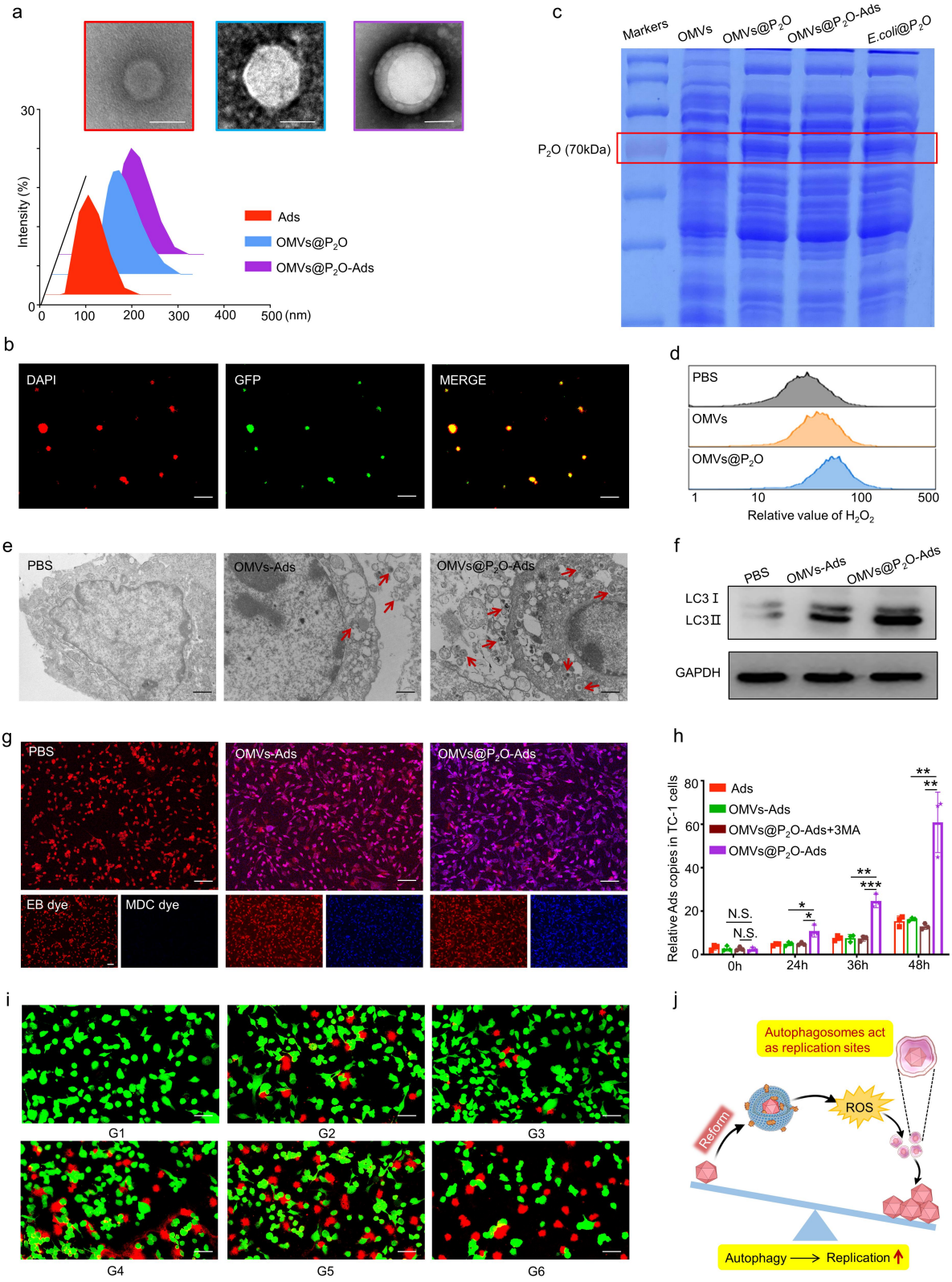

788 **Figure 2. Preparation and *in vitro* evaluation of the microbial nanocomposite.** (a) TEM and size distribution
789 images of Ads, OMVs@P_2O, and OMVs@P_2O-Ads. Scale bar=100 nm. (b) CLSM images of the microbial
790 nanocomposite. Ads were stained with DAPI dye (red) and OMVs carried a GFP marker (green). Scale bar=1 μm.
791 (c) The expression of P_2O was investigated by the SDS-PAGE method. (d) The ROS level assessment in TC-1

cells by flow cytometry. (e) TEM images of autophagosomes. Scale bar=1 μm. (f) The expression of autophagy-related protein LC3-I and LC3-II by western bolt analyses. (g) CLSM images of autophagosomes. Cells were stained with EB dye (red) and autophagosomes were stained with MDC dye (blue). Scale bar=50 μm. (h) The Ads replication in TC-1 cells was quantified using real-time PCR at 0, 24, 36, and 48 h sequentially. 3MA is an autophagy inhibitor: 3-Methyladenine. (i) Cytotoxicity of different formulations in TC-1 cells by CLSM. Living cells were stained with Calcein (green) and dead cells were stained with PI (red). Scale bar=20 μm. (j) Schematic diagram of bridging ROS with oncolytic Ads replication. *p<0.05, **p<0.01, ***p<0.001, ****p<0.0001 versus control. G1: PBS, G2: Ads, G3: OMVs, G4: OMVs@P_2O, G5: OMVs-Ads, G6: OMVs@P_2O-Ads.

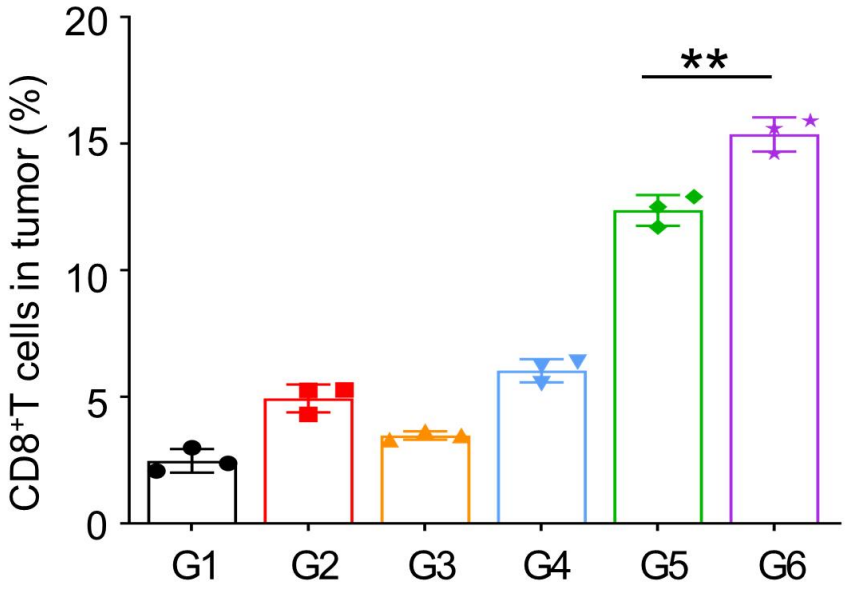

Figure S14. The infiltration of $CD8^+$ T cells in tumor of mice treated with different agents on the 18th day.

Reviewer #4: This is a meaningful work for the present autophagy-cascade-boosted immunotherapeutic method. The authors stated that OMVs@P_2O promoted Ads replication and resulted in Ads-overactivated autophagy, further remolded immunosuppressive TME. However, several problems that must be clarified need to be solved.

Question 1: As we all known, oncolytic adenovirus enters tumor cells through CAR receptor to play an anti-tumor role. What mechanism does OMVs@P_2O or OMVs@P_2O-Ads enter tumor cells through? Does it have practical significance in tumor cells with high or low CAR expression?

Response: Thanks for reviewer's meaningful question. Human serotype 5 adenovirus (Ad5) is a non-enveloped virus and its internalization into cells primarily relies on the interaction between fiber knob of Ad and coxsackie adenovirus receptor (CAR) expressed on cell surface. Once Ad fiber binds with CAR, a RGD motif at the penton base of Ad interacts with cellular integrin (αvβ1, αvβ3, or αvβ5) to induce clathrin-mediated Endocytosis. However, in our manuscript, the oncolytic virus used in this study is Ad11, which relies on CD46 receptor rather than CAR receptor for entry into cells. In addition, as is reported in related papers, the entry route of OMVs@P_2O or OMVs@P_2O-Ads is different from that of Ads[1]. Concretely, OMVs can bind to certain receptors, such as Toll-like receptor 2, and activate receptor-induced intracellular signaling in recipient cells. Besides, OMVs can also be taken up by recipient cells through direct membrane fusion or by using various endocytic routes, including macropinocytosis, phagocytosis, and endocytosis.

References

1. Li M, et al. Bacterial outer membrane vesicles as a platform for biomedical applications: An update. J Control Release 323, 253-268 (2020).

Question 2: The reason of the low intratumoral content of intravenous-delivered Ads is that the higher level of anti-adenovirus antibody in human body eliminates the exogenous injected Ads. Can OMVs@P_2O or OMVs@P_2O-Ads effectively avoid the elimination of neutralizing antibodies? Whether the expression level of anti-adenovirus antibody has been improved in the mouse model in advance? This is a very necessary experiment.

Response: We appreciate the reviewer's comments. The experiment of neutralizing antibody binding with OMVs@P_2O-Ads has been conducted, and the result image and experimental method

are as follow. As shown in figure, OMVs@P_2O-Ads possess abilities to protect 91.8% Ads from recognition and clearance by neutralizing antibodies.

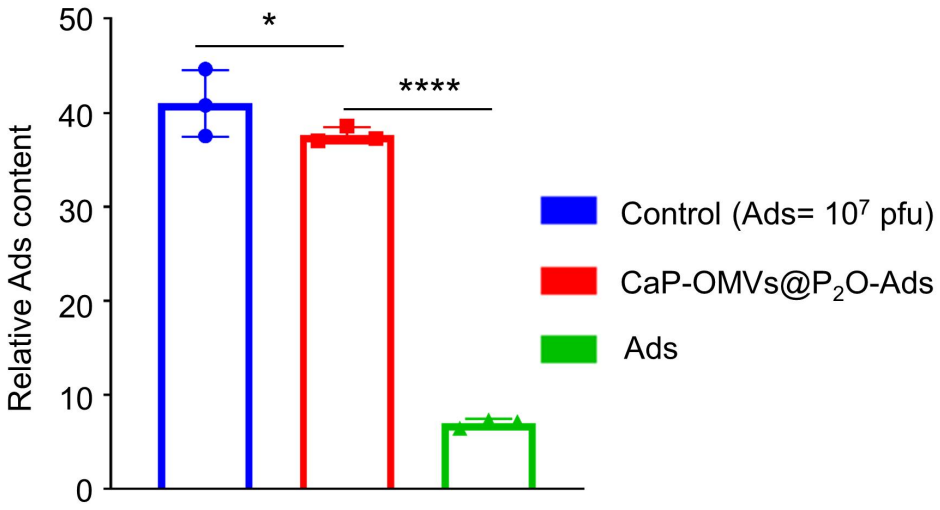

Figure. The result of neutralizing antibody binding with OMVs@P_2O-Ads experiment.

Method: The serum containing neutralizing antibodies of ads was diluted as 1:100. Then the diluted neutralizing antibody was mixed with ads or OMVs@P_2O-Ads (10^7 pfu/mL) and incubated for 1 h at 4 ℃. Afterward, protein G-coated agarose beads (Beyotime, China) were added to the mixture and incubated for 1 h. The mixture was finally centrifuged at 6000 rpm for 1 min and the supernatant was collected. The number of ads remaining in the supernatant was determined by qPCR assay.

Question 3: Infection with oncolytic viruses leads to activation of type I IFN signaling pathways, which are crucial in oncolytic virus-mediated antitumor immunity. The authors stated that OMVs@P_2O promoted Ads replication. Is this pathway activated to a greater extent by OMVs@P_2O?

Response: We appreciate the reviewer's comments. As suggested by the reviewer, we have determined the content of type I IFN in the tumor tissue of mice after four different administrations (G1: PBS, G2: OMVs@P_2O-Ads, G3: CaP-OMVs-Ads, G4: Intra-Ads, G5: CaP-OMVs@P_2O-Ads, G6: Intra-Ads high does) *via* ELISA experiment. And the experimental result is as follows. As

shown in the figure, the concentration of type I IFN of G5 (CaP-OMVs@P_2O-Ads) was evidently higher than G3 (CaP-OMVs-Ads), indicating that the presence of P_2O could enhance the replication of Ads.

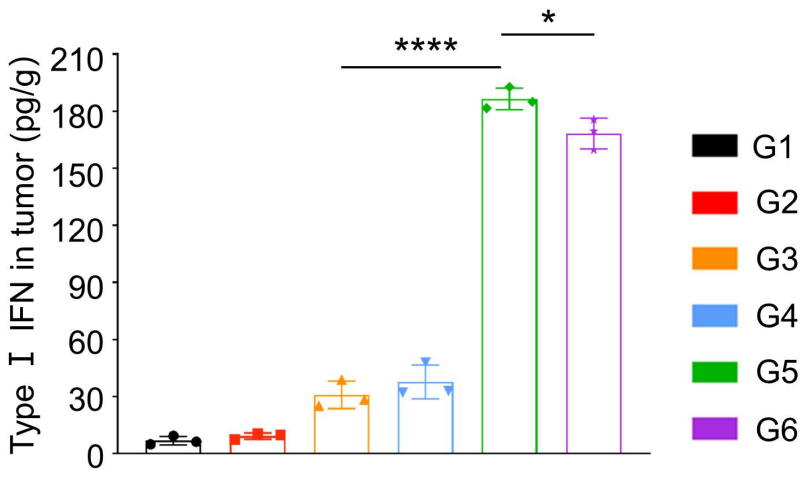

Figure. Images of concentration of type I IFN cytokines in tumor tissue.

Question 4: *In vivo* experiment on OMVs@P_2O-Ads or CaP-OMVs@P_2O-Ads regulating tumor immune microenvironment is not enough. The innate and adaptive immune cells, as well as the activation and exhausted markers of T cells, need to be detected.

Response: We appreciate the reviewer's comments. In this manuscript, we have performed a series of experiments on the investigation of tumor immune activation. First, to investigate the changes in gene expression after OMVs@P_2O-Ads treatments, a transcriptomic analysis of the tumor xenografts was conducted to determine the expression of immune-related genes (Figure 3i-k). Then we investigated the content of M1-like macrophages ($CD45^+F4/80^+CD80^+$), ($CD45^+F4/80^+CD206^+$) M2-like macrophages and activated DC ($CD45^+CD11c^+MHC\text{-}II^+$) at the tumor site (Figure S26-S29, Figure 5f and 5i). In addition, the amount of $CD8^+$ T cells ($CD45^+CD3^+CD8^+$), IFN-γ^+CD8^+ T cells ($CD45^+CD3^+CD8^+IFN\text{-}\gamma^+$) and Treg cells ($CD45^+CD3^+CD4^+Foxp3^+$) were measured (Figure 5c-e, g-h, S24 and S25). Furthermore, we performed T cells co-incubation experiment *in vitro* (Figure S32) and verified the dependence of CaP-OMVs@P_2O-Ads on $CD8^+$ T cells in the process of anti-tumor by depleting CD8 T cells with antibodies (Figure S33). Besides, the detection of cytokines (Figure 3f-h) in serum and memory T cells (Figure S30 and S31) in spleen can also reflect the immune status of tumor to a certain extent.

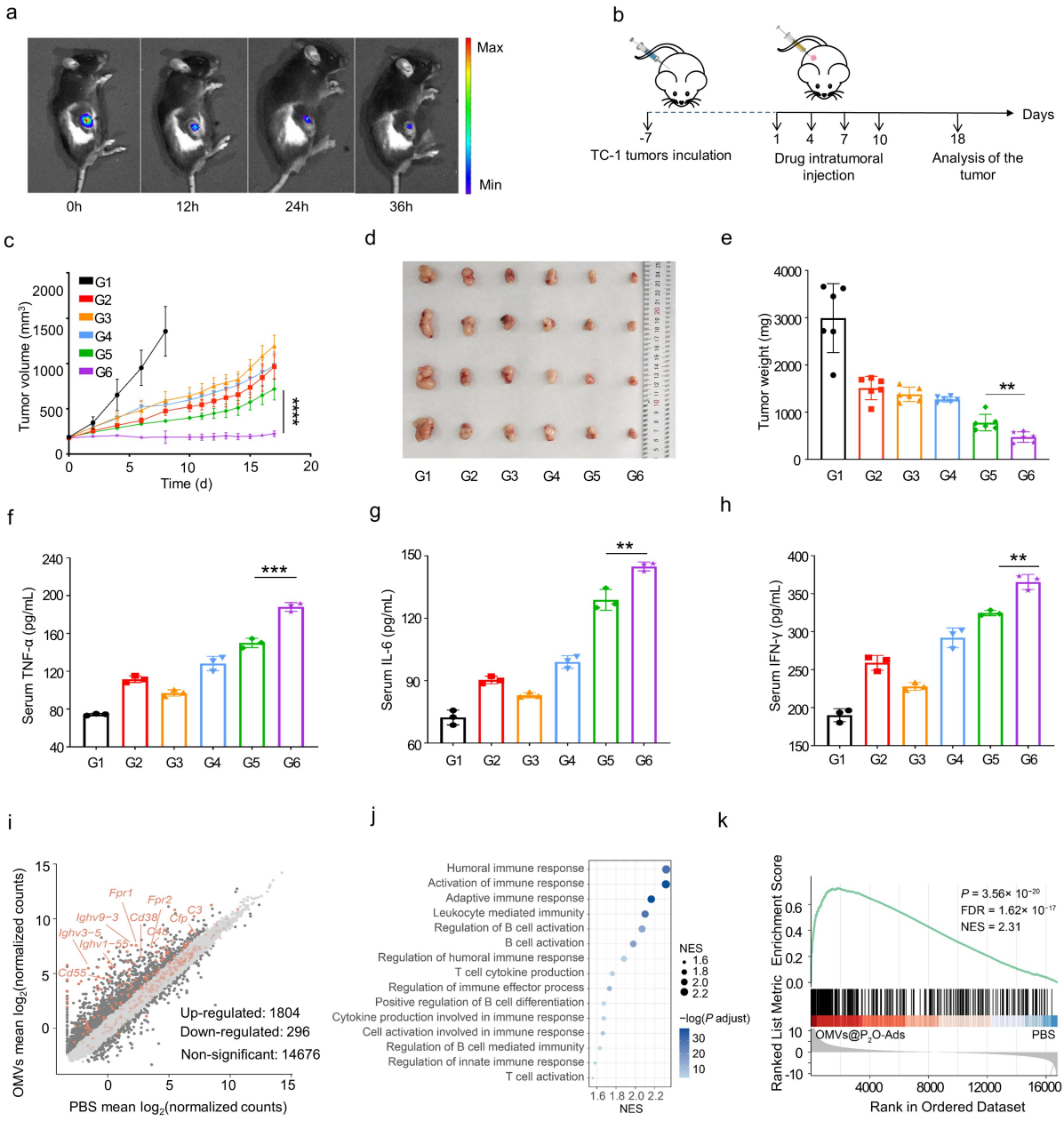

Figure 3. *In vivo* oncolytic efficacy of the microbial nanocomposite. (a) *In vivo* DIR fluorescent imaging of the microbial nanocomposite in TC-1-hCD46 xenograft tumor-bearing mice by IVIS. (b) Schematic illustration of the antitumor activity and immunology assessment experiments of the microbial nanocomposite using TC-1-hCD46 xenograft tumor-bearing C57 female mice model. TC-1 cells (10^6) were subcutaneously injected into the waist of female C57 mice, and the tumor-bearing mice were divided into six groups (n=6). When the tumor reached 100-150 mm^3, the mice were injected intratumorally with PBS, Ads (7×10^5 PFU), OMVs, OMVs@P_2O, OMVs-Ads (7×10^5 PFU), and OMVs@P_2O-Ads (7×10^5 PFU). The drug was given every three days for four consecutive times, the tumor volume was measured with a vernier caliper, and mice were weighed daily. (c) Tumor volume growth profiles of C57 mice bearing TC-1 xenografts. (d) Images of representative tumors of different treated groups on the 18th day (n=6). (e) Statistical graph of tumor weight of different treated groups on the 18th day (n=6). (f-h) Images of concentration of main cytokines in serum. (i) The differential gene expression between the samples treated with OMVs@P_2O-Ads and PBS, using the absolute value of logFC greater than 1 as

the threshold. (j) GSEA enriched pathways of the up-regulated genes in the samples treated with OMVs@P_2O-Ads, showing immune-related terms. (k) Gene set enrichment analysis (GSEA) of the term "Activation of immune response", and the genes included in this pathway are highlighted in (i) with light yellow brown. *p<0.05, **p<0.01, ***p<0.001, ****p<0.0001 versus control. (G1: PBS, G2: Ads, G3: OMVs, G4: OMVs@P_2O, G5: OMVs-Ads, G6: OMVs@P_2O-Ads).

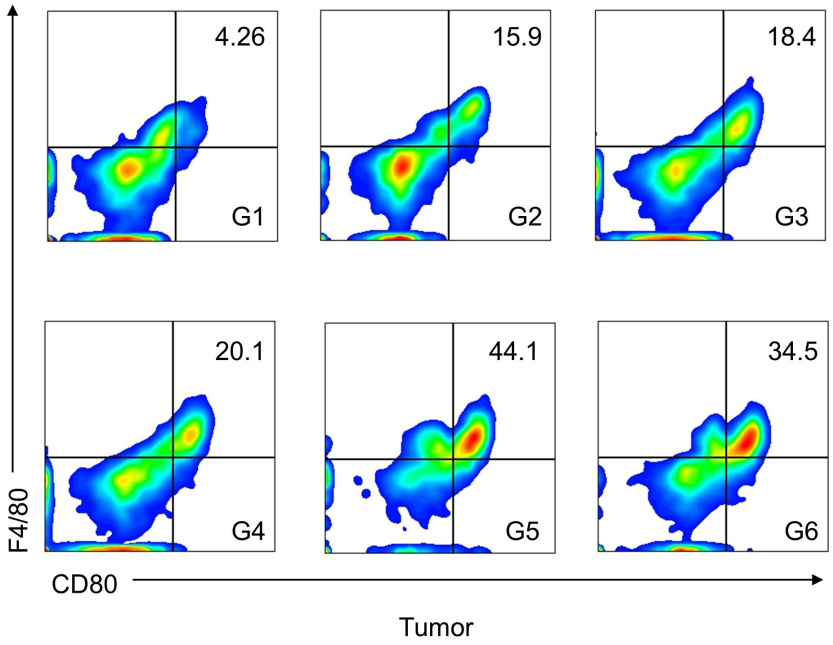

Figure S26. Representative flow cytometric evolution images of M1-like macrophages ($CD45^+F4/80^+CD80^+$) in tumor (n=3). (G1: PBS, G2: OMVs@P_2O-Ads, G3: CaP-OMVs-Ads, G4: Intra-Ads, G5: CaP-OMVs@P_2O-Ads, G6: Intra-Ads high does)

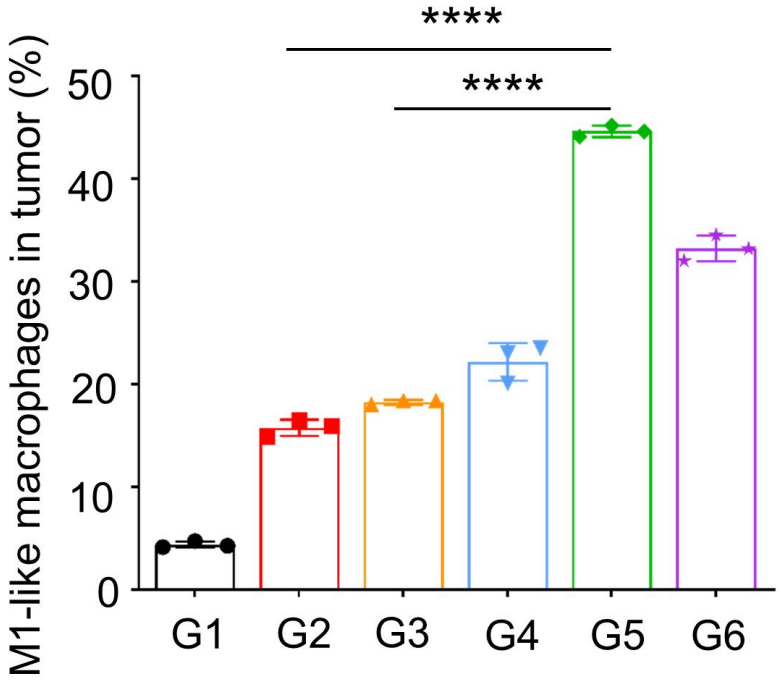

887 **Figure S27.** Relative quantification of M1-like macrophages ($CD45^+F4/80^+CD80^+$) in tumor (n=3). (G1: PBS, G2:
888 OMVs@P_2O-Ads, G3: CaP-OMVs-Ads, G4: Intra-Ads, G5: CaP-OMVs@P_2O-Ads, G6: Intra-Ads high does)

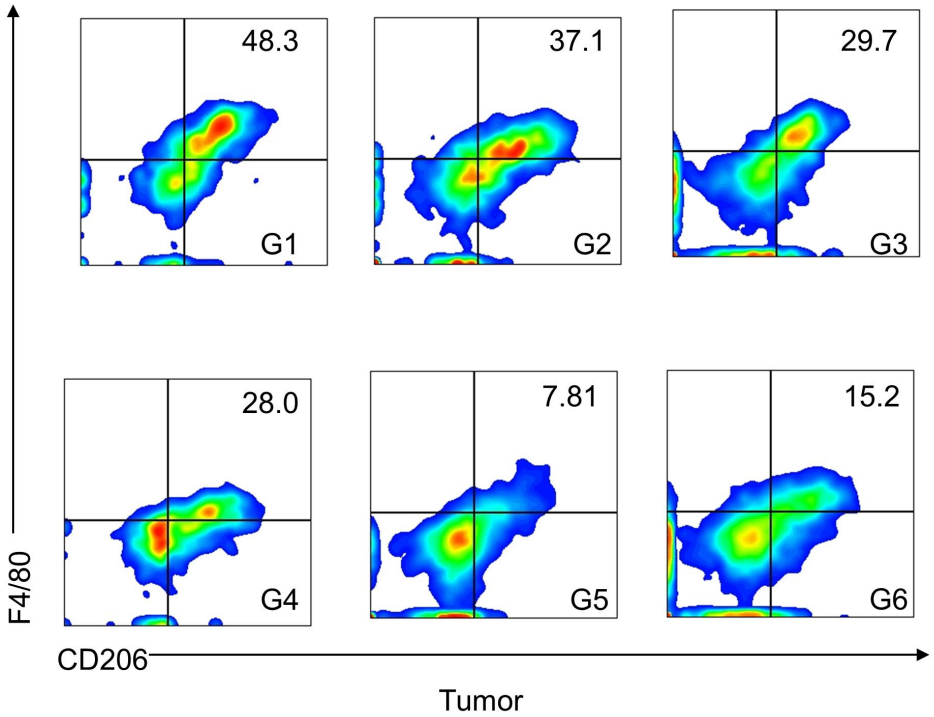

889 **Figure S28.** Representative flow cytometric evolution images of M2-like macrophages ($CD45^+F4/80^+CD206^+$) in
890 tumor (n=3). (G1: PBS, G2: OMVs@P_2O-Ads, G3: CaP-OMVs-Ads, G4: Intra-Ads, G5: CaP-OMVs@P_2O-Ads,
891 G6: Intra-Ads high does)

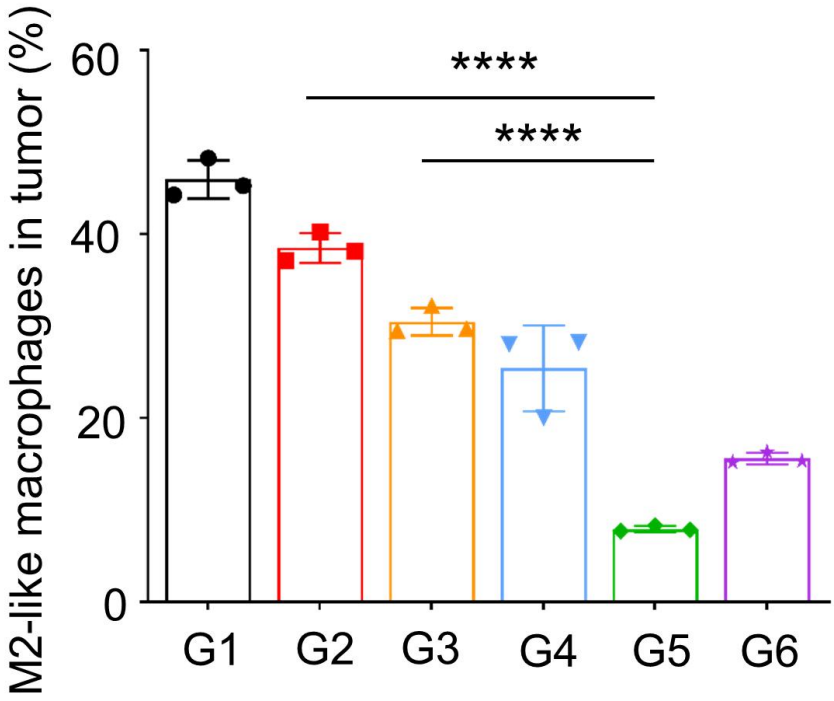

892 **Figure S29.** Relative quantification of M2-like macrophages ($CD45^+F4/80^+CD206^+$) in tumor (n=3). (G1: PBS,
893 G2: OMVs@P_2O-Ads, G3: CaP-OMVs-Ads, G4: Intra-Ads, G5: CaP-OMVs@P_2O-Ads, G6: Intra-Ads high does)

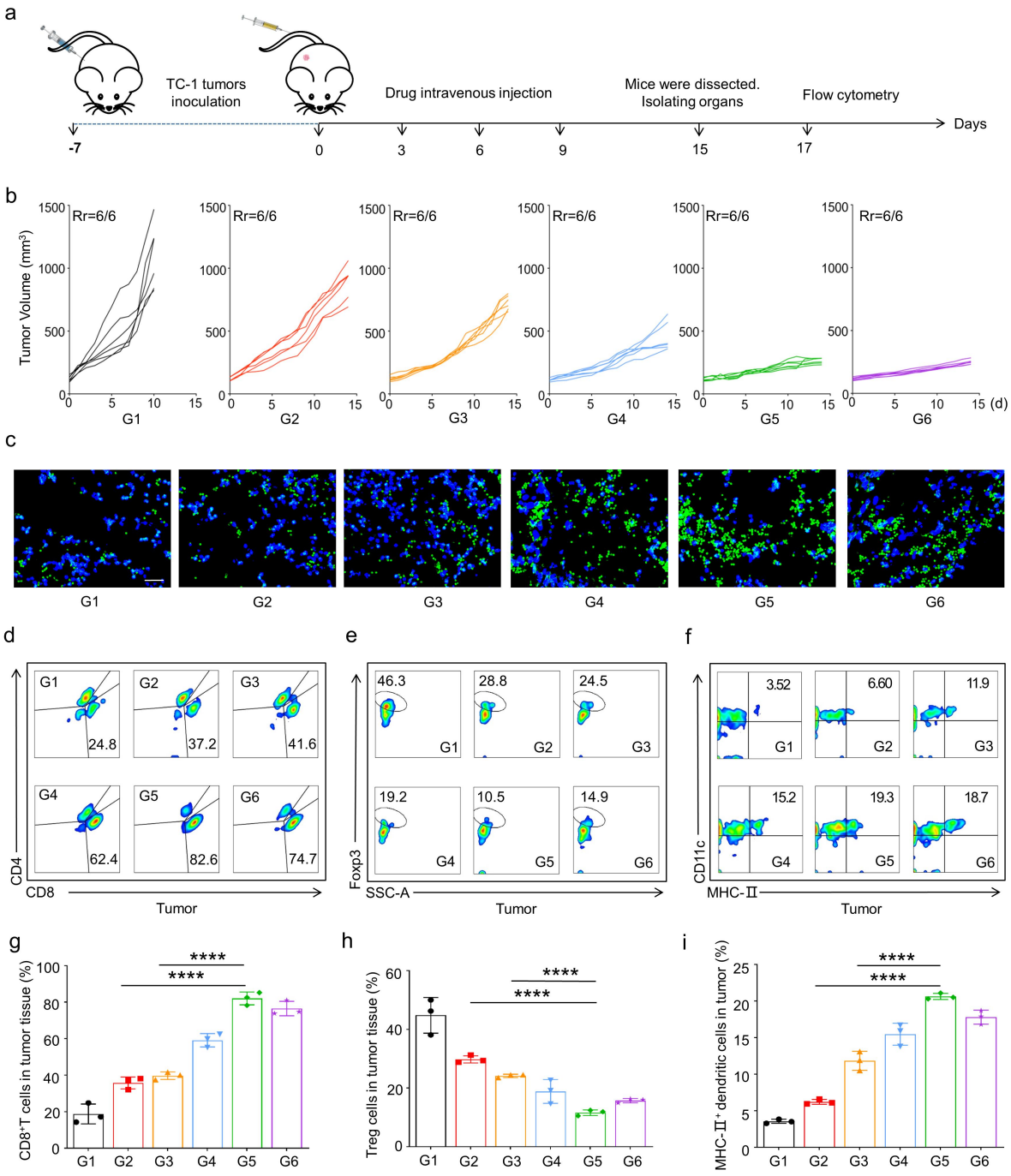

Figure 5. ***In vivo*** **oncolytic efficacy and immuneactivation capacity of the biomineralized microbial nanocomposite.** (a) Schematic illustration of the antitumor activity and immunity investigation of the biomineralized microbial nanocomposite on TC-1-hCD46 xenograft tumor-bearing C57 female mice model. (b) Individual tumor growth kinetics in different groups (n=6). (c) The immunofluorescence images of $CD8^+$ T cells in tumor tissues. Scale bars=50μm. (d) Representative flow cytometric evolution images (g) as well as relative quantification of $CD8^+$ T cells ($CD45^+CD3^+CD8^+$) in the tumor (n=3). (e) Representative flow cytometric evolution images (h) as well as relative quantification of Treg cells ($CD45^+CD3^+CD4^+Foxp3^+$) in the tumor (n=3). (f) Representative flow cytometric evolution images (i) and relative quantification of MHC-II^+ DC cells ($CD45^+CD11C^+$MHC-II^+) in the tumor (n=3). *p<0.05, **p<0.01, ***p<0.001, ****p<0.0001 versus control. (G1:

PBS, G2: OMVs@P_2O-Ads, G3: CaP-OMVs-Ads, G4: Intra-Ads, G5: CaP-OMVs@P_2O-Ads, G6: Intra-Ads high does).

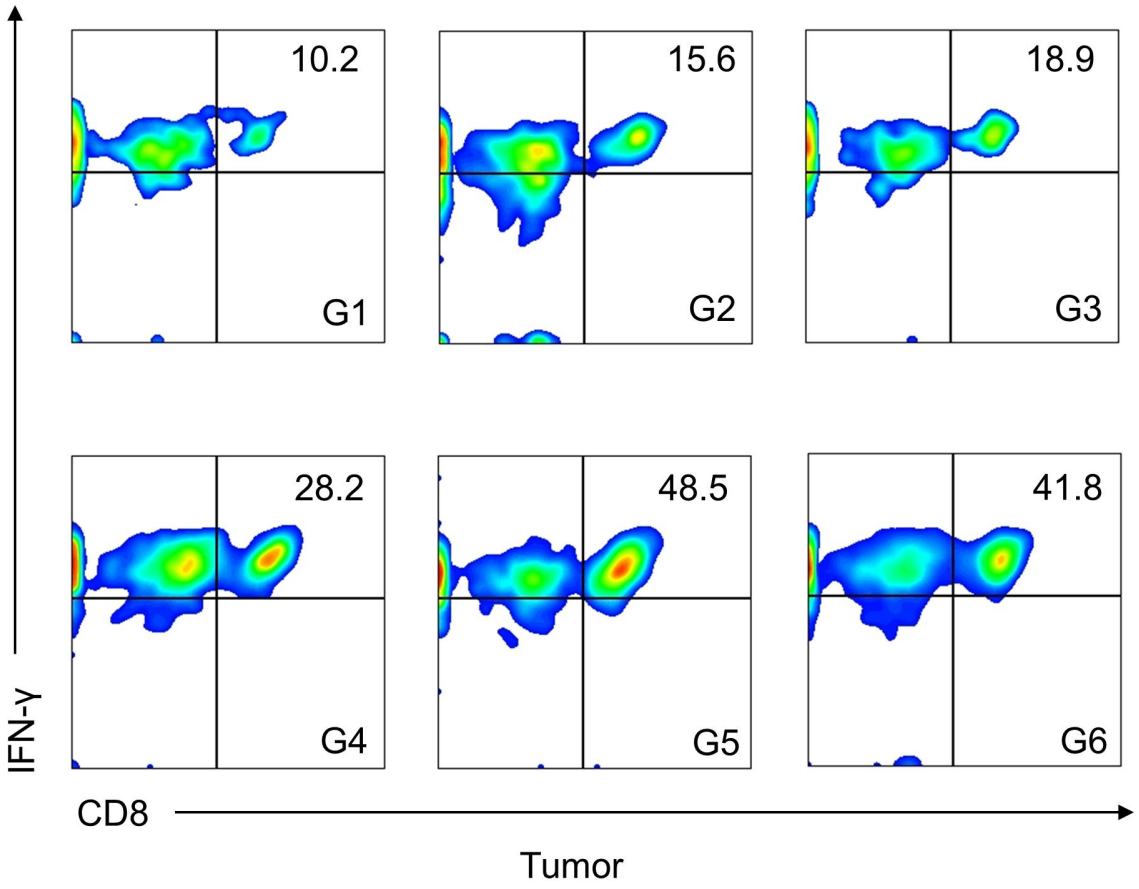

Figure S24. Representative flow cytometric evolution images of IFN-γ^+CD8$^+$ T cells (CD45$^+$CD3$^+$CD8$^+$IFN-γ^+) in tumor (n=3). (G1: PBS, G2: OMVs@P_2O-Ads, G3: CaP-OMVs-Ads, G4: Intra-Ads, G5: CaP-OMVs@P_2O-Ads, G6: Intra-Ads high does)

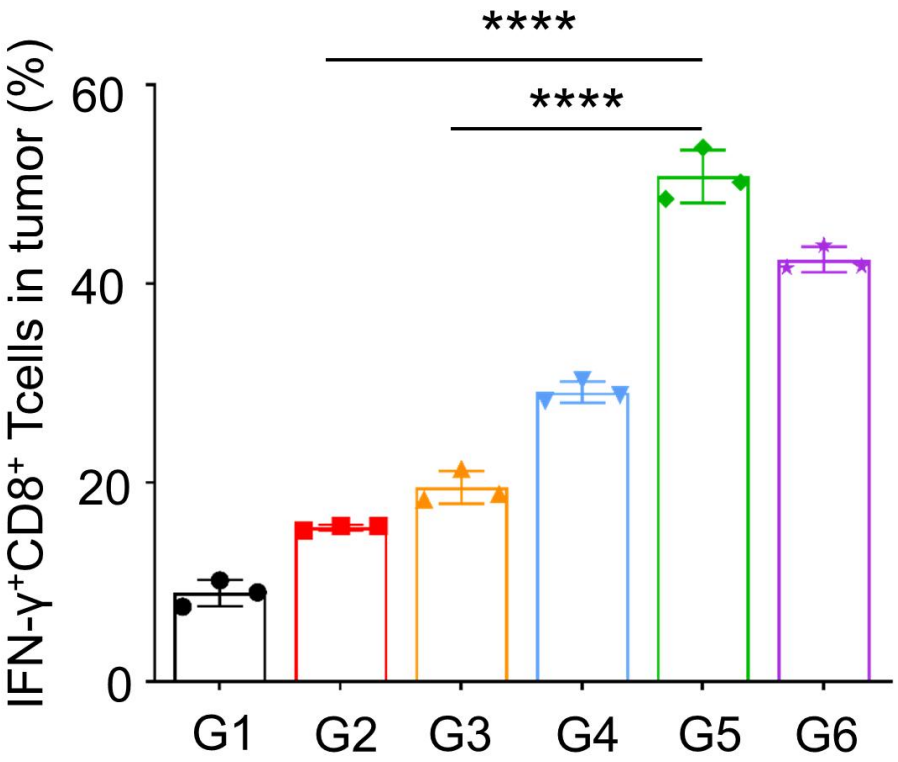

908 **Figure S25.** Relative quantification of IFN-γ$^+$CD8$^+$ T cells (CD45$^+$CD3$^+$CD8$^+$IFN-γ$^+$) in tumor (n=3). (G1: PBS,
909 G2: OMVs@P$_2$O-Ads, G3: CaP-OMVs-Ads, G4: Intra-Ads, G5: CaP-OMVs@P$_2$O-Ads, G6: Intra-Ads high
910 does)

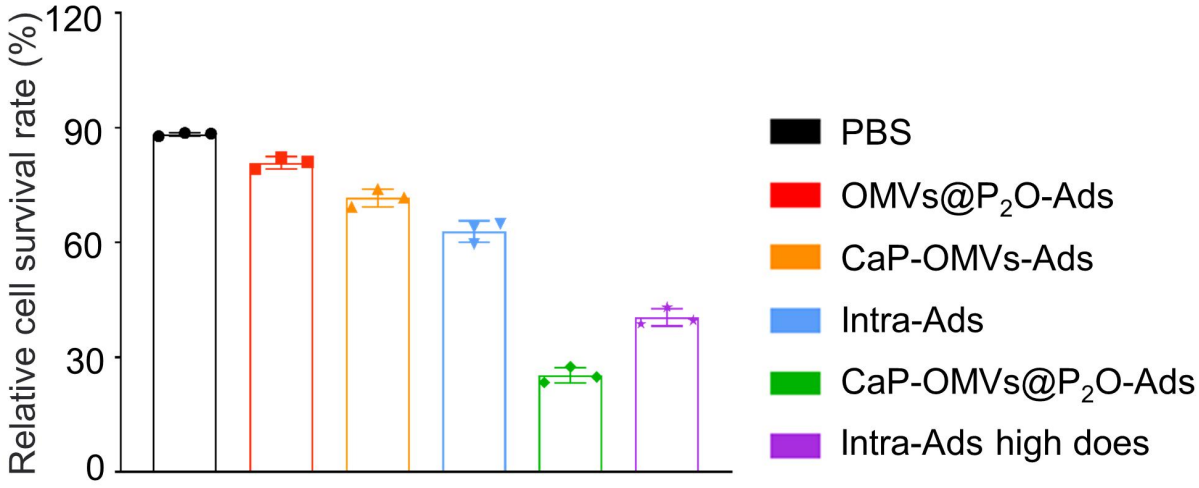

911 **Figure S32.** The experimental result of the co-culture assay. (It's worth noting here that PBS represents T cells
912 extracted from mice in the PBS group, and other groups as above.)

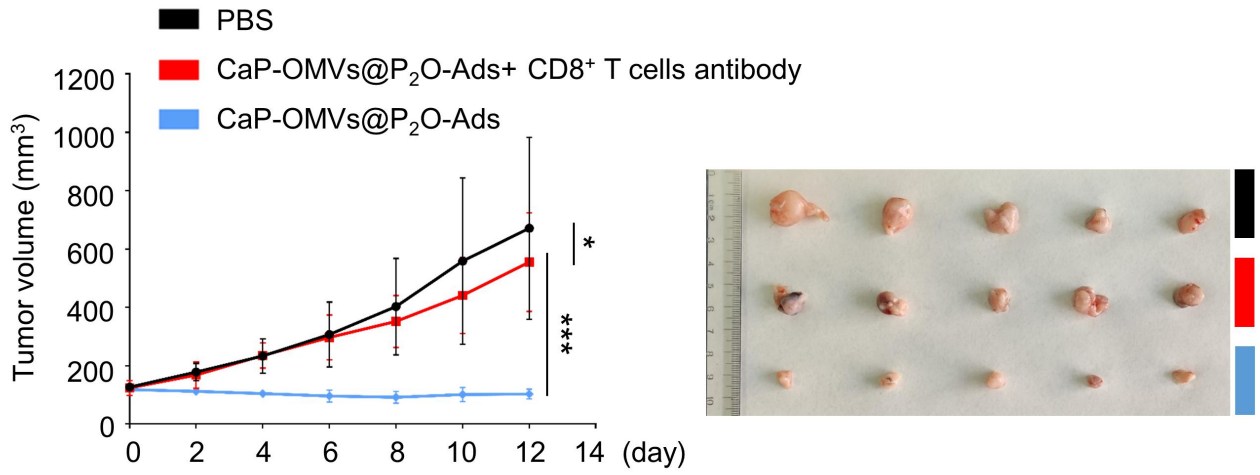

913 **Figure S33.** Tumor volume during the treatments and images of representative tumors of different treated groups
914 on the 12th day (n=5).

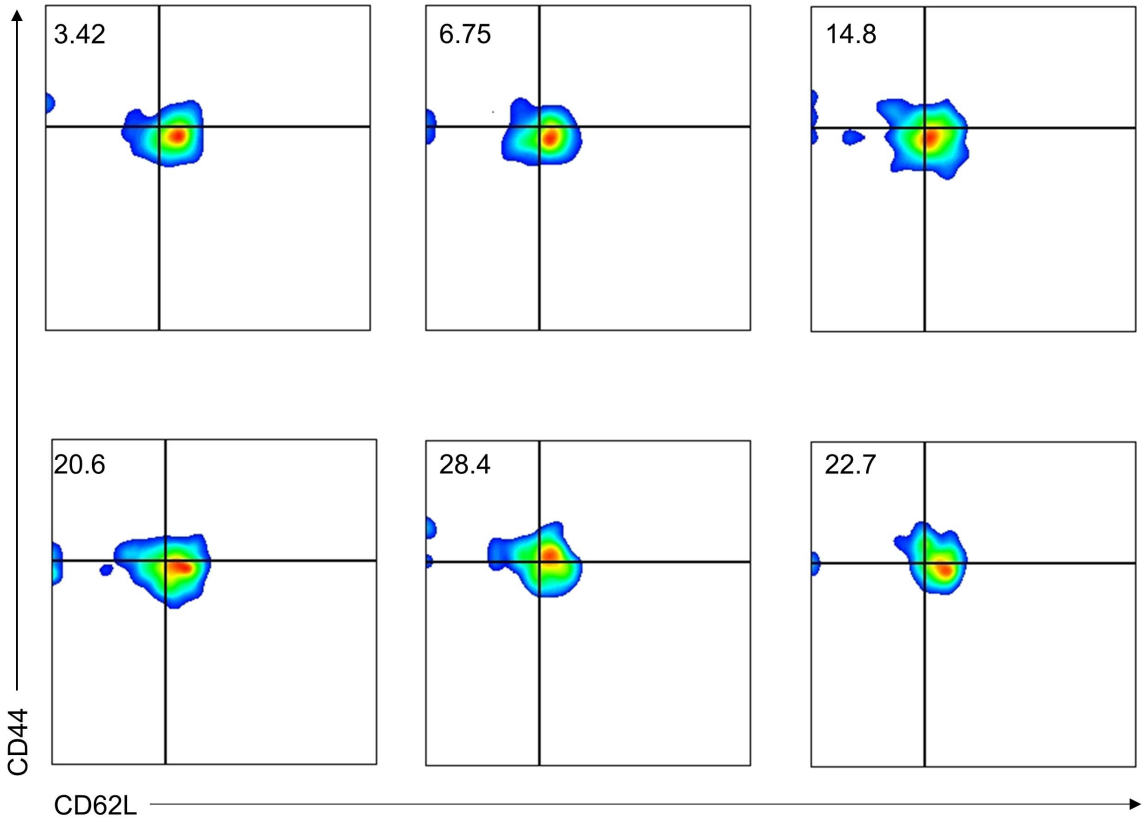

915 **Figure S30.** The gating strategy of effector memory T cells ($CD3^+$ $CD8^+$ $CD62L^-$ $CD44^+$) in spleen (n=3). (G1:
916 PBS, G2: OMVs@P_2O-Ads, G3: CaP-OMVs-Ads, G4: Intra-Ads, G5: CaP-OMVs@P_2O-Ads, G6: Intra-Ads high
917 does).

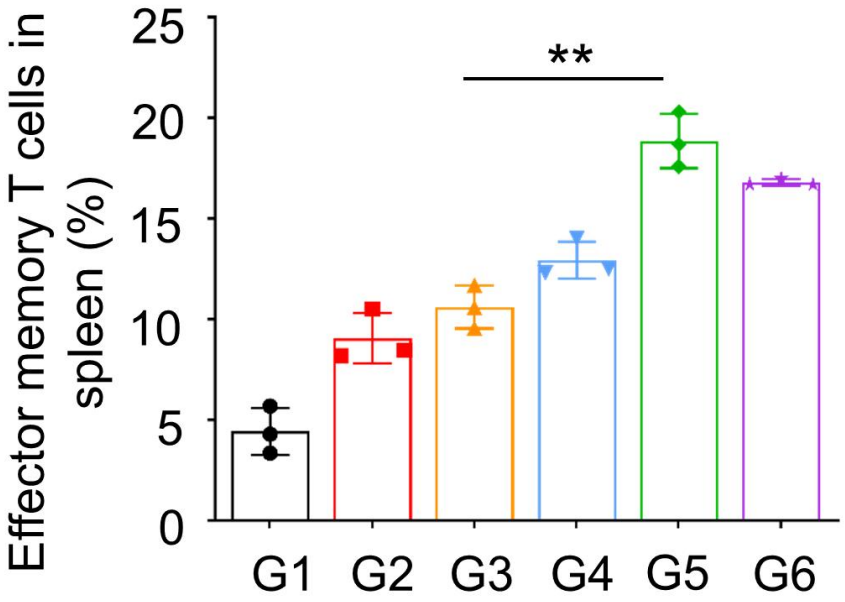

Figure S31. Relative quantification of effector memory T cells ($CD3^+$ $CD8^+$ $CD62L^-$ $CD44^+$) in spleen (n=3). (G1: PBS, G2: OMVs@P_2O-Ads, G3: CaP-OMVs-Ads, G4: Intra-Ads, G5: CaP-OMVs@P_2O-Ads, G6: Intra-Ads high does).

REVIEWERS' COMMENTS

Reviewer #2 (Remarks to the Author):

The authors have addressed all my concerns by conducting additional experiments and analysis. The results are solid.

Reviewer #3 (Remarks to the Author):

Reviewer #4 (Remarks to the Author):

The revised manuscript, “Autophagy-overactivated microbial nanocomposite engineeredfromoncolytic2 adenoviruses for the cascade enhancement of cancer immunotherapy” are very effective in addressing all the reviewer’s comments and concerns. The manuscript is clearly to be accepted.

Responses to the reviewers' comments

Reviewer #2: The authors have addressed all my concerns by conducting additional experiments and analysis. The results are solid.

Response: Thanks for the reviewer's recognition and support of our work.

Reviewer #4: The revised manuscript, “Autophagy-overactivated microbial nanocomposite engineered from oncolytic adenoviruses for the cascade enhancement of cancer immunotherapy” are very effective in addressing all the reviewer’s comments and concerns. The manuscript is clearly to be accepted.

Response: We are truly grateful to your valuable comments and approval.